

INFLUENCE OF ALUMINIUM ADDITIONS  
UPON THE OXIDATION BEHAVIOUR OF  
(SOME) IRON-CHROMIUM ALLOYS.

BY

SARDER ELIUS SADIQUE

A thesis submitted to the Department of Metallurgical Engineering,  
Bangladesh University of Engineering and Technology, Dhaka, in  
partial fulfilment of the requirements for the Degree of Master of  
Science in Engineering (Metallurgical).

January, 1996



BANGLADESH UNIVERSITY OF ENGINEERING AND TECHNOLOGY, DHAKA,  
BANGLADESH.



## DECLARATION

I do, hereby declare that this research work has been carried out by the author under the supervision of Dr. Md. Mohar Ali, Professor, Department of Metallurgical Engineering, BUET, Dhaka, and it has not been submitted elsewhere for the award of any other degree or diploma.



Countersigned

*Md. Mohar Ali*  
22.1.96

Supervisor

A handwritten signature in cursive script, appearing to read "S. S. S.", written over a horizontal line.

Signature of the Author

The undersigned examiners appointed by the Committee of Advanced Studies and Research (CASR) hereby recommend to the Department of Metallurgical Engineering of the Bangladesh University of Engineering and Technology, Dhaka, the acceptance of the thesis entitled "INFLUENCE OF ALUMINIUM ADDITIONS UPON THE OXIDATION BEHAVIOUR OF (SOME) IRON-CHROMIUM ALLOYS" submitted by Sarder Elius Sadique, B.Sc. Engg. (Metallurgical), in partial fulfilment of the requirements for the Degree of Master of Science in Engineering (Metallurgical).

1. Md. Mohar Ali 22.1.96 Chairman  
Dr. Md. Mohar Ali (Supervisor)  
Professor  
Dept. of Metallurgical Engg.  
BUET, Dhaka.
2. 628 22/01/96 Member  
Head  
Dept. of Metallurgical Engg.  
BUET, Dhaka.
3. Rezaul Haque 22/1/96 Member  
Dr. A.K. Md. Rezaul Haque  
Professor  
Dept. of Metallurgical Engg.  
BUET, Dhaka.
4. [Signature] 22-1-96 Member  
Prof. Dr. Md. Serajul Islam  
(External)  
256/2A Sultanganj  
Rayer Bazar, Dhaka.

## ACKNOWLEDGMENT

The author wishes to record his immeasurable gratitude and thankfulness of the One and the Almighty Allah, the most Merciful, the Lord and Sustainer of the Universe, and of mankind in particular. All praise and glory are due to Him. Peace and - blessings be upon His chosen servants - His messengers and upon all those who follow the path of Guidance.

The author expresses his thanks and indebtedness to his supervisor Dr. Md. Mohar Ali, Professor, Dept. of Metallurgical Engineering, BUET for his support, valuable guidance, profitable discussions and congenial co-operation in the project all through.

The author is very much grateful and expresses his profound gratitude to his former supervisor, Professor Dr. Md. Serajul Islam who got retired from the Dept. of Metallurgical Engineering, BUET, Dhaka, for his valuable suggestions, constant guidance, encouragement and kind help throughout the research work and in writing this thesis.

He expresses his deep sense of appreciation and gratefulness: To Dr. Md. Mohafizul Haque, Professor and Head, Dept. of Metallurgical Engineering, BUET, for his immeasurable and valuable suggestions, encouragement and for providing research facilities, to Dr. Md. Nasrul Haque, Professor, for his valuable co-operation in obtaining the X-ray analysis and relevant suggestions and to Dr. Md. Fakhrul Islam, Assistant Professor, for his encouragement and constant care in completing this work.

Thanks are also due to Mr. Mohammad Zahirul Islam, Librarian and Mr. Mirza Mohd. Rezaul Islam, Assistant Librarian, Central Library, BUET.

The author gratefully acknowledge the help of Mr. Fazlul Haque Bhuian, Senior Foundry Instructor, and of Mr. Yousuf Khan, Sub Assistant Engineer, in carrying out his experiments.

Thanks are also due to: Md. Lutfur Rahman, Senior Crafts Instructor, Babu Binoy Bhushan Shaha, Senior Laboratory Instructor, Md. Ashequr Rahman, Senior Laboratory Assistant, and Feroz Hamid Khan, Laboratory Instructor, Dil Mohammed, Senior Craft Instructor, Md. Shamsul Alam, Craft Instructor, Md. Younus Miah, Head Assistant and Md. Abu Taher, Accounts Assistant and other staff members in the Department for their kind help and co-operation.

## ABSTRACT

An investigation has been undertaken to study the oxidation behaviour of Fe-10Cr alloys containing Aluminium in the range of 2-8% by weight in pure oxygen at 1 atmosphere pressure and the general effects of the additions. The investigations were performed in the temperature range of 950<sup>b</sup>C-1050<sup>d</sup>C under cyclic conditions (3-hour cycles) in each case.

The cyclic oxidation resistance as measured by the specific weight gain values was observed to have progressively improved with increasing aluminium-contents in the alloy. For a particular aluminium-content in the alloy, however, the oxidation resistance decreased with increasing temperatures. The lower aluminium-containing alloys (2-4%Al) were observed to end up with Fe-rich oxide scales under the experimental conditions at all the temperatures, whereas those containing aluminium in the range of 6-8% formed  $\alpha$ -Al<sub>2</sub>O<sub>3</sub> scales. Both the weight of spall released and the size of individual spall particles decreased with increasing aluminium contents. Spall particles released from the lower aluminium-containing alloys were fragmental, blackish and magnetic in nature whereas those from the higher aluminium-containing alloys were powdery, creamy brown and non-magnetic in nature.

Healing layers of Cr<sub>2</sub>O<sub>3</sub> and of Cr<sub>2</sub>O<sub>3</sub>/ $\alpha$ -Al<sub>2</sub>O<sub>3</sub> subscale could be observed under the optical microscope after breakaway of the initial protective scales in the case of the 2% Al and 4% Al alloys

respectively almost at all the temperatures of investigation, but the 6% Al and 8% Al alloys re-formed external  $\alpha$ - $\text{Al}_2\text{O}_3$  scales at all the temperatures. Convolutated growth of  $\alpha$ - $\text{Al}_2\text{O}_3$  scale with limited localized spinel growth could be observed upon these two alloy surfaces.

## CONTENTS

	Page
CHAPTER 1 : INTRODUCTION	1
1.1 General	1
1.2 General Nature of the Problems	4
1.3 Materials	5
1.4 Present Trends	7
1.5 Present state of the Art in Bangladesh	9
CHAPTER 2: A REVIEW OF LITERATURE	11
2.1 Nature and Properties of Iron Oxides	11
2.2 Oxidation of Chromium	13
2.3 Oxidation of Fe-Cr Alloys	17
2.31 Breakaway Oxidation	21
2.32 Healing	26
2.4 Thermal Cycling	31
2.41 Influence of Cycle Frequency	33
2.42 Compositional Changes	36
2.43 Effect of Variables	39
2.5 Spalling of Oxide Scales	39
2.51 Formation of voids at metal-scale interface	40
2.52 Stresses in Growing Oxide Films	43
2.53 Stress Generation due to Thermal Cycling	45
2.54 Other Factors Associated with Oxide Spallation	45
2.6 Effect of Reactive Metal Additions	50



<b>CHAPTER 3:EXPERIMENTAL TECHNIQUES</b>	<b>57</b>
3.1 Materials and Preparation	57
3.2 Apparatus and Oxidation Procedure	58
3.21 Cyclic Oxidation	58
3.3 Examination Techniques	61
<b>CHAPTER 4:RESULTS AND DISCUSSION</b>	<b>64</b>
4.1 Introduction	64
4.2 Results	68
4.21 Fe-10Cr-2Al Alloy	68
4.22 Fe-10Cr-4Al Alloy	76
4.23 Fe-10Cr-6Al Alloy	82
4.24 Fe-10Cr-8Al Alloy	93
4.25 Effect of Aluminium Content	98
4.26 Effect of Temperature	107
4.3 Discussions	107
<b>CHAPTER 5: CONCLUDING REMARKS</b>	<b>129</b>
5.1 Conclusions	129
5.2 Suggestions for future Work	131
<b>REFERENCES</b>	



## CHAPTER 1 : INTRODUCTION

### 1.1 General

The continuously mounting demand for higher power ratings in industry has resulted in a demand for metal components having superior mechanical and chemical properties at higher temperature. Since the efficiency and performance of aircraft gas turbine and similar stationary power plants engines are significantly improved with the use of higher operating temperature, the demand for alloys having strength and resistance to oxidation and corrosion at higher temperature are enthusiastically felt in this field. In such applications, the temperature of the metal components frequently exceeds  $1000^{\circ}\text{C}$  or even  $1100^{\circ}\text{C}$  and furthermore they may be highly stressed. Also the radioactivity (1) build-up around the primary coolant system of nuclear water reactor is one of the important problems from the point of view of the personal exposure. To reduce radioactivity buildup in boiling water reactor (BWR), the injection of some amounts of oxygen into the coolant has been carried out in order to protect corrosion. The suitability of metallic alloys (2) as construction materials in high temperature components is mainly determined by their mechanical properties and their resistance against the service environment. The latter is governed by the ability of the material to form slowly growing protective surface oxide scales on exposure to high temperature. Fe-Cr-Al based alloys with about 5 wt% Al can fulfil this requirement due to the

formation of alumina surface scales by selective oxidation of the aluminium.


The gaseous environment in these engines are highly oxidizing and in many cases, are contaminated with corrosive alkali salts such as the chlorides and sulphates of Na, Ca, and even Hg and Pb. The problem involved, therefore, can broadly be looked upon as a combination of two part processes: (a) Oxidation due to the oxidizing influence of the products of combustion including excess air at high temperature and (b) sulphatization of the component parts due to the influence of some of the alkali salts formed during combustion of the fuel. The damage to metals and alloys by loss of strength at high temperature may be of three general types (3) : (i) by oxidation or exposure to contaminating media with resultant loss of metal; (ii) by incipient surface cracks brought about by cyclic thermal stresses and (iii) by changes in the properties of the metal with increasing temperature with or without attendant phase changes.

Although these phenomena normally proceed together in a practical internal combustion (I.C) engines and are, therefore, bound to influence each other, the present investigation is directly concerned with the phenomenon of oxidation only. Furthermore, due to inherent nature of their use, the conditions obtained in such components are normally of cyclic nature either of a long or short duration, and the major part of the efforts have,

therefore, been directed towards investigation under cyclic conditions.

The basic materials that are used in the constituent parts of such high temperature equipments are generally based on three major alloy systems: the Fe-Cr alloys, the Ni-Cr alloys and the Co-Cr, alloys. Of these, the first group forms the basic materials in the preparation of stainless steels which find wide application amongst others, in the construction of certain component parts in the reactor vessels in atomic power plants, supersonic aircraft, missiles, cracking stills, steam turbines, gas turbines, turbosuperchargers, aircraft power plants, rocket motors, nuclear energy fields etc. Work in the field of this group of alloys including only aluminium does not appear to have been as extensive as in the two other groups of alloys, especially under cyclic conditions.

Chromium is the principal alloying element (3) in many of these alloys, but other elements, such as nickel, aluminium, silicon enhance the properties imparted by chromium. Steels containing 5 percent or more of Cr are of great interest to the engineer because they are more resistant to corrosion and stronger at elevated temperature than the low-alloy steels. Small amounts of reactive alloy additions have been known to produce numerous beneficial effects upon the rate of oxidation, the nature and morphology of the oxides formed and upon the extent of alloy-scale adhesion. Some attempt have , therefore, been made to study the



effect of minor additions of relatively common metal (like Al) to the binary alloys. Successive additions of Al have, therefore, been made to the base alloy, Fe-10% Cr, and the effects studied under cyclic conditions. Quite encouraging results are believed to have been obtained.

## 1.2 General Nature of the Problems

The metallurgical problems associated with the operation of high temperature machines nearly arise from the very high temperatures used for the working fluid, usually gases. Those parts of the machine in contact with the hot gases must, therefore, be made of some suitable materials which will maintain adequate strength at its working temperature, will not oxidize or corrode appreciably at that temperature, will not become brittle and not be seriously subject to the effect of creep.

Early tests were often made to measure the highest stress at which no creep would occur. It gradually became customary to stipulate either that the average rate of creep under the imposed conditions of stress and temperature should be such that the total deformation during the expected life of the component would be within tolerable limits, or that the observed deformation within a given time should not be more than a given amount.

The importance of 'creep' will be apparent from the following data in relation to a well-known British alloy widely used(4) for gas turbine blading : Whereas at 690°C, an indefinite period of

life is expected, an increase of temperature by only 60°C (from 710°C to 770°C) reduces the useful life of the material to less than 1/6 th of its life at 710°C and only by another 20°C (from 770°C to 790°C) reduces it to about 1/30 th of its life at 710°C.

In addition to the above, the hot impinging gases may lead to the oxidation and/or corrosion of the component parts. This will result in a loss of useful material from these parts, which will aggravate the problems of creep and loss of strength at high temperature. The corrosion which thus occurs, is broadly divided into two parts: Oxidation and hot corrosion.

Oxidation occurs due to the contact of the hot oxidizing gases with the metal parts. Detailed discussion of this vital problem concerning the materials under investigation appears in the later chapters. The problems of hot corrosion are essentially those of oxidation, in fact an accelerated form of oxidation resulting in general from the combination of oxidation and reactions with S, Na, V and other contaminants which may be contained in fuels ingested with the inlet air. Due to obvious reasons no further discussion about hot-corrosion may be made.

### 1.3 Materials

The development of modern high temperature materials was inaugurated with the test of alloys intended for the blading of exhaust gas turbines in aircraft engines. It described a range of commercial and experimental austenitic Ni-Cr steels with additions

of W, Mo, V, Ti or Ta together with a range of extremely complex Fe-Ni-Cr-Co-W-Mo alloys with additions of Ti or Ta. With the outbreak of the war, the development of the aircraft gas turbines assumed the character of a race, and the behaviour of the contestants was determined by their circumstances.

In Great Britain, the consciousness of limited resources led to the effort being concentrated upon a few materials to be studied in detail. These were mostly modifications of the already familiar earlier austenitic Ni-Cr alloys (5). Aware of their resources, the Americans started an investigation which grew to be almost a complete survey of the alloys based on Fe, Ni, Cr, and Co with various additions of Mo, W, Nb and Ti. The emphasis on reaching the highest possible working temperature was greater than in Great Britain.

The new alloys were few in number, but they represented in each case the result of a series of experiments, and the excellence of British engines owed something to the confidence with which the full properties of the materials could be employed. The earlier materials were not, of course discarded, but continued to be used where appropriate. Gas turbine rotors at first were made of austenitic steels but it was soon found possible to cool rotors sufficiently to keep the temperature below 550°C and so enable ferritic steels to be used. Cr-Si-Mo and Cr-Mo steels were the first to be chosen, but as engines became powerful, stronger materials were needed. Vanadium was introduced, and a change was

made to the more complex 3% Cr-Mo-W-V steels with which, by a modification of the heat resistant and an adjustment of the C content, a steel capable of maintaining high strength at temperature approaching 600°C could be obtained.

#### 1.4 Present Trends

It has been realized that in high temperature oxidation operations a scale is formed and maintained on the alloy surface which prevents or at least reduces the rate of contact between the reactants and thus offers protection in service.

For the scale to be protective, it is not actually necessary for it to be in intimate contact with the metal, but since the scale has usually very poor mechanical properties (e.g. resistance to shock and abrasion) it must be supported by the metal or alloy for its continued existence over the surface of the component part. For all practical purposes, therefore, a scale that is supposed to be protective must necessarily be adherent as well. A number of alloys, as already discussed, have been developed to possess sufficient strength and high temperature properties; but their usefulness, at present, is limited, besides other factors by their resistance to high temperature oxidation and subsequent spallation of their oxide scale.

Almost all the general-purpose high temperature materials used at present are derived from one or the other of Fe-Cr-Al, Ni-Cr-Al, or Co-Cr-Al alloys. Depending on their composition, these materials



usually develop and maintain either a  $\text{Cr}_2\text{O}_3$  scale, or an  $\alpha$ - $\text{Al}_2\text{O}_3$  scale on their surface for their protective ability. Also Fe-Cr-Al alloys (6) have good oxidation resistance at high temperatures due to the formation of a protective oxide layer of  $\text{Al}_2\text{O}_3$ . A wide range of alloys are now known which will operate satisfactorily under isothermal conditions, but most of these materials lose, either in part or whole, their effectiveness under changing thermal conditions i.e. cyclic conditions. The oxides that are protective (for all practical purposes) at the operating temperature under isothermal conditions, usually spall and the alloy, therefore, loses its protective ability, at least to a certain degree, at the end of a particular operating cycle and more so in subsequent cycles. This usually results, as is well-known, in a more rapid oxidation of the parent material in the subsequent cycles. A material which is resistant under isothermal conditions may not, therefore, be so under cyclic conditions. Primarily, therefore, although superior scale adhesion is certainly desirable but not indispensable under isothermal conditions where the component part is not subject to shock or abrasion, it is absolutely so under cyclic conditions, even when the possibilities for the occurrence of shock or abrasion are apparently absent (due to the spontaneous development of thermal stresses on cooling). Furthermore, even if the material does possess the requisite strength and resistance to creep in service, it will prove to be a failure if it lacks in the requisite degree of oxidation/corrosion resistance, and scale

spallation under cyclic operating conditions will still pose a challenge towards solving this problem. The major part of recent research effort in the field of high temperature oxidation and/or corrosion, therefore, seems to be rightly directed towards tackling the problem of scale adhesion and its stabilization on the surface of the component part.

As already known, certain reactive metal additions decrease the oxidation rate and increase the metal-scale adhesion. As indicated earlier in this chapter, since Fe-base alloys possess some degree of advantage in the field of high temperature operation, efforts are being directed towards more effectively handling this vital problem of metal-scale adhesion with this series of alloys in particular along with the endeavour for the development of newer alloys having improved mechanical properties at elevated temperatures. Admittedly, however, no material having yet been discovered which will carry high stresses continuously at elevated temperatures, particularly under the severe conditions encounterable in modern engines, the successful use of high temperature with available materials is a matter calling for close co-operation between the engineering designers and the metallurgists.

### 1.5 Present State of Art in Bangladesh

Although studies upon the oxidation resistance of binary iron-chromium alloys have been rather plentiful, but sufficient

information about the effects of aluminium additions to these alloys have not been so much available. Data upon the properties of such alloys and their oxidation resistance will be useful in the development and selection of substitute materials for our industries.

The more economical design of machine parts which are used at high temperatures such as air-craft gas turbines, steam engines, stationary power plants etc. need information about the properties such as oxidation resistance at high temperatures. Information about the high temperature performance of the proposed alloys will be helpful in the selection and production of substitute materials for the construction of heat-resistant machine components used in our local industries and this will also serve as a pointer towards their relative effectiveness against high temperature oxidation. Possibility of using locally manufactured substitute materials in the construction of high temperature machine parts will give impetus to our local industries. This may ultimately go to reduce our dependence upon external resources to some extent.

## CHAPTER 2: A REVIEW OF LITERATURE

### 2.1 Nature and Properties of Iron Oxides

Several stable oxides of iron are known to be formed on oxidation of iron, as revealed by Biswas (7): hematite ( $\text{Fe}_2\text{O}_3$ ), magnetite ( $\text{Fe}_3\text{O}_4$ ) and wustite ( $\text{FeO}_{1.05}$ ). Their fields of existence have been studied by Darken and Gurry and some important, salient and relevant information of the three oxides are detailed below:

Ferric oxide (8),  $\text{Fe}_2\text{O}_3$ , is the stable oxide at ordinary temperature. The rust which forms on the surfaces of iron and steel exposed to moist air is a hydrated form of ferric oxide. Pure ferric oxide is reddish in colour.

Hematite contains 30.05% oxygen and at  $1457^\circ\text{C}$  decomposes into magnetite and oxygen ( $P_{\text{O}_2} = 1 \text{ atm}$ ). Hematite occurs in two modifications: (a)  $\alpha\text{-Fe}_2\text{O}_3$ : hexagonal; much more prevalent: (b)  $\gamma\text{-Fe}_2\text{O}_3$ : cubic; forms only under special circumstances below  $400\text{-}500^\circ\text{C}$  (7).

The  $\text{Fe}_2\text{O}_3$  is a metal excess (n-type) semiconductor (9), according to Wagner's concept and the excess cations and an equivalent number of electrons are located on interstitial lattice sites. The observation that electron conductivity decreases with increasing pressure of the negative component (i.e. oxygen) is, thus, an indication of an excess of metal in the semiconductor just like  $\text{ZnO}$ ,  $\text{Al}_2\text{O}_3$ ,  $\text{MgO}$  etc. which are n-type semiconductors.

Magnetite,  $\text{Fe}_3\text{O}_4$  (8) , is formed when either of  $\text{FeO}$  or  $\text{Fe}_2\text{O}_3$  is strongly heated in air and is quite stable at elevated temperatures. The "scale" which forms on the surfaces of heated iron and steel is practically pure  $\text{Fe}_3\text{O}_4$  and , as might be anticipated, this oxide is strongly magnetic. Chemically the magnetic oxide behaves as a mixture of ferrous and ferric oxides.

Magnetite is cubic in structure and possesses a stoichiometric composition. It forms solid solutions with hematite at higher temperatures, the O/Fe ratio becoming more than the stoichiometric. Thus, it becomes deficient in iron ions resulting in the occurrence of iron ion vacancies, i.e. while oxygen atoms occupy fixed positions in the magnetite lattice, some positions in the iron sublattice remain unoccupied by iron ions. Such holes or defects facilitate diffusion of iron ions (or any foreign cations of comparable size) and permit migration through them. In fact the reduction of hematite produces a porous product and the structural metamorphosis from hexagonal to cubic gives rise to volume expansion , increased porosity, cracks and fissures. Magnetite has a very high melting temperature, about  $1597^\circ\text{C}$ . At this temperature it contains 27.64% oxygen (7).

Ferrous oxide,  $\text{FeO}$ , is unstable and in contact with air is rapidly oxidized to ferric oxide. At  $1524^\circ\text{C}$ , oxygen-saturated liquid iron (0.16% O) is in equilibrium with an immiscible liquid phase of ferrous oxide containing 22.6% O. The composition of

wustite saturated with iron corresponds approximately to  $\text{FeO}_{1.05}$  or  $\text{Fe}_{0.95}\text{O}$  (7).

According to Wagner's model (9),  $\text{FeO}$  (wustite) is a p-type (metal-deficit) semiconductors. Yet wustite is deficient in divalent iron ions and in order to maintain electro-neutrality there must be present some ferric ions, the latter increasing with the oxygen content of wustite. The occurrence of iron ion vacancies greatly facilitates diffusion of iron ions through the lattice and influences the reduction rate and product morphology. Thus just like  $\text{NiO}$  and  $\text{CoO}$ ,  $\text{FeO}$  is a metal deficit or an electron-deficit semiconductor.

Kubaschewski and Hopkins (9) reported that iron forms wustite,  $\text{FeO}$ , is normally unstable below  $570^\circ\text{C}$  but on iron oxidized below this temperature formed a thin layer of  $\text{FeO}$  underneath on  $\text{Fe}_3\text{O}_4$  scale. The oxide layers of iron and the position of the various oxides at  $625^\circ\text{C}$  after 24 hours of exposure are indicated in Fig. 2-1.

## 2.2 Oxidation of Chromium

Chromium oxidizes in air or oxygen to form the oxide,  $\text{Cr}_2\text{O}_3$ , which is stable upto a very high temperature. Other oxides,  $\text{CrO}_2$  (rutile) and  $\text{CrO}_3$  (orthorhombic) are also formed, but they are unstable. The volatile oxide,  $\text{CrO}_3$  is formed under very strong oxidizing conditions (9). Although  $\text{Cr}_2\text{O}_3$  has been found to exist in more than one phase, the rhombohedral structure is found in scales

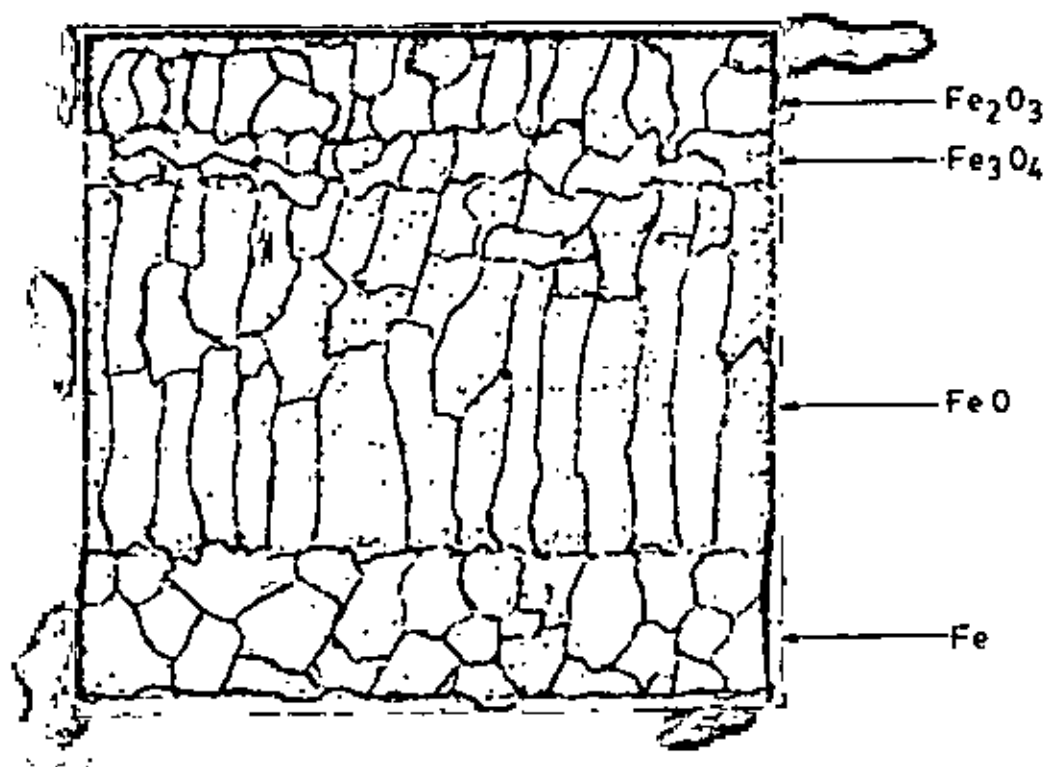


Fig.2-1 : Microsection of scale formed on iron in air at  $625^\circ\text{C}$  after 24 hour, (9).

and films.  $\text{Cr}_2\text{O}_3$  is stable to direct decomposition at temperatures of  $1000^\circ\text{C}$  in high vacuo of the order of  $10^{-6}$  mm Hg and less. At temperatures greater than about  $1100$ – $1200^\circ\text{C}$  vaporization losses from  $\text{Cr}_2\text{O}_3$  in the form of the volatile trioxide,  $\text{CrO}_3$  becomes excessive, and the oxidation of Cr and high Cr superalloys conforms to the so-called "paralinear" kinetics (10).

Gulbransen and Andrew(11) studied in detail the oxidation behaviour of high purity Cr in 76 torr oxygen over the temperature range of  $700^\circ$ – $1100^\circ\text{C}$ . Below  $900^\circ\text{C}$ , they obtained oxidation curves which fitted to the parabolic rate law. Above  $900^\circ\text{C}$  and for a film thickness of approximately  $4800\text{\AA}$ , the rate of oxidation was observed to increase in an unusual manner. This increase in the rate of oxidation disappeared on further oxidation. At a temperature of  $1050^\circ\text{C}$  and higher, a large increase occurred in the rate of oxidation suggesting that the oxide film was no longer protective for film thicknesses greater than  $42000\text{\AA}$ .

At lower temperatures in air ( $500^\circ$ – $700^\circ\text{C}$ ), an adherent green scale of  $\text{Cr}_2\text{O}_3$  was formed, whereas above about  $800^\circ\text{C}$  the scale was a gray black one on the outer surface, which on scraping showed the characteristic green colour of  $\text{Cr}_2\text{O}_3$ . It was suggested that only  $\text{Cr}_2\text{O}_3$  formed at lower temperatures. At  $900^\circ\text{C}$  and above, the black scale formed in air was presumably  $\text{Cr}_2\text{O}_3$  with some quadrivalent N<sub>2</sub> dissolved in it. In fact, X-ray results on the black scale, 260 hours at  $900^\circ\text{C}$  in air, indicated the presence of  $\beta$ - $\text{Cr}_2\text{N}$  along with  $\text{Cr}_2\text{O}_3$  which could conceivably change the defect structure of  $\text{Cr}_2\text{O}_3$ ,



thereby increasing the oxidation rate. As an alternative explanation, they also suggested that extensive cracks occurring in the metal at higher temperatures was responsible for the observed increase in the rate of oxidation (12).

Mortimer and Post (13) has suggested that the oxidation of Cr is remarkably dependent upon the experimental technique. Commencing the experiment by heating in vacuo shows a reduction in subsequent oxidation at 950°C by a factor of three, while heating relatively slowly in oxygen does not alter the rate but hastens the onset of scale cracking.

Seong et al (14), after checking the possibility of vaporization of  $\text{Cr}_2\text{O}_3$  via  $\text{CrO}_3$  (g), concluded that there was little vaporization of  $\text{Cr}_2\text{O}_3$ . It has been known that chromia ( $\text{Cr}_2\text{O}_3$ ) forms a highly volatile  $\text{CrO}_3$  above 900°C. The Cr-content of the scale deposit from total metal weight was compared with the Cr-content of the alloy. The result showed that Cr remained mostly in the deposit. This indicated that there was little vaporization of the chromium oxide in this case.

The addition of Ni to Cr causes a reduction in oxidation rate and a minimum is reached at the solubility limit of Ni-ions in  $\text{Cr}_2\text{O}_3$ . Although  $\text{Cr}_2\text{O}_3$  is generally believed to be a metal-deficit p-type semiconductor and scale-forming reaction proceeds by the diffusion of the cation outward through the scale, changes are evidenced in the oxidation mechanism in presence of certain reactive metals in the form of alloy additions (15).

### 2.3 Oxidation of Fe-Cr Alloys

Oxidation of dilute Fe-Cr alloys has been stated to obey, in general, a parabolic law (6):  $(\Delta W/A)^2 = K_p \cdot t$ , where  $\Delta W$  is the weight of oxygen reacted,  $A$  is the area of the specimen and  $t$  is the time of oxidation. Thus, if the square of the specific weight gain,  $(\Delta W/A)^2$ , be plotted against time,  $t$ , it will generate a straight line, where the slope of the parabolic rate constant,  $K_p$  in proper units. Isothermal oxidation kinetics of Fe-10Cr alloy at  $1000^\circ$  has been represented in Fig.2-2 as observed by Rhys-Jhones et al (16).

Gardiner et al (17) reported that the oxide film formed on iron-chromium alloys less than 5 wt% Cr below 873K consisted of two layers of magnetite and hematite. It has been found by Tjong et al (18) and Tjong (19) that for the Cr addition of 3 wt%, the oxide consisted mainly of iron, and the addition of Cr from 9 up to 18 wt% resulted in the formation of layered oxides, i.e.  $Fe_2O_3$  existed in the outer oxide/gas interface and  $Fe_{2-x}Cr_xO_4$  in the inner region with the predominant chromium oxide next to the substrate.

The scales formed on Fe-28Cr alloy (20) at  $1000^\circ C$  were grey chromium oxide. The alloy substrate beneath the spalled scale was very smooth with deep channels along the original abrasion grooves consistent with little contact between the scale and the alloy at the groove location .

Reichards and White (21) remarks from their quantitative findings relating to the  $M_2O_3 - M_3O_4$  equilibria in Fe-Cr-O system are in agreement with results obtained. Rickett and Wood (22) oxidized

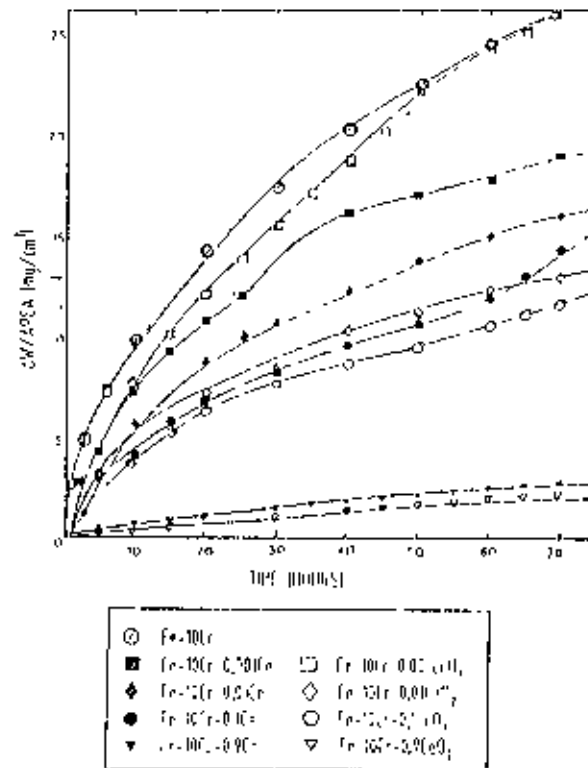


Fig.2-2 : The effects of various amounts of cerium in both metal and oxide form on the high temperature oxidation of Fe-10Cr at 1000°C in 0.1315 bar O<sub>2</sub> ( the % Ce metal is shown for both Ce and CeO<sub>2</sub>), (16).

12-28%Cr-Fe alloys in oxygen at 980°C and 1090°C and found spinel ( $\text{FeCr}_2\text{O}_4$ ) and  $\text{Cr}_2\text{O}_3$  on the inside and  $\text{Fe}_2\text{O}_3$  on the outside of the scale. The nature and number of the layers depended on Cr-content and temperature. McCullough and Fontana (23) found that spinel formed next to the metal on stainless steels heated in oxygen to 980°C, but as the oxidation proceeded  $\text{Fe}_2\text{O}_3$  was predominant in the scale.

Yearian et al (24) illustrated that two kinds of scale can be summarized: type A (low rates of attack) consisting primarily of  $\text{Cr}_2\text{O}_3$  with some dissolved  $\text{Fe}_2\text{O}_3$  and type B scales where attack is severe. In the latter scales, the spinel of the type  $\text{FeCr}_2\text{O}_4$  is predominant. They also added that the types of scale formed are a sensitive function of temperature, Cr-content, atmosphere, time of exposure, impurities present and possibly other factors. It has been established by Wretblad and Arong (25) that  $\text{Fe}_2\text{O}_3$  and  $\text{Cr}_2\text{O}_3$  form a continuous series of solid solutions. In addition Yearian et al (24) and Caplan and Cohen (26) found evidence for some  $\text{Fe}_2\text{O}_3$  dissolved in the  $\text{Cr}_2\text{O}_3$  - type scales. The spinel  $\text{FeCr}_2\text{O}_4$  is not necessarily stoichiometric, but this cubic oxide forms a solid solution series with  $\text{Fe}_3\text{O}_4$ .

From the findings of Seybolt (27), thermodynamically, the scales of lowest oxygen pressure lie closest to the metal and the scale nearest the gas phase must be of the highest dissociation pressure. In a non-equilibrium experiment, if  $\text{Cr}_2\text{O}_3$ ,  $\text{FeCr}_2\text{O}_4$  and  $\text{Fe}_2\text{O}_3$  are all found in the scale, they must be present in the order

listed from metal to gas phase. In this case, one expects an outer layer of nearly pure  $\text{Cr}_2\text{O}_3$ , next a spinel layer, and finally a  $\text{Cr}_2\text{O}_3$  -  $\text{Fe}_2\text{O}_3$  rhombohedral solid solution of variable composition.

Caplan and Cohen found (26) by X-ray diffraction that the lattice parameter of the oxide corresponded to pure  $\text{Cr}_2\text{O}_3$  which signifies an  $\text{Fe}_2\text{O}_3$  content less than 3% during oxidation of Fe-26Cr alloy between  $870^\circ$ - $1200^\circ\text{C}$ . Also chemical analysis revealed the  $\text{Fe}_2\text{O}_3$  content ranged from 0.4-2.5% consistent with the x-ray result. Thermodynamically, a spinel is possible if the surface metal were to become depleted in Cr below 13%.

Rhys-Jones et al (16) postulates that, after 70 hours oxidation, the scale formed on the base of Fe-20Cr material was thick, porous and non-protective with  $\text{Fe}_2\text{O}_3$  and  $\text{Fe}_3\text{O}_4$  being identified by X-ray diffractometry. By contrast, after 70 hours oxidation, the Fe-10Cr alloy had formed a thick, non adherent and non-protective scale with a surface comprising cone-shaped grains. X-ray diffractometer detected  $\text{Fe}_3\text{O}_4$  and  $\text{Fe}_2\text{O}_3$  phases.

Mosely et al (28) illustrated by x-ray diffractometry that Fe-16Cr-5Al alloy heated to  $1200^\circ\text{C}$  in air for 17.5 hours show some evidence of oxidation of the base metal to give an  $\text{M}_2\text{O}_3$  phase but because of the similarity in lattice parameters it is not possible to decide whether M represents Fe, Cr or mixture of the two.

### 2.31 Breakaway Oxidation

The oxidation process can be divided into three stages (6) : oxidation following a parabolic rate law (1st stage), less oxidation following a linear rate law in comparison to that in the 1st stage (2nd stage) and the so called breakaway oxidation (3rd stage).

This phenomenon appears to be quite general and has been observed in many binary alloy systems as well as complex superalloys. Fe-Cr alloys have been known to exhibit a rapid increase in the oxidation rate, typically in the range of 14-25%Cr, following an initial protective induction period during which doped  $\text{Cr}_2\text{O}_3$  scale only is formed (29). To a lesser extent, Ni-Cr alloys show a similar behaviour (30). Wolf and Sandrock (31) while attempting to determine the influence of Si on the oxidation of L-605, a complex Co-base super-alloy, noticed that certain samples of the alloy with low Si or Mn contents showed an excessive rate of oxidation at  $1100^\circ\text{C}$ . They termed this behaviour as "an anomalous weight increment" to mean that these alloys started to oxidize parabolically, but then at some time less than 20 hours, the rate increased abruptly by more than 100 times. After a period of less than an hour, the rate once again slowed down to approximately the initial rate. It was possible to reproduce the results only qualitatively. Identical compositions would differ in the time of the increase by a factor of ten. Thus it is fairly common for an alloy to oxidize protectively for a period, then to exhibit one or

more stages of accelerated oxidation. Sometimes the first breach of protective oxide spreads, to degenerate completely, into a linear rate of growth.

The mechanism involved in this type of oxidation behaviour, has been discussed in detail by Wood and Whittle (32). Briefly this involves a loss of contact between the initial  $\text{Cr}_2\text{O}_3$  scale and the underlying alloy due to stresses developed in the system and vacancy coalescence at the alloy-oxide interface producing ballooning often above grain boundaries and specimen corners. This can happen isothermally, but is more prevalent on cooling or cycling, due to differential contraction effects. The lifted oxide eventually cracks and is completely removed, exposing the underlying depleted alloy, to the full severity of the oxidizing atmosphere resulting in rapid oxidation rate. Stratified scale formation takes place and parabolic oxidation is eventually established. Fig. 2-3 represents the model proposed by Lowell et al (33) for this type of oxidation.

An alternative mechanism (34) for breakaway oxidation is based on "Chemical" or "diffusional" phenomenon. This postulates that the initially formed  $\text{Cr}_2\text{O}_3$  type layer is transformed from within by iron from the depleted alloy. Transformation to  $\text{Cr}_2\text{O}_3\text{-Fe}_2\text{O}_3$  solid solution and finally  $\text{FeFe}_{1-x}\text{Cr}_x\text{O}_4$  spinel occurs, enabling the rapid outward diffusion of  $\text{Fe}^{2+}$  ions to form  $\text{Fe}_3\text{O}_4$  and  $\text{Fe}_2\text{O}_3$  layers.

But the validity of the chemical breakaway mechanism seems to have been seriously challenged by the dramatic suddenness of the

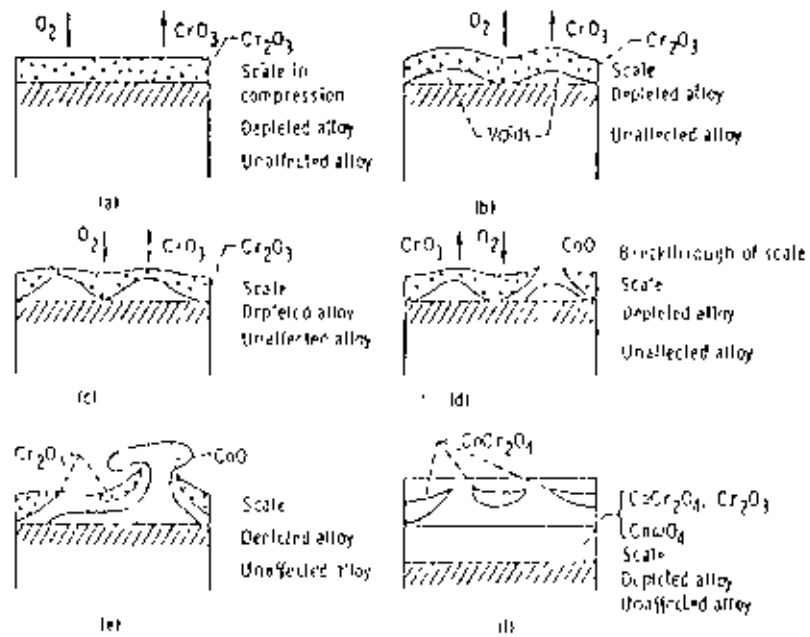


Fig.2-3 : Model to illustrate the oxidation mechanism of higher chromium Co-Cr alloys, (33).



onset of rapid oxidation, together with the observance of only protective  $\text{Cr}_2\text{O}_3$  immediately before breakaway. Such a situation was actually observed by Islam (35) in his work with binary Co-25Cr alloy at  $1100^\circ\text{C}$  after 1 hour of exposure as shown in Fig.2-4.. where he actually observed grains of CoO breaking out through an window formed by partial spallation of the external  $\text{Cr}_2\text{O}_3$  scale. No  $\text{CoCr}_2\text{O}_4$  spinel formation could be observed underneath the  $\text{Cr}_2\text{O}_3$  scale in the region of breakaway, as suggested by the chemical mechanism of breakaway.

Breakaway is likeliest in some respects when the alloy surface  $\text{Cr}$  concentration is low (i.e. in the early stages of oxidation), but it lasts longer when the depletion has penetrated deeply, because healing is then more difficult. Potentially, breakaway could be severed with Ni-Cr alloys because the interface Cr depletion is greater than for Fe-Cr alloys (due to the lower alloy interdiffusion coefficient), but isothermal breakaway is much more rare (29). The irregular and interlocked alloy-oxide interface, at least partly caused by the relatively low alloy interdiffusion coefficient, promotes adhesion both isothermally (29) and presumably under cyclic conditions as well. Whereas Ni-20Cr alloy shows little spalling and scale re-formation on cycling, Fe-28Cr alloy cycled for a number of periods at  $1000^\circ\text{C}$  shows areas with one, two, three, four or five doped  $\text{Cr}_2\text{O}_3$  layers (36) depending on the number of times scale failure occurred and re-formation took place in a certain location. With Fe-14Cr alloy, cycling favours

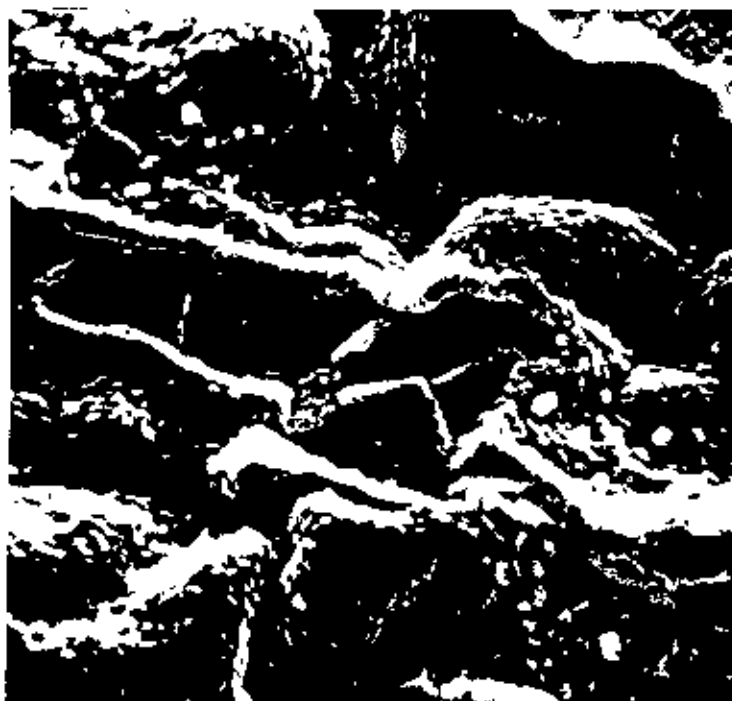


Fig.2-4 : Scanning electron micrograph of the oxide scale on a Co-25Cr alloy specimen exposed for 1 hour at 1100<sup>0</sup>C representing the occurrence of a typical breakthrough phenomenon in a Cr<sub>2</sub>O<sub>3</sub> scale. In the center, exposed CoO grains can be seen breaking out through the external scale, while lifting of the Cr<sub>2</sub>O<sub>3</sub> scale by CoO grains underneath is apparent in the surrounding regions, x 4200 (35).

breakdown of the initial doped  $\text{Cr}_2\text{O}_3$  layer, but subsequent failure and progressive layering is rare as the scale is relatively adherent.  $\text{Al}_2\text{O}_3$  scales on Fe-Cr-Al alloys (37) exhibit breakaway behaviour of essentially the same nature, Fig.2-5.

### 2.32 Healing

If the composition of the alloy is such that there is insufficient concentration of the protective component to form a new protective external scale layer (which is the case with alloys showing breakaway behaviour), then the protective oxide will still be formed at the surface of the alloy, but this will take the form of a discontinuous precipitate rather than a continuous layer. Simultaneous oxidation of the less protective component will also take place in such cases resulting in a faster oxidation rate. Oxygen diffusion and dissolution into the alloy will now take place, as the effective oxygen pressure behind the less protective scale is much higher. This process of oxygen diffusion and dissolution will result in the internal oxidation of the preferentially oxidizing component in regions of its higher local concentration leading to the formation of discrete particles which may eventually form a coherent layer by coalescence, a so called "healing layer" underneath the stratified scale layer, preventing or reducing further oxidation. It is interesting to note that although a doped  $\text{Cr}_2\text{O}_3$  scale layer is more readily established on Fe-Cr alloys than on comparable Ni-Cr alloys (29) because of the

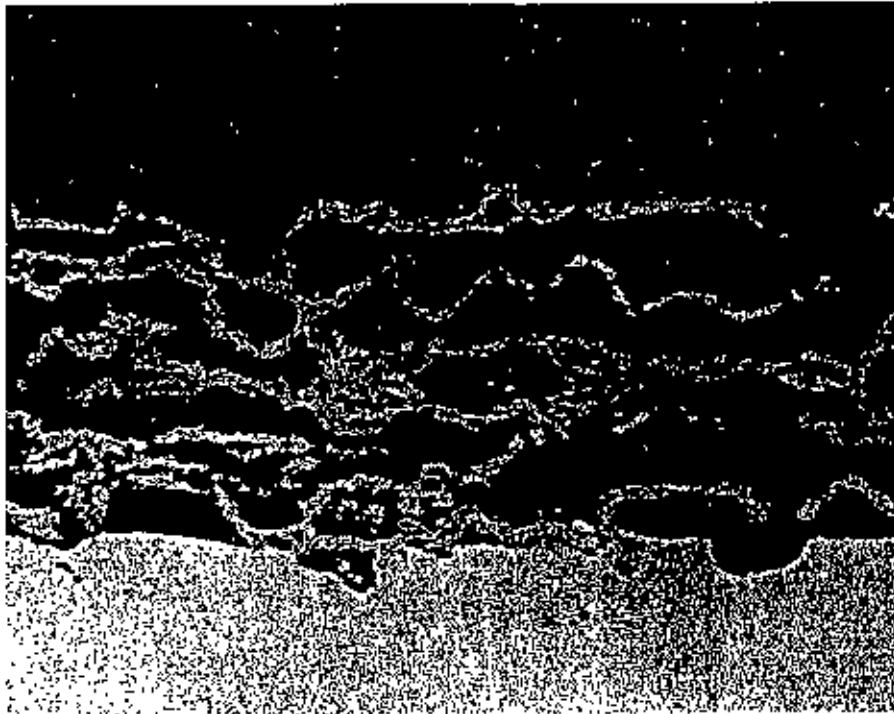


Fig.2-5 : Typical multiple breakaway of oxide scale on an Fe-14Cr-4Al alloy exposed for 7 6-hour cycles at 1200<sup>0</sup>C, (37).

greater alloy interdiffusion coefficient, it is less difficult to heal a stratified non-protective scale on Ni-Cr alloys because the Ni-rich oxides grow slower than the Fe-rich oxides thereby giving less scale encroachment on the alloy and absorption of the coalescing internal oxide. Additionally, the oxygen solution characteristics in the Ni-Cr alloys are more favourable to the formation of a dense-linking internal oxide layer.

Because the intrinsic diffusion coefficient for Cr is higher than that for the solvent component in alloys of Fe-Cr, Ni-Cr and Co-Cr, some fraction of the interstitials supporting scale growth on these alloys results in vacancy insertion at the alloy/scale interface and these vacancies are annihilated at dislocation sinks within the diffusion zone of the alloy. Interstitial cation creation or vacancy annihilation by this mechanism introduces elastic tensile stresses in the metal by changing the spacing or misfit dislocations at the interface. If this interfacial mechanism would be blocked somehow scale growth by cation diffusion could not continue, the associated growth stresses would be avoided and an alternative growth mechanism (anion diffusion) would become operative (38).

Wei and Stott (20) observed the development of  $\text{Cr}_2\text{O}_3$  scales on Fe-Cr alloys. Although the growth rates of iron oxides are much faster than that of  $\text{Cr}_2\text{O}_3$ , a continuous healing layer of  $\text{Cr}_2\text{O}_3$  is established rapidly by selective oxidation at the base of the transient oxides. Very little iron has been detected at the

surface of the scale indicating that this process occurs rapidly for this alloy.

As the healing layer thickens, it loses contact with the alloy surface and develops a convoluted configuration, as shown schematically in Fig.2-6. There have been many reports of voids beneath  $\text{Cr}_2\text{O}_3$  scales on iron base alloys and these features may result from vacancy condensation effects or the scale growth process. One suggestion is that growth of the  $\text{Cr}_2\text{O}_3$  layer involves outward transport of  $\text{Cr}^{3+}$  ions through the oxide and inward transport of oxygen along the grain boundaries. Formation of new oxide in the oxide grain boundaries causes generation of compressive stresses due to volume expansion and wrinkling of the scales by plastic deformation. The large stresses generated cause the scales to become convoluted or cracked during oxidation at high oxygen pressures, but to deform plastically at low pressures (20):

For a given oxide scale, Huntz and Schutze (39) summarized that the growth mechanism depends on the temperature, the nature of the substrate, the incorporated impurities etc and is not always clearly defined. It can be noted the following: For  $\text{Cr}_2\text{O}_3$ , most of the results suggested that scale growth is promoted by cationic diffusion, unless the substrate is doped with active elements. Then the growth direction is reserved. But recent results on 'undoped' chromia scales indicate that the situation is not so clear: oxygen and chromium diffusion coefficients are of the same order of

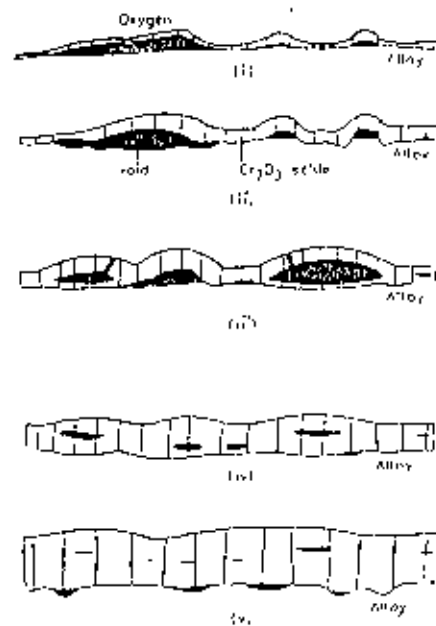


Fig.2-6 : Schematic representation of the progressive growth of a  $\text{Cr}_2\text{O}_3$  scale on Fe-28Cr at  $1000^\circ\text{C}$  (any transient iron-containing oxides are neglected), (20).

magnitude and oxygen can even diffuse faster than chromium as in massive oxide.

#### 2.4 Thermal Cycling

Most industrial processes involve use of superalloys at high temperature under oxidizing conditions in which the operation is of a cyclic nature. The cycles may vary from several hours (aircraft engines) to hundreds or even thousands of hours (ground power station turbines). It is essentially the cyclic nature of the operation, and not the duration of the individual cycles that often makes the difference causing loss of material in the form of oxide spallation. The sequence of events in such operations can be enumerated as follows:

- (a) During the initial heating period, oxidation takes place forming a protective scale at a more or less constant temperature. The growth of such an oxide scale is essentially parabolic, since either or both the reacting components must diffuse through the thickening scale. For most commercial heat-resisting superalloys, this growth rate should be sufficiently slow in order that metal loss under isothermal oxidation is negligible.
- (b) When the material cools down at the end of the heating cycle, part or all of the oxide scale formed spalls off as a result of thermal stresses generated.



- (c) When the material is reheated for the next cycle, it is now effectively less protective due to partial or complete spallation, the oxide being effectively thinner or locally absent on the material. Furthermore, the alloy has been more or less depleted of the protective component as a result of oxide formation and/or spallation.
- (d) Due to repeated cycling, the process of oxide formation and spallation also repeats. The alloy by now, might have been so much depleted of the protective component that it may fail to re-produce the protective scale and thus lose its protective nature altogether.
- (e) With continued cycling, therefore, other oxides form (and these form at much higher rates) resulting in a rapid oxidation and such, in metal losses, at a much higher rate.

Oxidation under such thermal cycling conditions, promote spallation of the protective oxide scale that may initially form on an alloy surface. The exposed alloy surface then oxidizes in a manner depending on its composition now different from that of the original alloy. Consequently, formation of a different less protective oxide on the surface may take place, leading to catastrophic scaling. Thus in systems where the initially formed protective oxide is susceptible to spalling, the alloy composition at the alloy-oxide interface during selective oxidation is of vital importance in determining the oxidation behavior in subsequent stages.

#### 2.41 Influence of Cycle Frequency

Whittle (40) has pointed out that when the specimen is being thermally cycled, repeated spalling of the protective oxide becomes a distinct possibility with many alloy systems. The concentration of the protective component B at the interface is, therefore, of paramount importance in such cases. Sufficient time must elapse between successive losses of oxides in order for the concentration of B at the alloy-oxide interface to return to the value it had before the loss of the first oxide. If the alloy interdiffusion coefficient is high (as is the case with B.C.C. Fe-Cr alloy compared to F.C.C. Ni-Cr and Co-Cr alloys), the limiting concentration of a B at the alloy-oxide interface is quickly restored, and second protective layer can be quickly formed, provided the concentration of B in the bulk alloy is sufficient for the re-formation of the protective scale. If a loss of the protective scale again occurs during the next cycle, the sequence is repeated if the conditions continue to be favourable. This is illustrated in Fig. 2-7. On the other hand, due to repeated thermal cycling and loss of oxide scale as a result, the alloy may be so much depleted of the protective component that it fails to reproduce the protective scale and thus lose its protective nature altogether. This results in the oxidation of the other metal components in the alloy which oxidize much faster as a rule, causing metal losses at a much higher rate.

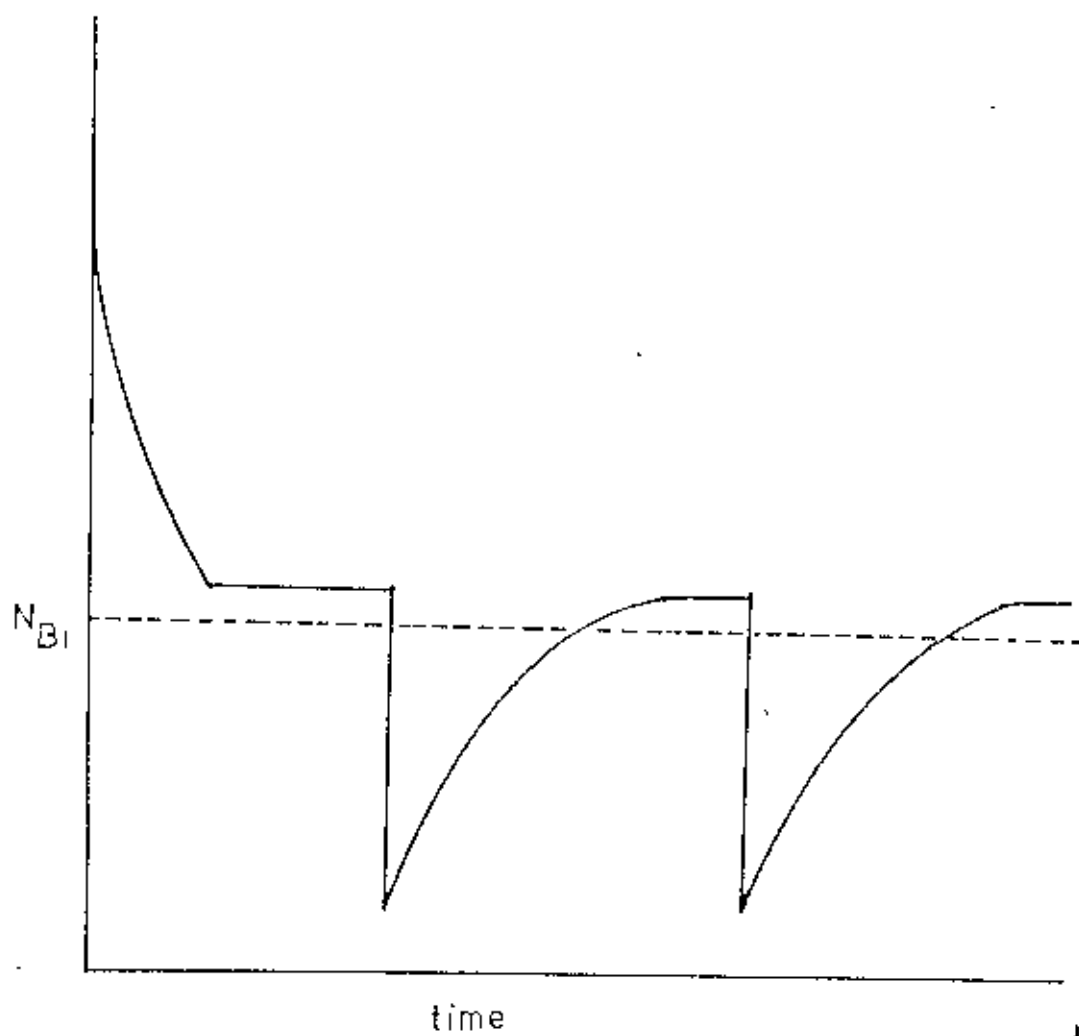


Fig.2-7 : Schematic variation of interface chromium content with time due to spallation, (40).

The variation of the interface composition with time after the second layer of protective oxide formation is then important as the subsequent mode of oxidation will depend on the surface composition at the time immediately after spalling has taken place. A third layer of protective oxide would, or would not be formed, depending on whether the interfacial concentration of B were above or below the limiting concentration for the formation of protective oxide. This limiting mole fraction  $N_{Bi}$  is indicated by the horizontal dashed line in the figure. During the time interval when the curve representing the interfacial composition of B lies below this horizontal line, a protective oxide layer would not be formed forthwith. Thus to a first approximation, it may be said that if the spalling frequency is greater than this time interval, continued protection against high temperature oxidation is unlikely. On the other hand, there are alloys containing higher mole fractions of B in the bulk alloy, for which the interfacial concentration does not fall below that necessary for re-establishment of a protective layer. The concentration of B at the metal-oxide interface may be considered to be maintained above the dashed line in the above figure at all times for all practical purposes. Thus with these alloys, unless the frequency of thermal cycling and consequently that of spalling is exceptionally rapid, continued formation and maintenance of the protective oxide would be expected.

Fe-Cr alloys containing over 30% Cr form multiple protective oxide layers (36, 37). Fe-Cr alloys containing 12-20%Cr and Ni-Cr alloys containing 18-30% Cr form a protective layer at first, but suffer rapid spalling because a new protective layer is not immediately formed again, (30). Fe-Cr alloys having less than 18%Cr do not generally form a second protective oxide layer.

It should be mentioned here that with alloys containing sufficient concentration of the easily oxidizable element B to form the protective oxide  $BO$ , this oxide may not form immediately on exposure of the alloy to the oxidizing environment. The re-formation of the second layer of protective scale is often preceded by a non-steady state period when both the elements A and B enter the oxide scale. But this non-steady state period is usually of short duration (41) and the protective scale is eventually established in a very short period of time.

#### 2.42 Compositional Changes

Compositional changes taking place in the underlying alloy during protective oxidation (during an individual cycle under cyclic oxidation conditions) have been discussed in detail by Whittle et al (42) and by Whittle (40).

It is shown for a  $Cr_2O_3$ -forming Fe-Cr alloy that during an infinitesimally short time at the start of oxidation, formation of  $Cr_2O_3$  would cause the Cr concentration at the surface of the alloy to drop virtually to zero. However, the chromium concentration soon

risers and continues to increase, approaching a constant value A. This will necessarily mean that Cr from within the bulk alloy diffuses towards the interface producing a Cr depletion zone AB with varying Cr concentration. This is schematically shown in Fig. 2-8, in which C represents the bulk alloy chromium concentration at the start of the cycle (i.e. the initial bulk alloy Cr concentration). Evidently, the depth of the Cr-depleted zone increases with time of oxidation, the concentration gradient becoming less steep. At corresponding times, the depth of depletion measured from the original alloy surface is dependent only upon the alloy interdiffusion coefficient. Considering that the oxidizing specimen is in the form of a slab so that only one-dimensional diffusion is involved and as such will be symmetrical about the middle plane of the slab, concentration profile for Cr in the alloy at an initial stage can be represented by ABCCBA in Fig. 2-9. At a later stage, the zone of depletion will be widened, curves OB, due to continued oxidation/spallation. At some time in course of the oxidation, the depletion zone will be wide enough so that the corresponding concentration profiles OC-OC will come together at the middle plane of the specimen. Further oxidation will produce Cr depletion to an extent such that the Cr concentration at the center will fall below that of the original bulk concentration, and as a result will even change the Cr concentration at the metal-oxide interface to a lower value, curve POP, and thus the surface scale will become thermodynamically unstable, leading to what is known as

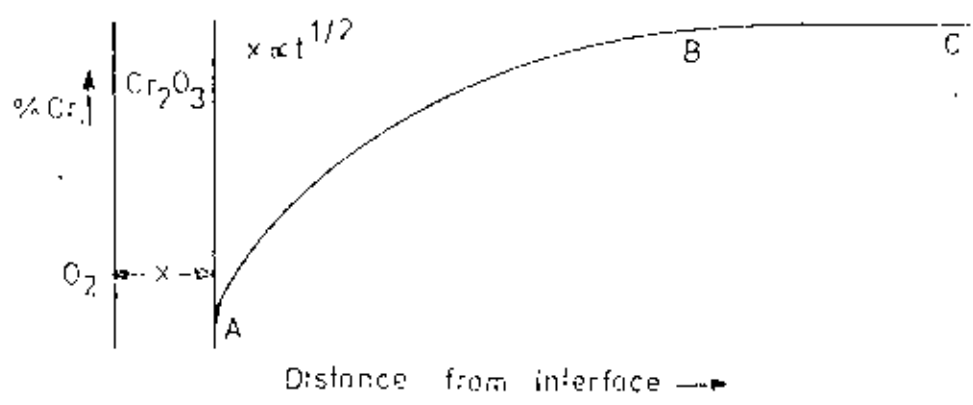


Fig. 2-8 · Schematic representation of alloy Cr-depletion, (42)

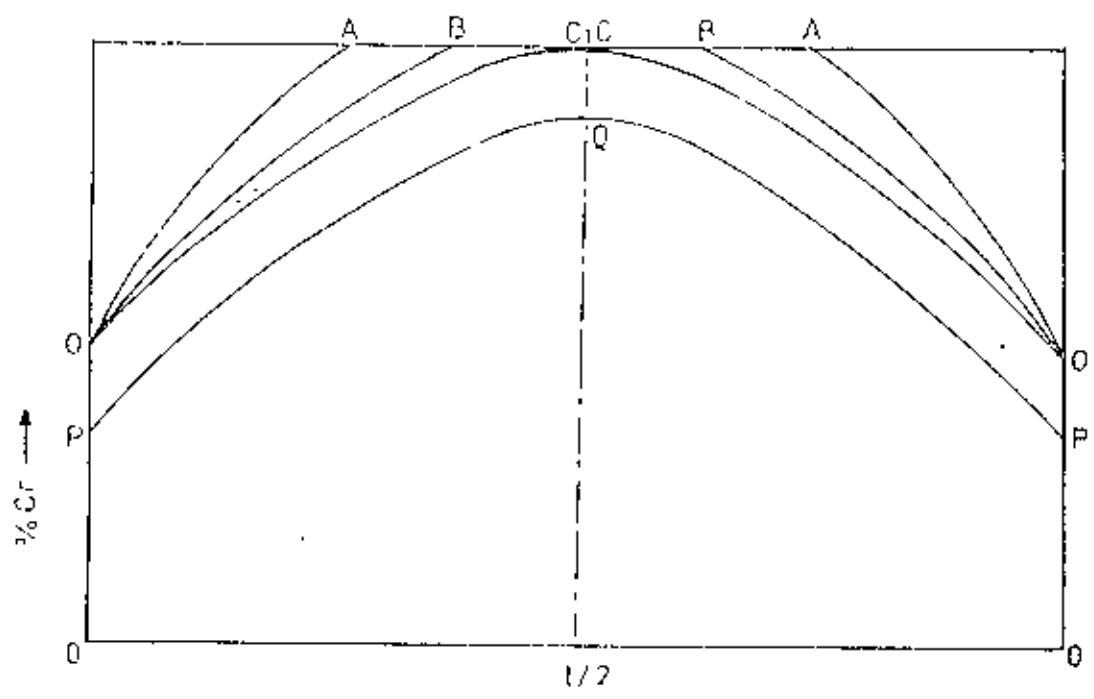


Fig. 2-9 · Schematic variation of alloy Cr-content with time, (42)

a "chemical breakthrough". The time at which this chemical breakthrough occurs corresponds to the time at which the Cr concentration at the alloy-oxide interface falls below that for the thermodynamic equilibrium of  $\text{Cr}_2\text{O}_3$  in contact with the alloy. Practically, this limiting concentration may be taken as zero, as  $\text{Cr}_2\text{O}_3$  is thermodynamically very stable.

#### 2.43 Effect of Variables

The effect of increasing the maximum temperature was found to result in an increased rate of attack with an earlier initiation of spallation (43). Failure of protective scale occurred with increase of temperature resulting in an increase in the oxidation rate. Increasing the peak temperature also meant increased rates of Cr-volatilization from the  $\text{Cr}_2\text{O}_3$  scales hastening their failure, or resulting in a parabolic type of oxidation.

#### 2.5 Spalling of Oxide Scales

Hou and Stringer (44) observed, while attempting to determine the influence of thermal cycling on spallation, that the protection of high temperature alloys against oxidation is provided by the formation of slow-growing oxide films which often contain  $\text{Al}_2\text{O}_3$  and/or  $\text{Cr}_2\text{O}_3$ . One major factor inhibiting the protection is the tendency of the oxides to break away from the metal surface or spall, under thermal cycling conditions. The degree of spallation depends on many factors: the specific oxide growth mechanism, the stresses in



the oxide-metal system, the ability of the system to relieve such stresses, and the fracture resistance of the oxide, the metal and the scale/metal interface.

Oxidation resistance of an alloy at high temperature depends on the production and maintenance of a protective oxide film upon the alloy. To offer continued protection, this film must be adherent and have a low or negligible growth rate in the environment. The utility of such a protective scale exists only as long as the film remains in tact and can provide a barrier between the reactants. Unfortunately, this is the exception rather than the rule and most of the protective scales formed would spall off either at temperature, or on cooling, for one reason or another. Progress in the science of oxidation requires an understanding of the causes of such failure of the protective oxide scales (35).

Two main causes are believed to act independently to bring about the failure of protective oxide scales. These are: (a) formation of interfacial voids which results in progressive loss of scale-metal contact, eventually ending up in a failure of the scale, and (b) stresses developing in the growing oxide and upon cooling, which again lead to lifting and cracking of the scale (35).

#### 2.51 Formation of Voids at Metal-Scale Interface

When metal atom is transferred from the metal to the oxide, one of the two things happen: either oxide formation occurs at the

gas-scale interface, or it occurs at the metal-scale interface. In the former case, the metal ion must bodily move across the scale layer to the outer surface and a vacancy is thus created as a result of the cation migration. If no mechanism is available to fill up this vacancy, void formation will occur at the scale-metal interface as a result of coalescence of such vacancies and adherence will eventually be lost. In the latter instance, when oxide formation takes place at the metal-scale interface, the oxide molecule will fill up the space left by the metal atom and in this case a mechanism should again be operative to accommodate this volume change (as in many cases, the volume of the oxide formed is more than the metal from which it formed).

Such a situation was actually observed by Islam (35) in his work with binary Co-25Cr alloy at 1100°C after exposure for 112 hours as shown in Fig. 2-10 where he found considerable voids on the substrate surface. This alloy showed initially breakaway behaviour for which spallation of initial protective scale on thermal cycling took place and considerable depletion of Cr behind the Cr<sub>2</sub>O<sub>3</sub> subscale was also apparent. It is believable that some more alloy Cr depletion was yet to take place on continued thermal cycling to induce a higher degree of plasticity in the substrate alloy to bring about a further reduction in the number of voids by plastic flow.

Formation of voids at metal-scale interface has been reported in the oxidation of a range of iron-chromium alloys (45) resulting

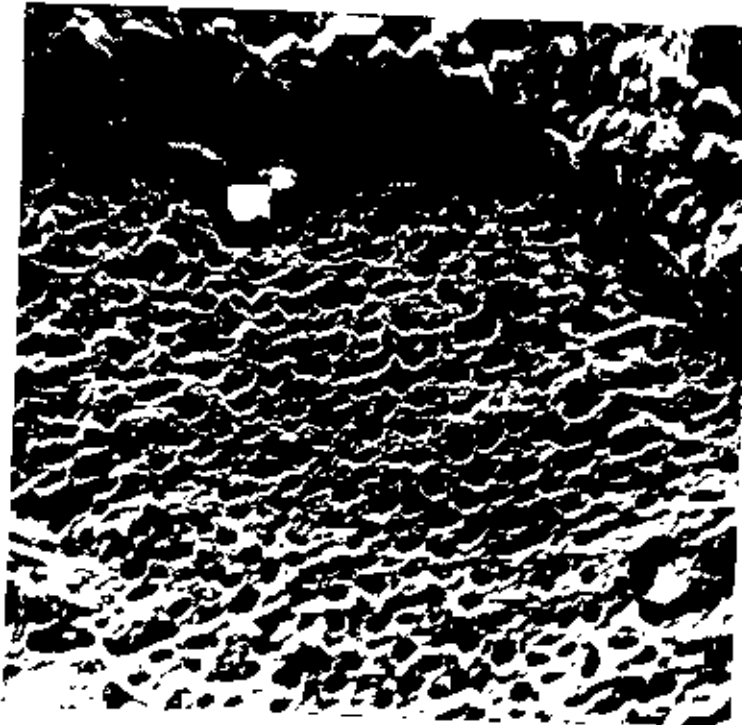


Fig.2-10 : Scanning electron micrograph of Co-28Cr alloy showing the substrate surface appearance after oxidation for 12 hours (isothermal) at  $1100^{\circ}\text{C}$ ,  $\times 1000$ . The extent of void formation is significant, (35).

in loss of contact in the regions of void formation and a negative deviation in oxidation rate. Such void formation is also known to take place during the oxidation of Fe-Cr-Al alloy (46).

## 2.52 Stresses in Growing Oxide Films

The factors involved in the generation and relief of stresses in growing oxide films have been discussed in detail by Stringer (47). He points out the origin of the stresses and the mechanisms of relief of such stresses. While it is not intended to go into any details, these factors may be outlined as follows:

(a) Volume change considerations based on the Pilling Bedworth model:

This suggests that if the ratio, Volume of oxide/Volume of equivalent amount of metal exceeded unity, then the oxide will grow under compression and will be protective, but if this ratio was less than unity, the film will be non-protective due to crack formation as a result of tensile forces developed in the film (48). But it has been pointed out that this model is clearly an oversimplification since oxides with volume ratios less than unity have been known to be protective in some cases. Similarly oxides formed on some metals having volume ratios exceeding unity and supposed to be protective according to this model are known to be non-protective.

(b) Growth of Oxide within the Oxide Layer:

If the oxide film cracks after a certain time due to developing stresses, it would allow oxygen in and lead to the formation of new oxides within the existing oxide body leading to the generation of compressive stresses. Tylecote (49) has discussed the suggestion originally put forward by Czerski and Franik that the oxidation of 99.8% Ni at 1300°C proceed mainly by oxygen penetration along grain boundaries and only 30% of the oxide formed by cation diffusion outwards. Rhines and Wolf also qualitatively share this same view (50). They demonstrated the evidence for the presence of compressive stresses of the order of about 1500 lbs./in<sup>2</sup> within the scale layer during the oxidation of 99.95% purity nickel at a temperature of 1000°C. They report that this stress was over and above those due to differential thermal contraction. In a recent study, Golightly et al (51) have suggested this whereas the major reason for oxide spallation on an Fe-27Cr-4Al alloy on cooling from 1200°C was believed to be the result of highly convoluted oxide growth, this configuration itself was due to the formation of new oxide within the existing oxide layer following reaction between oxygen diffusing down through oxide grain boundaries and Al diffusing outward through the bulk oxide.

### 2.53 Stress Generation due to Thermal Cycling

Thermal stresses produced due to large temperature variations as in cyclic oxidations, is the largest single contributing factor towards oxide scale spallation. The thermal expansion coefficients of oxides are usually smaller than those of the metals from which they form. Changes of temperature, therefore, result in the generation of compressive stresses within the oxide scale via differential contraction of the oxide and the metal (33). These thermal stresses could be sufficient to cause scale failure and hence an increased subsequent oxidation rate.

Evidence for oxide growth stresses was also shown by the shape of the alloy specimen after long periods of exposure, with the alloy having been pushed out at the edges. This is evident from Fig.2-11 (20).

### 2.54 Other Factors Associated with Oxide Spallation

#### (a) Metal-Scale Interface Configuration:

Examination of the metal-oxide interface of different systems of metals and oxides show pronounced difference. In some cases, this surface remains fairly smooth even after a thick oxide film has built up, while in others, the interface is uneven and shows some penetrations along grain boundaries. This latter phenomenon is said to be responsible for the good adherence of  $\text{Cr}_2\text{O}_3$  scales on Ni-Cr alloys. This is evident from Fig.2-12 (52). A flat interface,

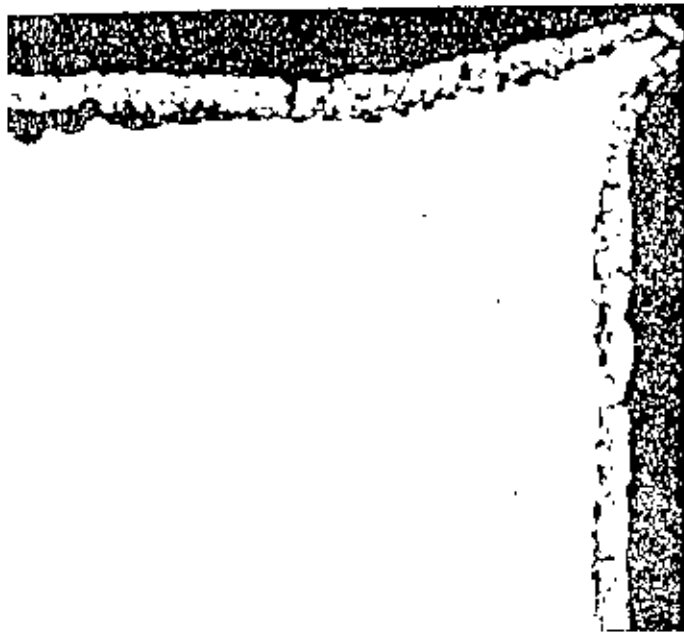


Fig.2-11 : Photomicrograph of oxide scale on Fe-28Cr alloy after oxidation for 1000 hours in oxygen at  $1000^{\circ}\text{C}$ , showing lateral growth of oxide at the specimen corner, (20).



Fig.2-12 : Oxide scale on Ni-40Cr alloy oxidized for 25 hours at 1200°C in 1. atmosphere oxygen, x 1500 approximate, representing some penetrations along the grain boundaries, (52).



on the other hand, is often considered to be favourable for non-adherence and exfoliation of oxide scales. A study of the effect of scale-metal interface configuration upon spallation, however, did not reveal any conclusive evidence to this effect (53).

**(b) Scale-Metal Plasticity:**

If the stresses generated in the growing oxide scale can be relieved in any form, either by deformation of the scale itself or the alloy substrate in contact, then spalling is avoided. The subject of high-temperature process for stress relief has been reviewed by Stringer (47). The question of scale plasticity would be meaningless if no stress existed in the film either at temperature (of oxidation) or upon subsequent cooling. For those systems where scale formation takes place primarily by anion diffusion and the newly-formed oxide is confined, compressive stresses sufficient to deform or even fracture the scale will be generated if there is an increase in volume on oxide formation. On the other hand, where the reaction occurs by cation diffusion, it is possible that no stresses will result from this source, even for adherent oxides with very large oxide/metal volume ratio. Moreover, in such cases the large number of vacancies lead to the formation of macroscopic porosities as a result of vacancy condensation and growth. If a growing porous oxide can withstand the stresses without fracturing, enhanced creep will take place resulting in the

collapse of vacancies by plastic deformation, and thus reduce the spalling tendency.

However, if considered in isolation, thermal expansion data can be misleading as pointed out by Tedmon (10). While investigating into the oxidation behaviour of a series of Fe-Cr alloys, he found that the deterioration in scale adhesion with increasing Cr-content could not be correlated with the thermal expansion coefficients of the alloys.

**(c) Effect of Purity:**

Small amounts of preferentially oxidizable impurities appear to accumulate at the metal-oxide interface and tend to increase the stresses at the point.

It is well-known that the lower layers of oxide films tend to have a fine grain size while the upper layers are coarser. This seems to be due to the accumulation of easily oxidizable impurities inhibiting grain growth. In the outer layers of the film where the purity is greater, large grains form, although in some cases intergranular films rich in impurity elements can be seen to be present in these layers (35).

For alumina scales, the impurity accumulation at the scale/alloy interface is believed to be the major cause for scale failure. For chromia scales, the dominated effect appeared to be the interfacial morphology which resulted from the oxidation

process, whereas impurity accumulation at the interface is only a secondary effect (44).

## 2.6 Effect of Reactive Metal Additions

It has been known for many years that small additions of reactive metals such as Th, Al, Y, Ce, Ca, Mg, Ti, V etc. improve oxidation resistance of high temperature alloys. Prominent amongst the benefits derived through such additions were:

Firstly, these additions visibly improved the casting quality by reducing the formation of voids, gas cavities etc., and

Secondly, the resultant metal possessed higher strength and better heat-resisting properties as a result of its inherent: fine-grained structure.

Two principal factors may be considered to be responsible for the observed beneficial effects of these reactive metal additions as reported by Islam (35) and others in their works. First, the effective partial pressure of oxygen behind the less protective  $Fe_2O_3/Fe_3O_4$  scale is much lower than the atmospheric and hence preferential oxidation of Al or Cr will tend to occur in case of 2% and 4% Al alloys. The new element, by virtue of its higher reactivity, enables the protective element being available at the interface region without being oxidized in the interior of the alloy. They, therefore, migrate freely to the interface region forming stable internal oxide particles ultimately coalescing into

an effective protective barrier at the base of any initially formed stratified scale.

The second reason for the observed beneficial effects of Al additions in the range of 2-4% follows as a corollary to the above phenomenon. It has been well known that these oxide particles form a zone or network of internal oxide particles close to the interface region and act as effective sinks for the incoming vacancies, thereby largely eliminating formation of voids at the interface. A better scale-metal contact is thus maintained resulting in improved scale-metal adhesion.

Fe-Cr-Al-based alloys (2) with about 5 at% Al can fulfil to form slowly growing protective surface oxide scales on exposure to high temperature due to the formation of alumina surface scales by selective oxidation of Aluminium.

Wang et al (54) discussed about the formation of protective oxide scale on high heat resistant alloys by reactive metal addition like Aluminium etc. They stated that high temperature alloys exhibit their oxidation resistance by forming a thin oxide scale on the surface. This oxide scale should remain adherent to the alloy during both isothermal and thermal cycling exposures, which is considered to be prerequisite to a protective oxide scale.

Recent investigations have further elaborated the effects of such alloy additions. It has been proposed that the effects of reactive metals is essentially the same as that of the dispersed

stable oxides, and that in fact the reactive metals oxidize internally ahead of the oxidation front.

For  $\text{Al}_2\text{O}_3$  at high temperatures (1000-1300°C) most results indicate growth controlled by anionic diffusion but this is not a general rule and impurities can have an important effect. At low temperatures (800-900°C) cationic diffusion seems predominant (39).

The oxide phases formed on Ni-Cr-Al alloys during oxidation at high temperature were investigated by Brumm and Grabke (55) who stated that on the oxide free metal surface oxides are formed of each alloying element for which the oxide formation pressure is exceeded. So oxide nuclei of NiO,  $\text{Cr}_2\text{O}_3$  and  $\text{Al}_2\text{O}_3$  are to be expected on the surface in the initial stage. After a closed oxide layer has formed, the oxygen partial pressure at the metal-oxide interface decreases to the formation pressure of  $\text{Al}_2\text{O}_3$  which is the lowest one. At this phase boundary the other oxides are no longer stable and are undergrown by  $\text{Al}_2\text{O}_3$ . The other oxides are only stable at the oxide-gas interface. NiO reacts with  $\text{Al}_2\text{O}_3$  to form  $\text{NiAl}_2\text{O}_4$ . The hexagonal  $\text{Cr}_2\text{O}_3$  and  $\alpha$ - $\text{Al}_2\text{O}_3$  form a continuous solid solution over the entire composition range. Thus the reaction of  $\theta$ - $\text{Al}_2\text{O}_3$  or  $\gamma$ - $\text{Al}_2\text{O}_3$  with  $\text{Cr}_2\text{O}_3$  leads to the formation of hexagonal  $(\text{Al}, \text{Cr})_2\text{O}_3$  crystals which can act as nuclei for the formation of hexagonal  $\alpha$ - $\text{Al}_2\text{O}_3$  (Fig. 2-13).

Jedlinski and Borchardt (56) observed that the change of the scale growth direction from the predominant outward metal to the prevailing oxygen inward transport occurred at the rather early

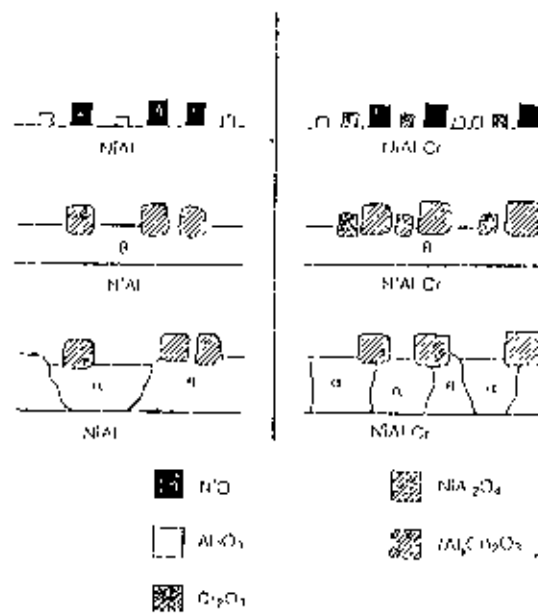


Fig.2-13 : Schematic model of the chromium effect on transformation kinetics, (55).

stages of oxidation of Fe-Cr-Al alloys. At these stages of reaction the development of unstable aluminas is very plausible as already demonstrated for scales on Fe-Cr-Al alloys. The scales formed due to the conditions in this study were analyzed by means of X-ray diffraction. The results indicated perfect correlation between the scale growth direction and its phase composition. In the cation-deficient unstable aluminas an outward metal transport prevailed, while in scales consisting essentially of  $\alpha$ -Al<sub>2</sub>O<sub>3</sub> an inward oxygen short circuit transport predominated.

Various explanations have been summarized by Ramanathan (57), Rhys-Jones et al (16) and Rapp and Pieraggi (38) to account for the beneficial effects of reactive metal additions for the growth of a chromia protective scale on pure Cr or on an alloy of Fe-, Ni-, or Co-base. The following effects have been demonstrated:

1. mechanical keying through formation of oxide pegs into the alloy;
2. promotion of preferential cationic or anionic diffusion in the scale and thus inducing the formation of oxide at one preferential interface;
3. formation of graded oxide or interlayers containing the reactive element;
4. reduction in accumulation of voids at the alloy/scale interface;
5. enhancement of scale plasticity by modification of the structure;

6. The adherence of the scale is improved greatly, especially in response to thermal cycling.
7. The parabolic scaling rate constant for steady state growth is reduced, by as much as a factor of ten or more.
8. For a binary alloy, the minimum concentration of chromium in the alloy required to achieve a steady state chromia scale is reduced considerably, from about 20-35 % Cr to about 10-13% Cr.
9. The dominant mechanism for scale growth is changed, from scale growth at the oxide/gas interface resulting from dominant outward cation diffusion (via grain boundaries or other short-circuits) in the scale to scale growth at the alloy/scale interface resulting from inward diffusion of oxygen anions (also via grain boundaries or short-circuits) in the scale.
10. provision of sites for vacancy condensation,
11. enhancement of oxide nucleation processes,
12. the rate of oxide growth is decreased;
13. the integrity of the oxide scale is improved;

Golightly (37) and Golightly et al (51) reported that the oxidation of Fe-14Cr-4Al and Fe-27Cr-4Al alloys proceeded by the outward diffusion of  $Al^{3+}$  ions and the inward diffusion of  $O^{2-}$  ions along grain boundaries occurring simultaneously. Where these two fluxes meet within the scale new oxide is formed and compressive stresses arise as a result and lead to spalling.

Clemendot et al (58), while attempting to determine the influence of Al on the oxidation of Fe-Cr alloys noticed that Fe-



Cr-Al type ferritic alloys are used for the manufacture of resistance wires for high temperature electric furnaces. These refractory alloys show a great resistance to high temperature oxidation. Their high Al content (>5%) allows the formation of an alumina refractory layer ( $\text{Al}_2\text{O}_3$ ) which protects them. However, the formation of this oxide layer is associated with the development of lateral stresses which favour spallation particularly during thermal cycling. The increase of oxidation rate which follows this spalling decreases the in-service lifetime of components.

Through the observation of Rapp and Pieraggi (38) for scale growth at the metal/scale interface resulting from inward anion diffusion, it has been reported that a very strong chemical bond is maintained at the metal/scale interface and adherence is excellent there. For inward scale growth, any insoluble internal or superficial particles are incorporated directly into the scale so that the metal/scale interface does not have to collect marker-like particles. Therefore, the metal/scale contact and the associated excellent bonding for inwardly grown scales are not reduced by interfacial impurities.

Relative to the grain size of such a scale, extremely small grains are formed inherently for scale growth via anion diffusion. Such an occurrence is also expected for chromia grains with the corundum lattice, so that chromia formed at the metal/scale interface by anion diffusion would be expected to be fine grained and tightly adherent.

## CHAPTER 3 : EXPERIMENTAL TECHNIQUES

### 3.1 Materials and Preparation

Mild Steel scrap, Ferro-Chrome and Aluminium were used as raw materials in the production of the alloys for the investigation. Mild steel scrap has been purchased in the form of bar, Ferro-chrome (containing 65% Cr) in the form of lump and Aluminium (Containing 99% Al) in the form of ingot have been also purchased from the local market.

The alloys were prepared in a high-frequency induction furnace. They were cast in the form of rod about 2.5 cm in diameter, 30 cm in length. Their nominal compositions are listed in Table 3-I.

Table 3-I : Nominal composition of alloys (by weight)

Serial No.	%Cr	% Al	% Fe
1	10	2	balance
2	10	4	balance
3	10	6	balance
4	10	8	balance

Alloys prepared in this way have compositions very close to their nominal values. The portions of the ingots, about 1 mm from the surface, were liable to be affected by segregation effects giving rise to compositional inhomogeneity and as such they were cut off. The specimens were cut out from the ingots by carborundum wheels to sizes varying usually between 13-15 mm diameter x 1.5-2.0 mm thick for cyclic oxidation.

The surface preparation of the specimens involved abrading on successively finer grades of SiC papers of fineness from 3 to 2/0 grit size. Proper care was taken to avoid overheating of the specimens during cutting and drilling operations.

### 3.2 Apparatus and Oxidation Procedure.

#### 3.21 Cyclic Oxidation:

The Cyclic oxidation kinetics were followed by oxidizing the samples in a horizontal electrically heated furnace followed by direct weight change measurements (after cooling for at least 20 minutes) in a manual type balance. A general view of the apparatus is presented in Fig. 3-1. The furnace used silicon carbide heating elements having approximately a 6-in. long hot zone with a temperature variation of about  $\pm 5^{\circ}\text{C}$ . The specimens for oxidation were placed on a refractory tray lean against the sides of the tray. The 'specimen' thermocouple was introduced through the long refractory tube at the one end of the reaction tube and was

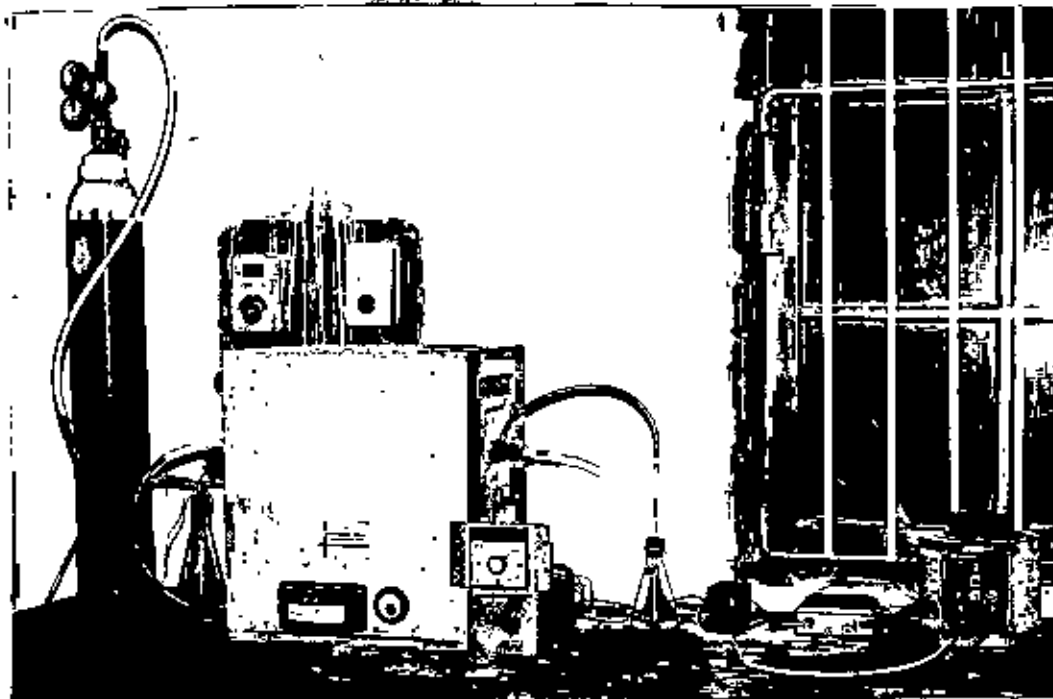


Fig.3-1 : General view of cyclic oxidation apparatus.

connected to a potentiometric measuring device to indicate accurately the specimen temperature.

The specimens were laid with their length across the width of the specimen carrying tray. Thus a fairly wide gap was maintained between the bottom of the tray and the specimen surface to avoid the effect of any probable temperature difference between the center and the bottom of the tray. Furthermore, both the broad faces of the specimen were thus subjected more closely to identical conditions of gas flow and pressure.

Necessary joints were provided at both ends of the reaction tube to ensure a proper flow of oxygen. The gas( $O_2$ ) was passed through sulfuric acid ( $H_2SO_4$ ) contained in the conical flux. At the exit end, the outgoing gases were bubbled through a column of liquid thus providing a visual indication of proper gas flow as well, besides acting as a protection against the possibility of any backward suction. Before the start of the run, the furnace was raised to the desired temperature. The distance from the center of the specimen carrying tray to the reaction tube end was measured. The same distance was marked on the thermocouple (bare). It has been ensured that the tip of the thermocouple was exactly at the central position on the specimen tray. After ensuring that the thermocouple had reached a steady temperature, the temperature reading was obtained with a temperature controller (pyrometer). Necessary adjustment on the controller temperature setting was made to get the exact desired temperature on the thermocouple for the

specimen (i.e. the specimen thermocouple). This procedure eliminated any probable difference between the actual specimen temperature on the tray and that at the thermocouple tip inside the protecting refractory sheath.

The clean ground/polished specimens were placed on the tray which was held near the end of the reaction tube with the help of a suitable clamping device. The gas was turned on and adjusted to approximately the required flow rate. After about 10 min. the specimens were introduced inside the furnace and the gas joints securely fitted. The furnace attained the set temperature in about 2 minutes. At the end of the cycle, the specimens were transferred quickly and cautiously into previously weighed porcelain crucibles for the collection of any spall particles likely to be released on cooling. Necessary weight change data were recorded.

### 3.3 Examination Techniques

The following tests were performed on the oxidized specimens:

#### (a) Macro Examination

It was performed, under ordinary light, to illustrate any prominent macroscopic feature on the specimen surface. The maximum magnification employed for the purpose was usually under x 6.

**(b) X-Ray Diffraction:**

The scale constituents were identified by the following procedures:

The oxidized specimens surface were analyzed on an X-Ray Diffractometer - JDX 8P, X-Ray Analytical Equipment, continuously evacuated version produced by the JEOL, Japan. A copper target in conjunction with a Nickel filter at a potential difference of 40 kV with a current of about 20 mA were used for the purpose. The different phases were identified by the resulting X-ray patterns as separate peaks using standard ASTM data.

**(c) Metallography:**

The structure and morphology of the scale in cross-section were examined extensively under the optical microscope. The oxidized samples were mounted on a slow heat setting solid mounting medium (plastic materials) and a quick setting liquid mounting medium (Quick Powder) using a chemical hardener. The materials for cold quick setting system have been collected from the Dept. of Physics, BUET, Dhaka. In heat setting system, the specimen was placed in a stainless steel mould supported by a tongs and plastic powders were poured well around the specimen. The specific size was attained under pressure as plastic powder allowed to set through an electrically heating device. The plastic materials helped to minimum technical damage to the scale during the subsequent grinding and polishing operations.

The resin had a low shrinkage coefficient on setting and helped to minimum technical damage to the scale during the subsequent grinding and polishing operations. Specimens were positioned and supported on edge in a small cast iron mould and liquid resin carefully poured around the specimen and allowed to harden.

The mounted specimens were then ground down on a dry SiC paper progressively from 3 to 4/0 grit size, followed by wheel polishing with velvet cloths and finally hand polishing was completed in velvet cloths thus minimizing "pull-out" of the scale.

The polished cross-sections were examined using a Swift Microscope supplied by Swift Instrument INC. (SWIFTMASTER II), Japan in ordinary light. The scale cross-sections were photographed using the 35 mm camera head attached to the microscope.

10568



## CHAPTER 4 : RESULTS AND DISCUSSION

### 4.1 Introduction

Most industrial processes involve the use of metals and alloys at elevated temperatures followed by cooling to room temperatures. When such heating goes on for quite a large number of times, the oxidation behaviour and the resultant effects may not necessarily be the same as those under isothermal conditions. The operating conditions in such plants conform more to cyclic rather than to isothermal processes. The concern of the present project has, therefore, been mainly the oxidation under cyclic conditions, and given due considerations to the effects of thermal cycling, cyclic oxidation studies may ultimately go to constitute a more realistic approach towards solving the problem of metal corrosion.

Thermal cycling generally consists in repeatedly heating the metal or alloy to the test temperature in either still or moving air, or any other suitable environment, followed by cooling to some desired lower temperature (usually room temperature) at any desired rate. In an isothermal process the oxide or scale formed normally retards further oxidation as a result of scale build-up with attendant metal consumption, whereas under cyclic conditions the scale usually spalls or flakes off as the metal is cooled or heated up. The more the spalling, the greater the rate of metal consumption due either to the exposure of fresh metal surface to the oxidizing environment or due to thinning down of the scale,

resulting in increased diffusion rates. Sometimes, one or more constituents of the alloy may be depleted which again may result in an increased oxidation rate. In other cases, the spalling may be so severe that parts of the substrate metal are also removed along with the spall.

If the alloys were used in an application where they are not thermally cycled or if they did not spall appreciably when cycled, then the alloys with the lowest rate constant (isothermal) would have the best oxidation resistance under service conditions. Although scale spallation usually takes place at a lower temperature in thermal cycling and the consequence may not be so severe as spallation under isothermal conditions when the exposed alloy surface, often depleted of the protective constituent, is immediately exposed to the full severity of the atmosphere at its highest temperature, but then the extent of spalling is often greatest during cycling and repeated removal of large pieces of scale can be catastrophic. As partial or complete scale adhesion can be as important as the scale composition itself, it does not follow that the most effective scale under isothermal conditions is the most effective during cycling.

Cyclic oxidation is difficult to study because there is no agreed upon experimental and interpretive approach such as that generally used in studying isothermal oxidation. In isothermal studies, the conventional technique is to measure weight change as a function of time at temperature which is generally a direct

measure of oxygen pick up, i.e. scale formation, as shown by the curve marked 'isothermal' in Fig.4-1. In cyclic oxidation, the sample is usually weighed after a given number of heating or cooling cycles when the sample is at the ambient temperature, and a specific weight change versus time curve is generated, but because of spallation, a resultant curve such as the one marked 'sample' in Fig.4-1 is typical. Alternatively, the weight change given for each cycle may represent the value at the middle point of the high temperature portion of each cycle, generating a curve which is again essentially of the same form. If on the other hand, the weight of the oxide spall is measured and plotted at each stage then a curve such as the one marked 'spall' in Fig.4-1 may be obtained and combining this with the sample weight change for each stage, one can readily obtain a curve such as that marked 'cyclic' in Fig.4-1 which represents 'total specific weight change' or 'cyclic (or combined) specific weight change' comparable to corresponding specific weight change data under isothermal conditions.

In all illustrations, unless otherwise stated the term  $\Delta W/A$  will have the usual significance of the weight of total oxygen pick up in  $\text{mg}/\text{cm}^2$  of specimen surface during any time 't'. Obviously, this quantity is the sum of the weight of oxygen in the oxide retained on the specimen surface and the weight of oxygen in the oxide spalled (per unit area of the specimen surface), neglecting of course, any loss of oxide due to volatilization. This quantity

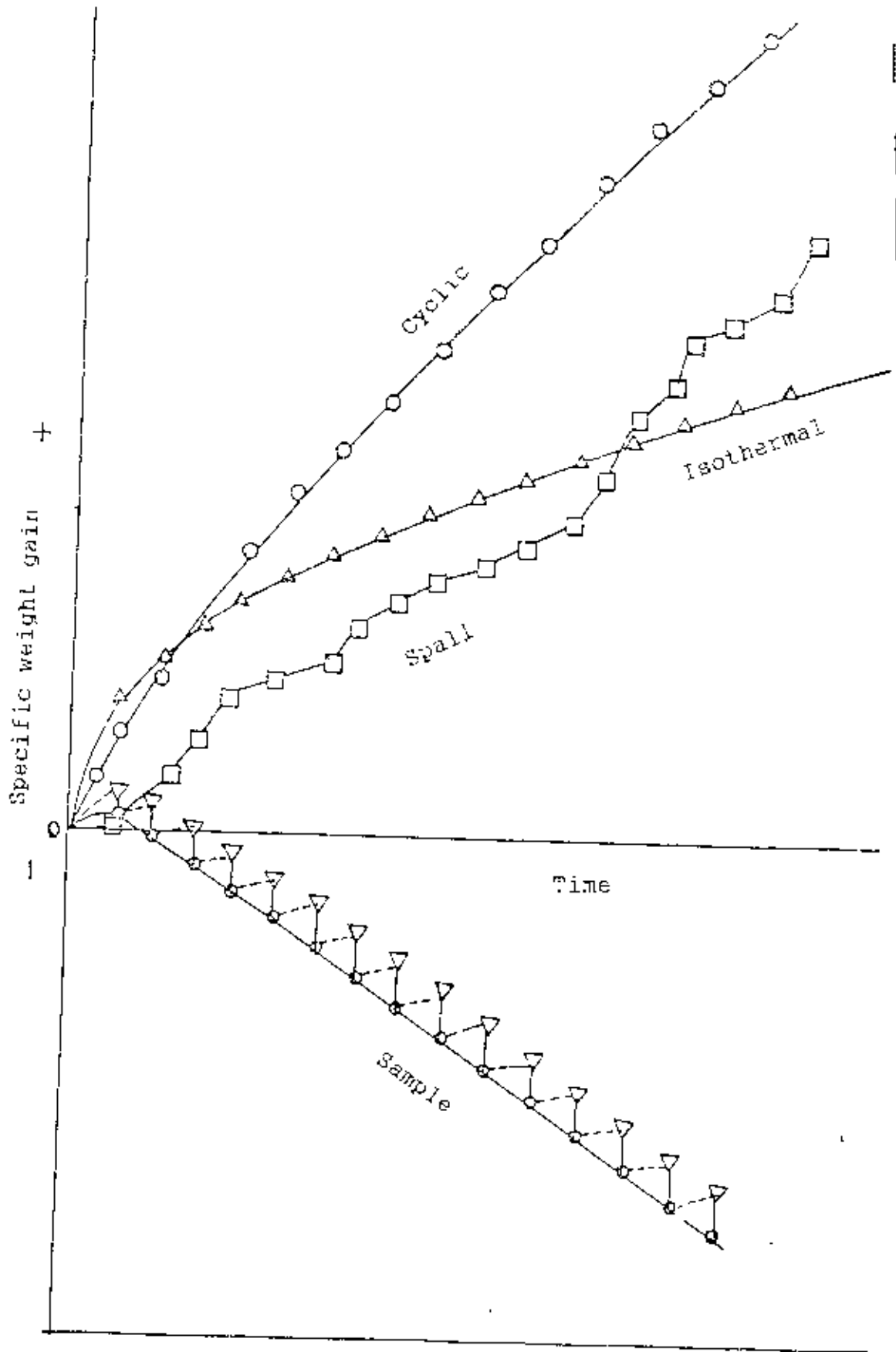


Fig.4-1 : Schematic representation of cyclic oxidation kinetic data. (35).

can, therefore, be regarded for all practical purposes, to be the cyclic specific weight gain.

Furthermore, the percentage compositions used in this work are all gravimetric percentages by weight and the oxidation in all cases has been carried out at or near the atmospheric pressure in flowing oxygen at an appropriate rate. The length of the individual cycles in the cyclic oxidation runs were of 3-hour duration in all cases.

## 4.2 Results

### 4.21 Fe-10Cr-2Al Alloy

The oxidation kinetics of Fe-10Cr-2Al alloy at 950°C in pure oxygen at 1 atmosphere pressure under thermal cycling for 17 3-hour cycles has been represented in Fig. 4-2.

It will be observed from the kinetics curves that a protective scale initially forms which persists upto about 9 hours (curves OA<sub>1</sub> and OA<sub>2</sub>) but eventually begins to cause breakaway within the next cycle resulting an increase in the oxidation rates (curves A<sub>1</sub>B<sub>1</sub> and A<sub>2</sub>B<sub>2</sub>). Subsequently, a protective scale further forms causing decrease in the oxidation rates (curves B<sub>1</sub>C<sub>1</sub> and B<sub>2</sub>C<sub>2</sub>), ultimately reaching a steady state values in the period of 27-51 hours (curves C<sub>1</sub>D<sub>1</sub> and C<sub>2</sub>D<sub>2</sub>).

Specific weight gain values, from thermogravimetric data, during 17 3-hour cycles (i.e. 51 hours) of the same alloy are

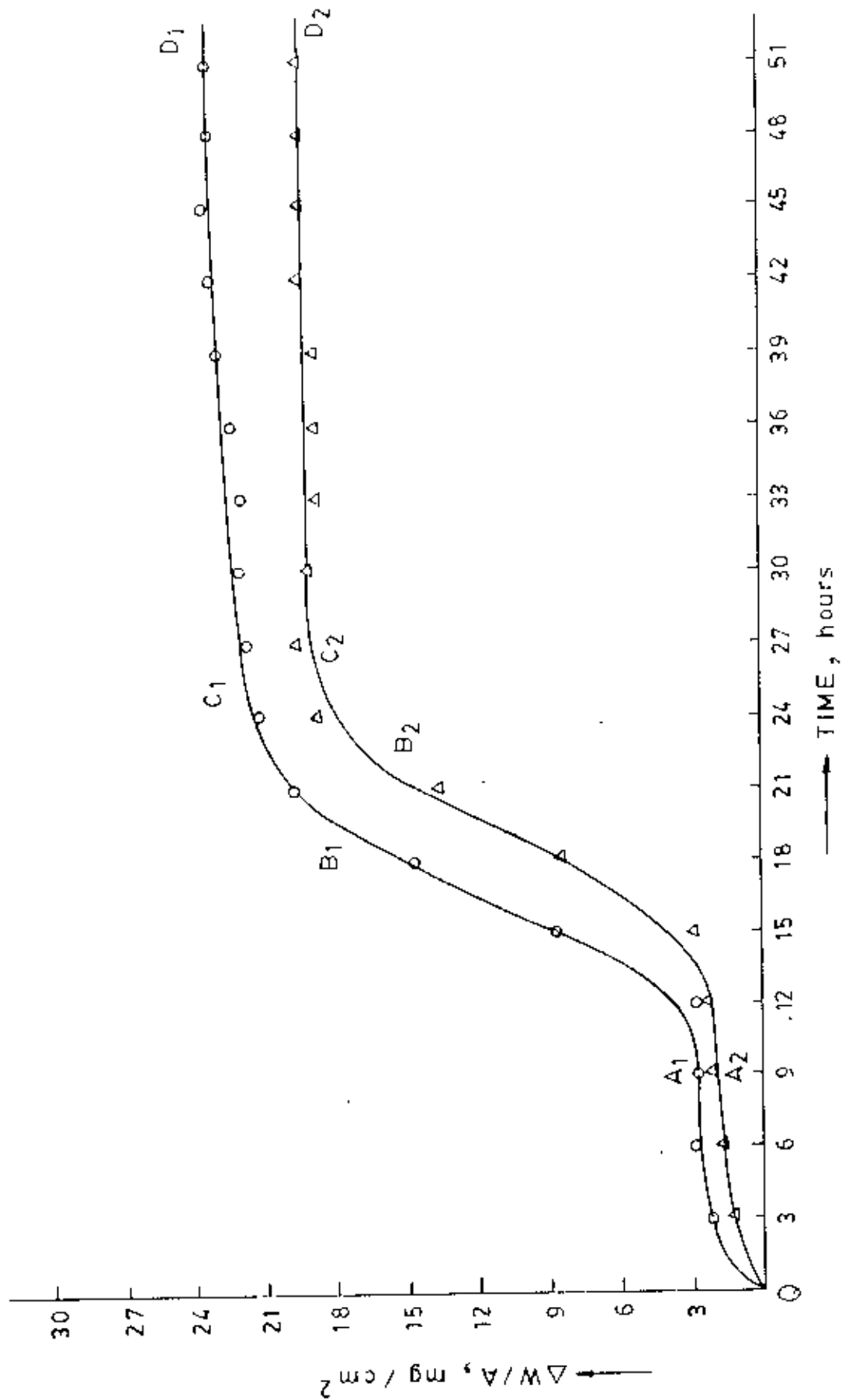


Fig. 4-2 : Cyclic oxidation kinetics of Fe-10Cr-2Al alloy at  $950^\circ\text{C}$ .

observed to be about  $23.67 \text{ mg/cm}^2$  on curve  $OD_1$  and  $19.65 \text{ mg/cm}^2$  on curve  $OD_2$  for the two specimens treated.

The kinetics curves for Fe-10Cr-2Al alloy at  $1000^\circ\text{C}$  in pure  $\text{O}_2$  at 1 atmosphere pressure after 16 3-hour cycles of oxidation are shown in Fig.4-3.

It reveals that initially the rate of oxidation (as measured by the specific weight gain value) is somewhat severe and rises to about  $35 \text{ mg/cm}^2$  in 2 hours which is much higher than that of  $950^\circ\text{C}$ . Although a protective scale on both the specimens forms but it subsequently breaks down and shows an increase in the rate of oxidation (curves  $A_1B_1$  and  $A_2B_2$ ) for the two specimens. The oxidation rate then begins to decrease (curves  $B_1C_1$  and  $B_2C_2$ ) as a result of the formation of a second protective scale eventually reaching a steady state rate of oxidation for the alloy (curves  $C_1D_1$  and  $C_2D_2$ ).

The thermogravimetric data shows that the specific weight gain values during 48 hours of oxidation at this temperature are about  $73.93 \text{ mg/cm}^2$  and  $60.39 \text{ mg/cm}^2$  for the two specimens tested (curves  $OD_1$  and  $OD_2$  respectively).

The oxidation kinetics of the Fe-10Cr-2Al alloy at  $1050^\circ\text{C}$  in pure  $\text{O}_2$  at 1 atmosphere pressure after 54 hours thermal cycling can be observed in Fig.4-4.

The alloy forms a protective scale which offers protection for about 2-3 hours (curves  $OA_1$  and  $OA_2$ ) suffering breakaway within the next few hours (curves  $A_1B_1$  and  $A_2B_2$ ). After this breakaway a second protective scale starts to form as shown by curves  $B_1C_1$  and  $B_2C_2$ .

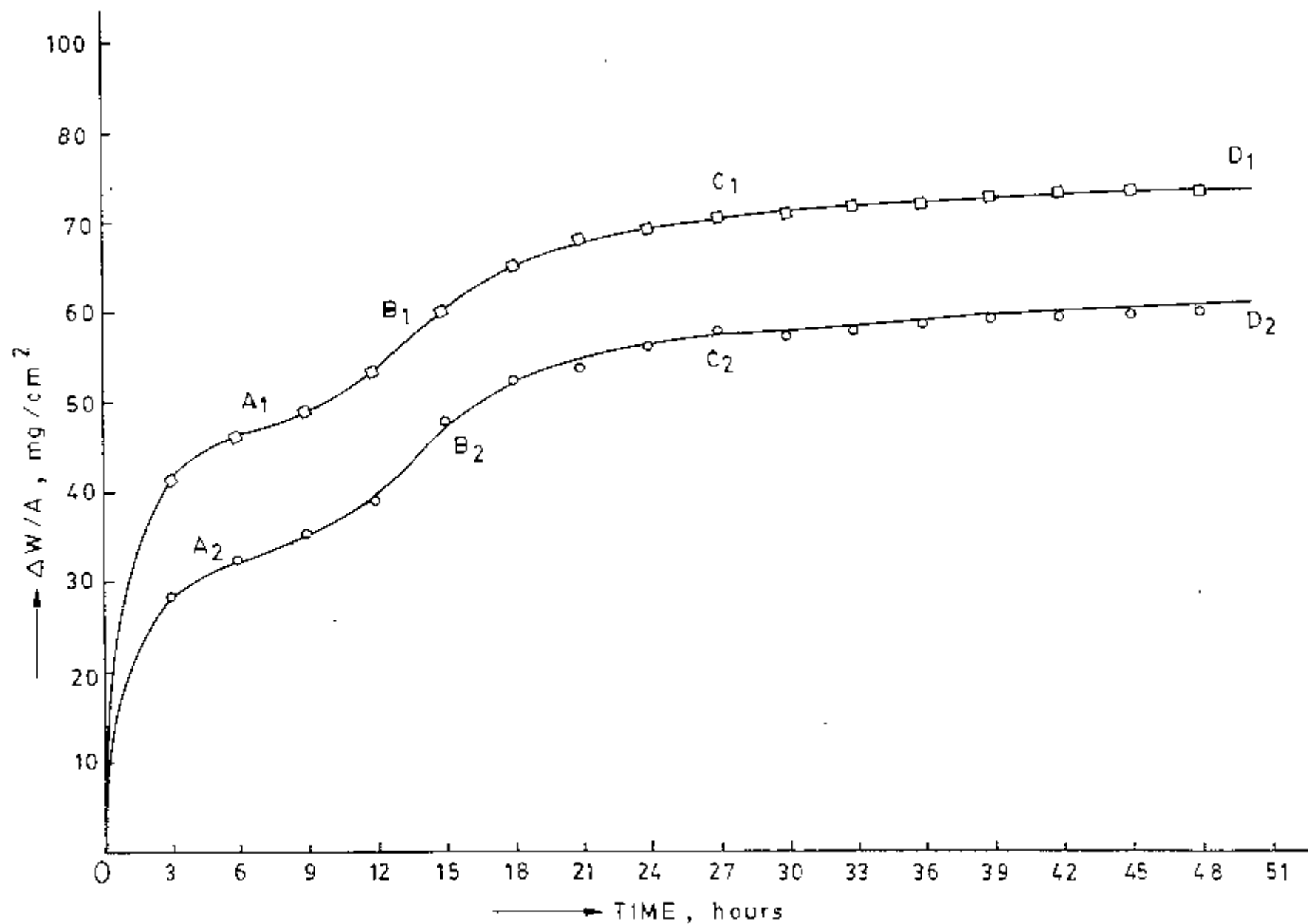


Fig. 4-3 : Cyclic oxidation kinetics of Fe-10Cr-2Al alloy at 1000°C.





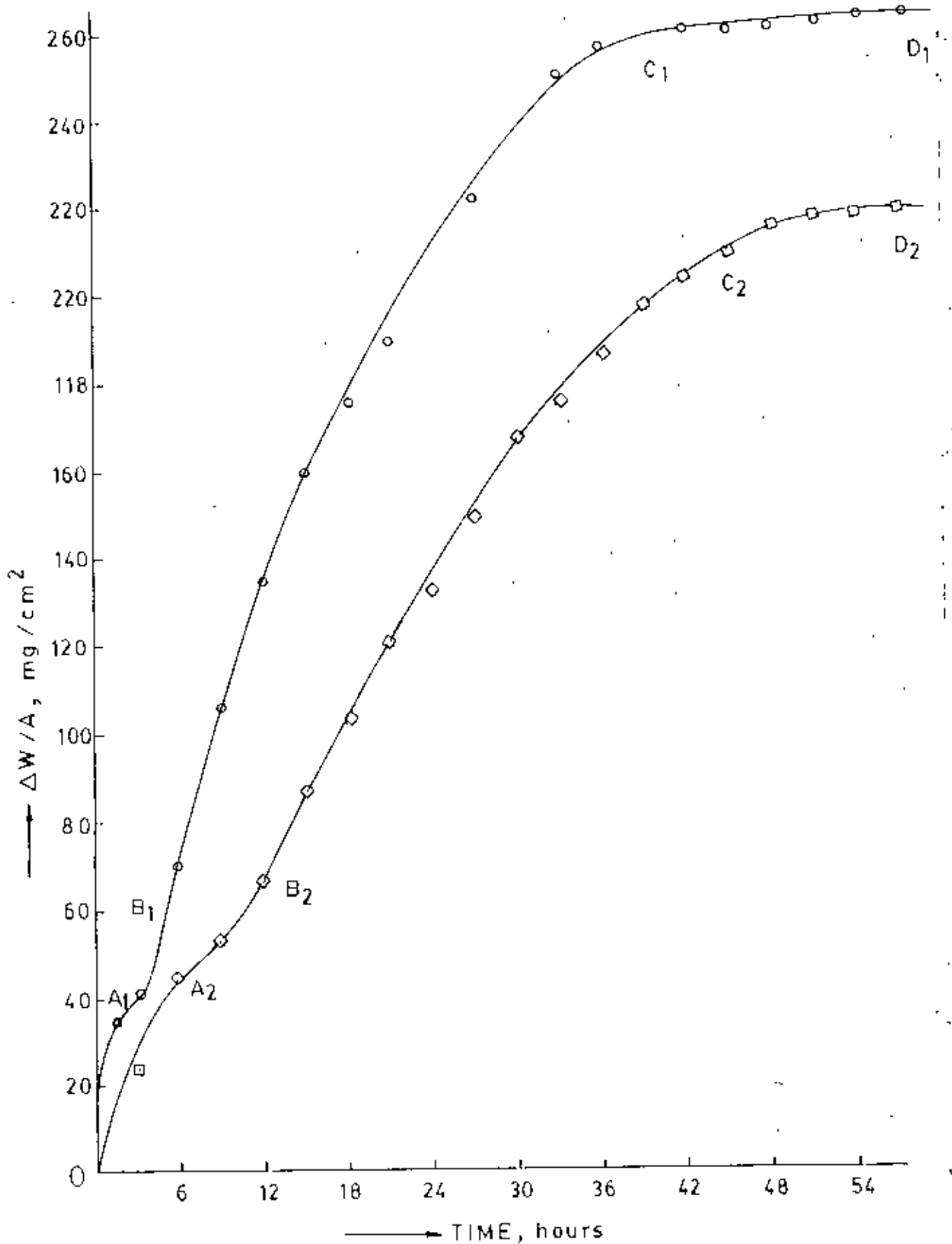


Fig. 4-4 : Cyclic oxidation kinetics of Fe-10Cr-2Al alloy at  $1050^\circ\text{C}$ .

Finally , the curves level down abruptly to a still lower rate of oxidation for the rest of the cycles (curves  $C_1D_1$  and  $C_2D_2$ ).

The specific weight gain values as observed from the thermogravimetric data after 18 3-hour cycles (i.e. 54 hours) of oxidation for the above alloy are about  $264 \text{ mg/cm}^2$  on curve  $OD_1$  and  $220 \text{ mg/cm}^2$  on curve  $OD_2$  for the two specimens treated.

Visual examination of the samples shows the existence of blackish patches running between gray to dark gray areas. After 17-3 hour cycles at  $950^\circ\text{C}$  a stratified duplex scale is noticeable in the optical cross-section of the alloy with a subscale at the base as shown in Fig.4-5. The substrate surface of the specimen shows the presence of voids as usual. This alloy also represents the almost identical microstructure at  $1000^\circ\text{C}$  in optical cross-section after 48 hours (16 3-hour cycles) as observed at  $950^\circ\text{C}$ . On optical examination of the alloy treated at  $1050^\circ\text{C}$  for 54 hours (18 3-hour cycles) reveals the same microstructure as that shown in Fig.4-5. It may be mentioned here that both the specimens heated at this temperature are found to be oxidized completely so that no parent metal can be observed. This is also evident from the macro-examination of the oxidized specimen for this alloy at  $1050^\circ\text{C}$  exposed for 54 hours (17 3-hour cycles) as shown in Fig.4-6.

Spall particles are mostly in the form of broken thin flakes with larger amounts of finer particles at the lower temperature and with progressively coarse particles at the higher temperature. They

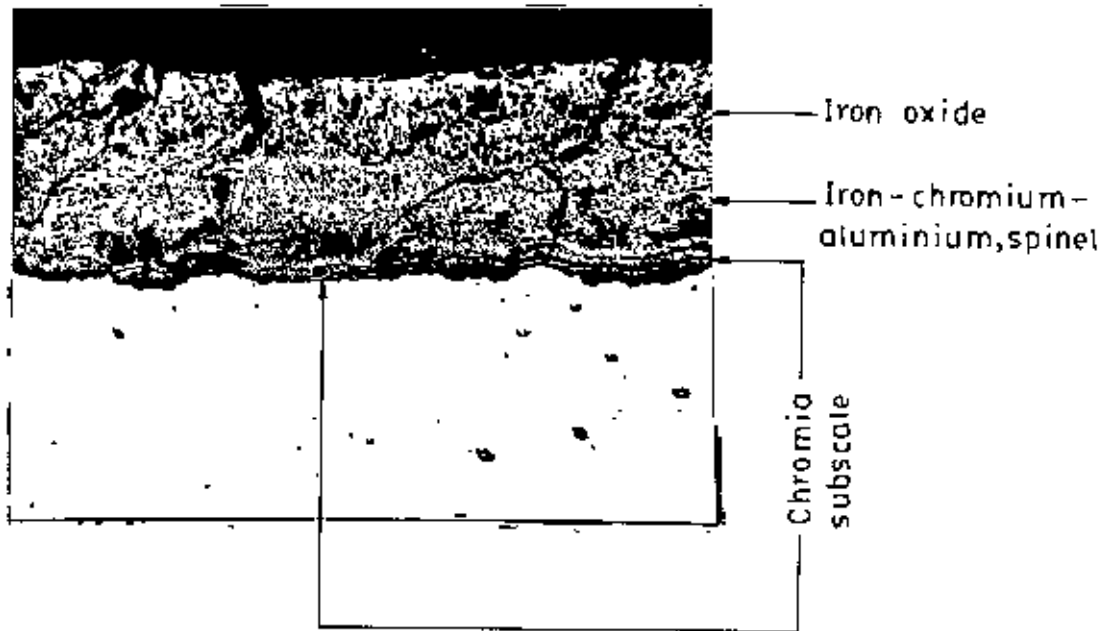


Fig. 4-5 : Optical cross-section of oxide scale on an Fe-10Cr-2Al alloy specimen after an exposure of 51 hours (17 3-hour cycles) at 950°C, x 300. This rapidly oxidizing specimen shows a usual duplex scale. A continuous, uniform Cr<sub>2</sub>O<sub>3</sub> subscale layer is also noticeable at the stratified scale base.

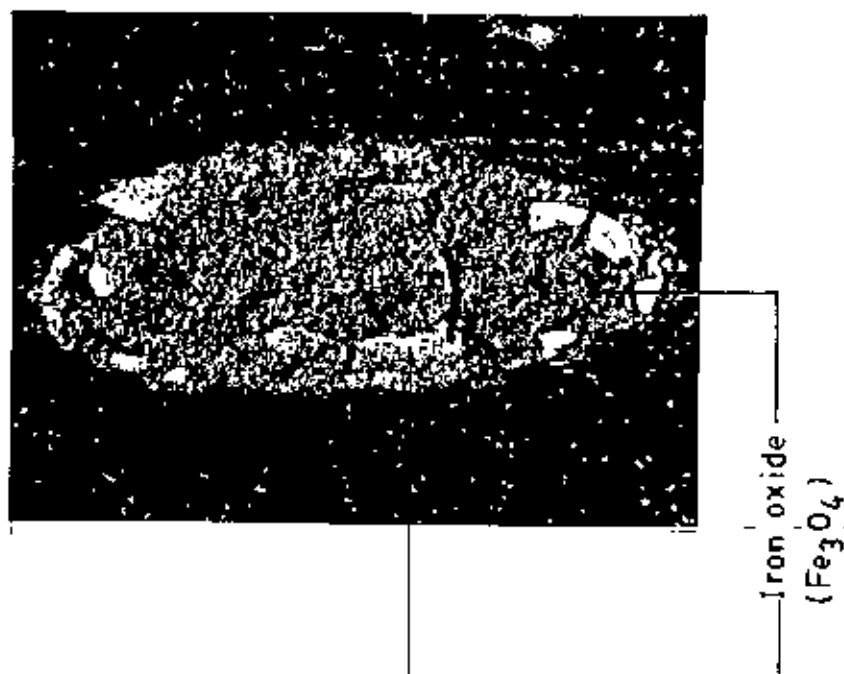


Fig. 4-6 : Photomicrograph of an Fe-10Cr- 2Al alloy specimen (cross-section) after oxidation for 18 3-hour cycles at 1050°C, x 6. The specimen can be observed to have been oxidized throughout as a result of the exposure.

are paramagnetic to magnetic in behaviour which is revealed under magnetic test.

#### 4.22 Fe-10Cr-4Al Alloy

The oxidation kinetics curves for Fe-10Cr-4Al alloy at 950°C in pure O<sub>2</sub> at 1 atmosphere pressure exposed for 15 3-hour cycles can be observed in Fig. 4-7.

The above alloy is supposed to form initially an external protective scale which persists for about 3-6 hours (curves OA<sub>1</sub> and OA<sub>2</sub>) and suffers breakaway through a rapid increase in its oxidation rate within a few hours (curves A<sub>1</sub>B<sub>1</sub> and A<sub>2</sub>B<sub>2</sub>). After this breakdown a second protective scale starts to form as apparent from the reduction in oxidation rates (curves C<sub>1</sub>D<sub>1</sub> and C<sub>2</sub>D<sub>2</sub>), which subsequently levels down to a more or less steady state value.

The specific weight gain values after 15 3-hour cycles (i.e. 45 hours) during oxidation is recorded to be 6.53 mg/cm<sup>2</sup> on curve OD<sub>1</sub> and 5.62 mg/cm<sup>2</sup> on curve OD<sub>2</sub> for the two specimens of the alloy treated.

The oxidation kinetics of the above alloy under thermal cycling at 1000°C in pure O<sub>2</sub> at 1 atmosphere pressure is represented in Fig. 4-8. The initial oxidation characteristics at this temperature is almost similar as at 950°C. Initially a protective scale forms at this temperature as well, which continues till about 1-3 hours (curves OA<sub>1</sub> and OA<sub>2</sub>). The very same scale then starts to breakdown as indicated by an abrupt acceleration in the

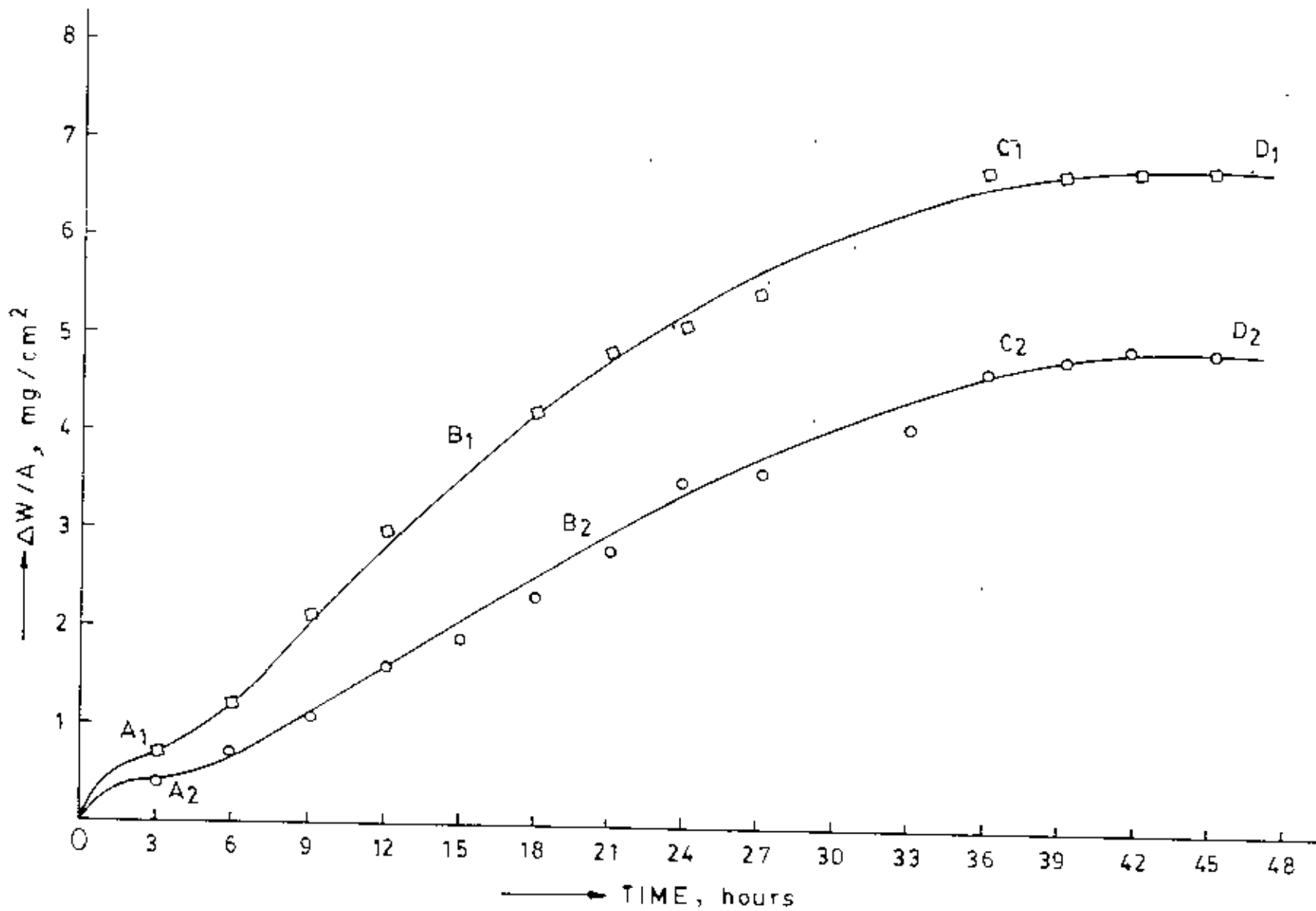


Fig. 4-7 : Cyclic oxidation kinetics of Fe-10Cr-4Al alloy at  $950^\circ\text{C}$ .



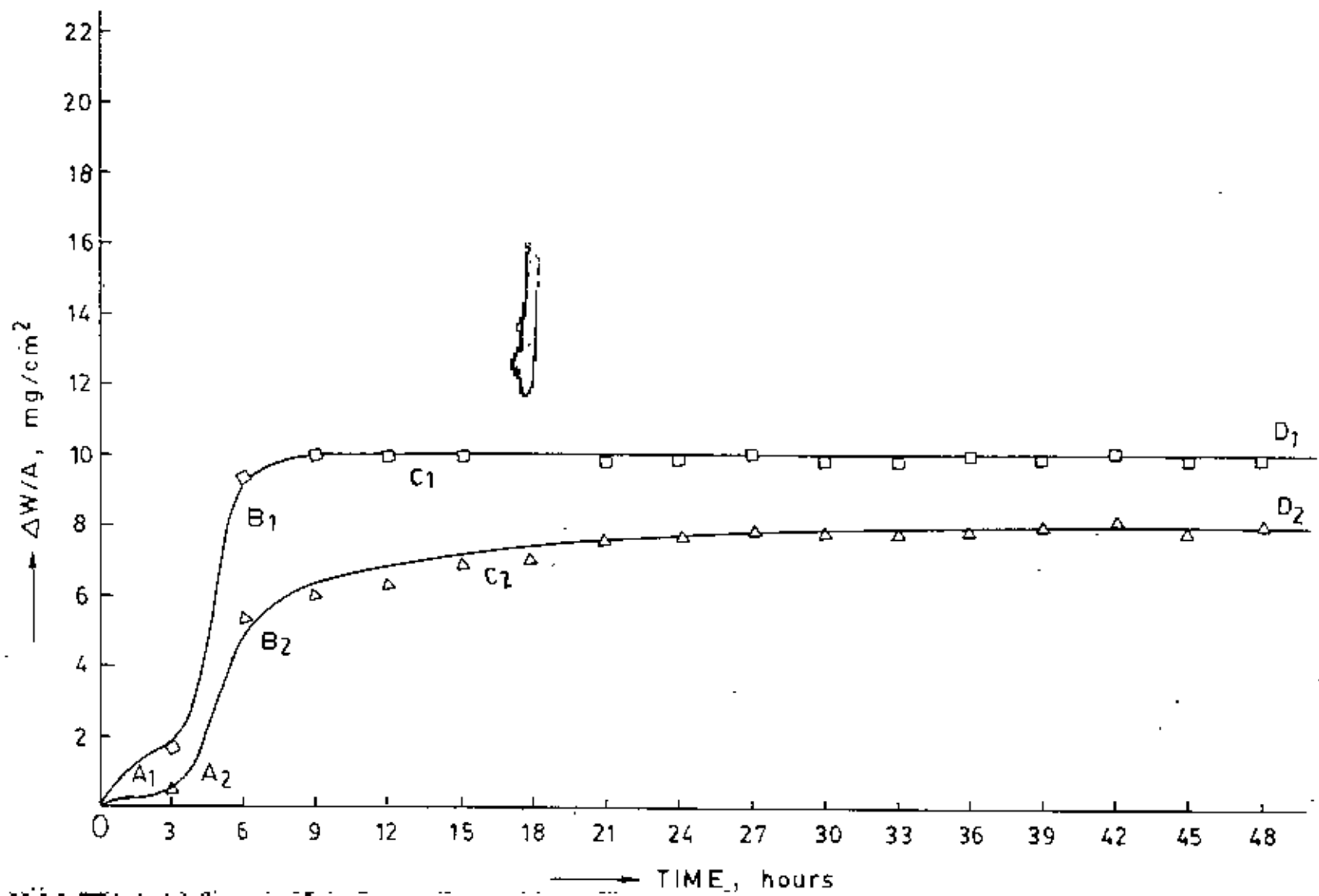


Fig. 4-8 : Cyclic oxidation kinetics of Fe-10Cr-4Al alloy at  $1000^\circ\text{C}$ .

oxidation rates (curves  $A_1B_1$  and  $A_2B_2$ ). A protective scale forms afterwards due to which the rates of oxidation for the three specimens subsequently settle down to steady state for the rest of the run.

The thermogravimetric data reveals that the specific weight gain values after 16 3-hour cycles at this temperature are about  $9.97 \text{ mg/cm}^2$  and  $8.07 \text{ mg/cm}^2$  for the two specimens of the above alloy under thermal cycling.

The oxidation kinetics of Fe-10Cr-4Al alloy at  $1050^\circ\text{C}$  during cyclic oxidation in pure  $\text{O}_2$  at 1 atmosphere pressure can be observed in Fig. 4-9.

This alloy is believed to form a protective scale initially which stays for about 2-3 hours (curves  $OA_1$ , and  $OA_2$ ) and suffers breakdown within the few subsequent hours as displayed by an increase in the oxidation rates and extends upto point  $B_1$  and  $B_2$ . After this breakaway the rate of oxidation begins to decline (curves  $B_1C_1$  and  $B_2C_2$ ) and in fact a second protective oxide forms and reduces the oxidation rate to a more or less steady state value (curves  $C_1D_1$  and  $C_2D_2$ ) for the rest of the run.

Thermogravimetric data reveals that the specific weight gain attains after 16 3-hour cycles (i.e. 48 hours) for the above alloy specimens are  $171.33 \text{ mg/cm}^2$  and  $166.24 \text{ mg/cm}^2$  at this temperature.

The optical cross-section of the alloy after 16 3-hour cycles (i.e. 48 hours) at  $1000^\circ\text{C}$  shows a stratified duplex scale with a subscale at the base as shown in Fig.4-10. The substrate surface of



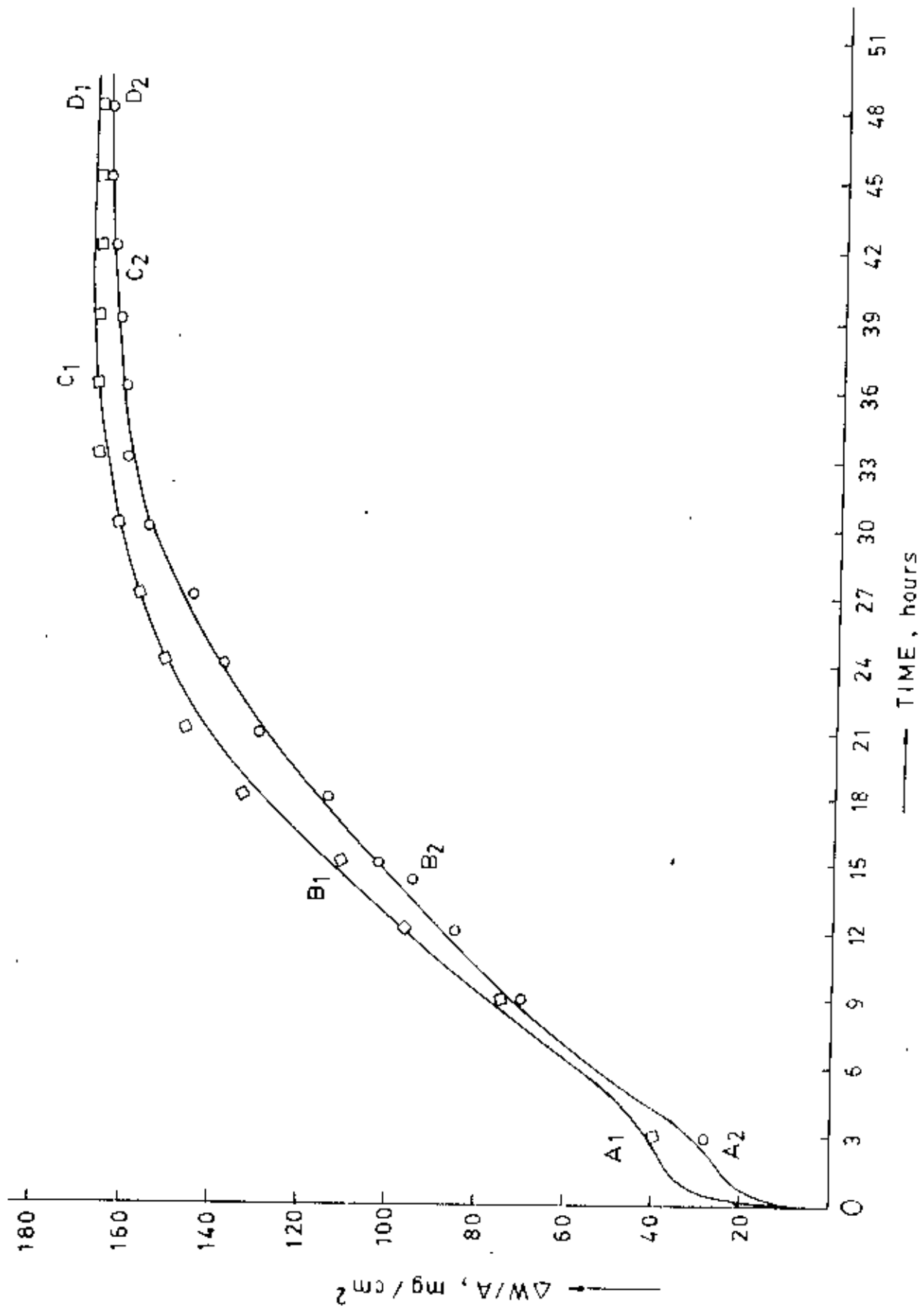


Fig. 4-9 : Cyclic oxidation kinetics of Fe-10Cr-4Al alloy at  $1050^\circ\text{C}$ .

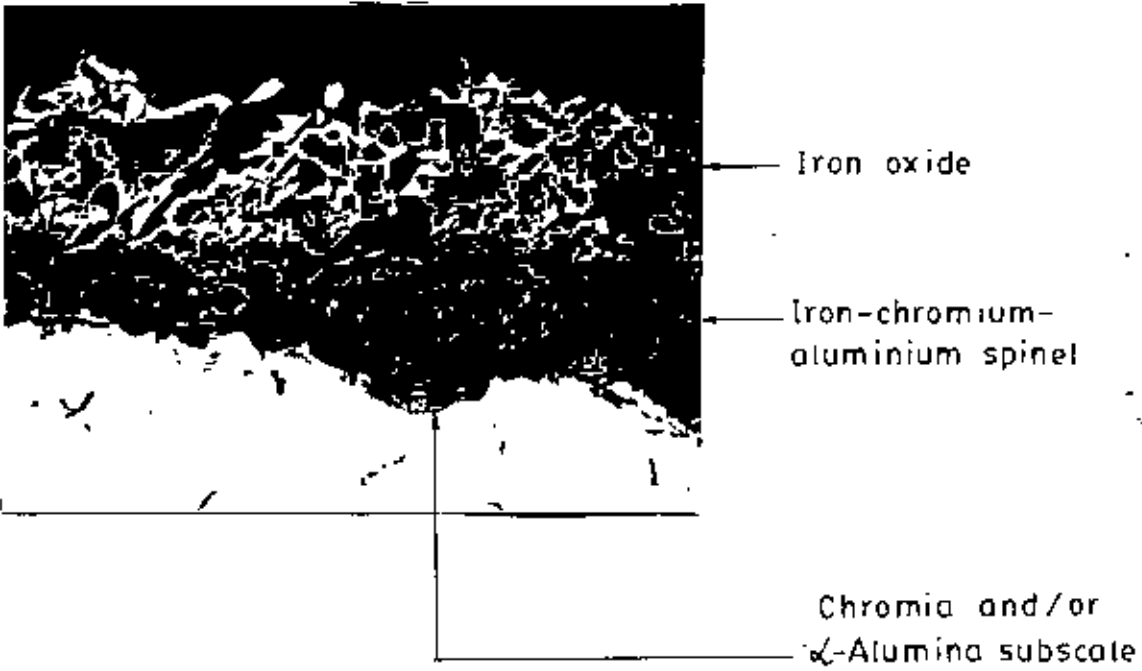


Fig. 4-10: Metallographic cross-section of oxide scale on an Fe-10Cr-4Al alloy specimen oxidized for 48 hours (16 3-hour cycles) at 1000°C, x 1200. A usual duplex scale with a continuous subscale layer at the scale base can be observed.

the specimen reveals the presence of voids as usual. The alloy also displays an almost identical microstructure in optical cross-section at both  $950^{\circ}\text{C}$  and  $1050^{\circ}\text{C}$  after 48 hours (16 3-hour cycles) of exposure as shown in Fig.4-11 and Fig.4-12 respectively that has been observed at  $1000^{\circ}\text{C}$ .

Visual examination of the specimens shows the existence of blackish patches running between gray to dark gray areas. Spall particles are mostly in the form of broken pieces of glass with larger amounts of finer particles at the lower temperatures and progressively larger particles at the higher temperatures. Spall particles are magnetic in nature, dark blackish in colour as well as weakly magnetic in nature.

#### 4.23 Fe-10Cr-6Al Alloy

The oxidation kinetics of Fe-10Cr-6Al alloy at  $950^{\circ}\text{C}$  in pure  $\text{O}_2$  at 1 atmosphere pressure after 48 hours (16 3-hour cycles) of oxidation is shown in Fig. 4-13.

This alloy is believed to form a protective scale initially which persists for about 9-12 hours (curves  $\text{OA}_1$  and  $\text{OA}_2$ ) but subsequently breaks away within a few hours as shown by an increase in the oxidation rates (curves  $\text{A}_1\text{B}_1$  and  $\text{A}_2\text{B}_2$ ). The oxidation rates then start decreasing (curves  $\text{B}_1\text{C}_1$  and  $\text{B}_2\text{C}_2$ ) and eventually levels down to a more or less steady state condition (curves  $\text{C}_1\text{D}_1$  and  $\text{C}_2\text{D}_2$ ).

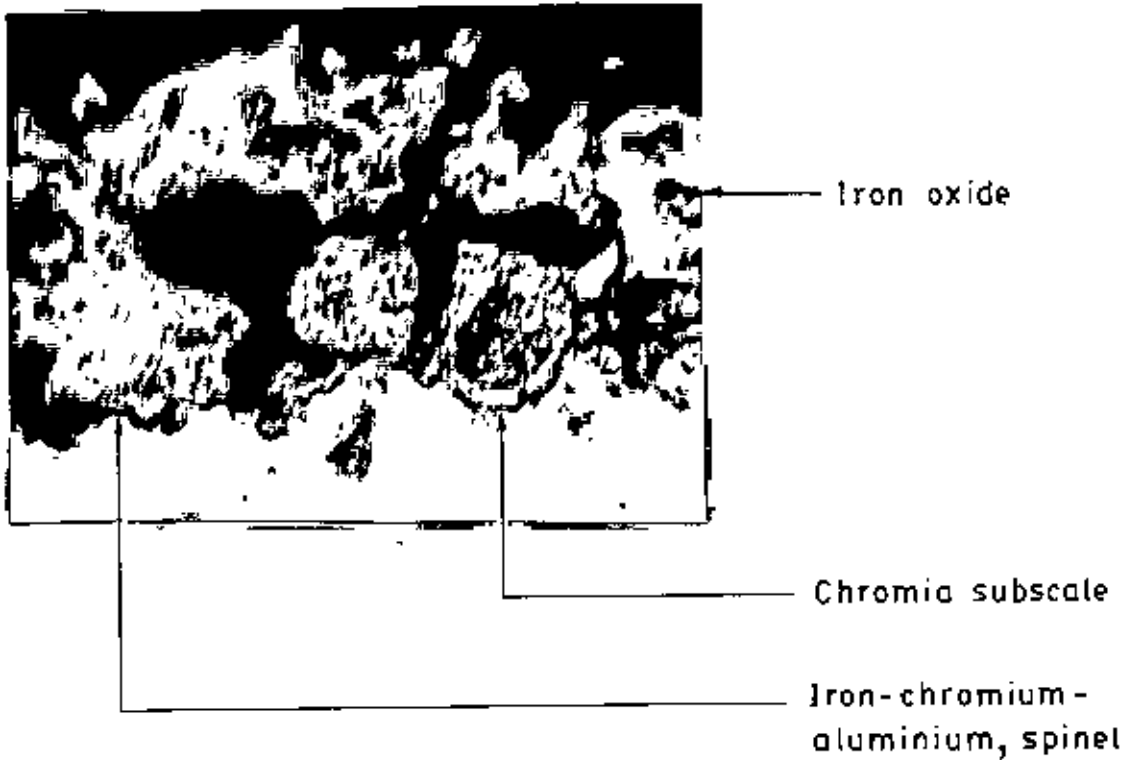


Fig. 4-11 : Photomicrograph of an Fe-10Cr-4Al alloy specimen after oxidation for 15 3-hour cycles at 950°C, x 1200.  $Cr_2O_3$  particles are visible at the scale base.

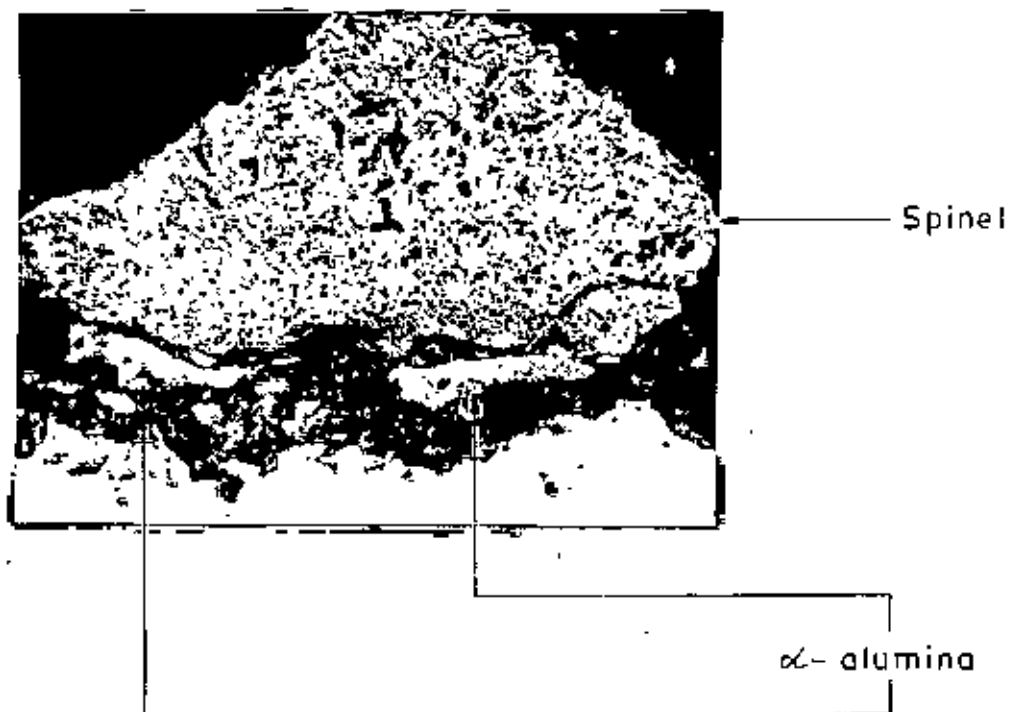


Fig. 4-12: Optical cross-section of oxide scale on an Fe-10Cr-4Al alloy specimen after an exposure of 48 hours (16 3-hour cycles) at 1050°C, x 600.  $\alpha$ -Al<sub>2</sub>O<sub>3</sub> particles are visible at the scale base.

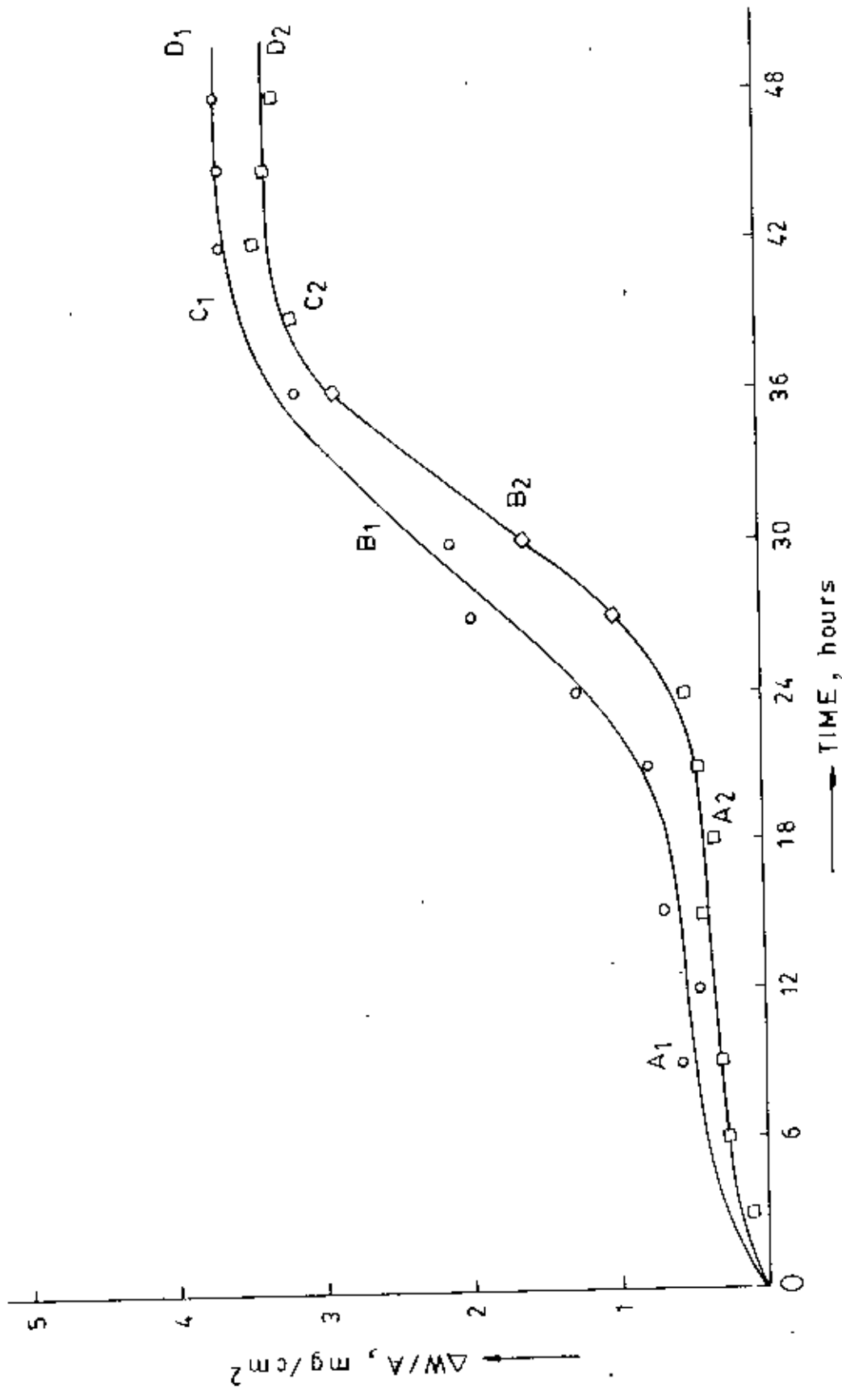


Fig. 4-13 : Cyclic oxidation kinetics of Fe-10Cr-6Al alloy at  $950^\circ\text{C}$ .

The thermogravimetric data shows that the specific weight gain values during 48 hours of oxidation of the alloy are about  $3.67 \text{ mg/cm}^2$  and  $3.33 \text{ mg/cm}^2$  for the two specimens tested.

The oxidation kinetics of the above alloy at  $1000^\circ\text{C}$  in pure  $\text{O}_2$  at 1 atmosphere pressure can be observed in Fig. 4-14. The initial oxidation characteristics at this temperature is of almost identical nature as the above (i.e. as at  $950^\circ\text{C}$ ).

A protective scale forms initially at this temperature as well, which prolongs upto only about 6 hours (curves  $\text{OA}_1$ ,  $\text{OA}_2$ ,  $\text{OA}_3$ ). The scale then starts breaking away as marked by a sudden increase in the oxidation rates (curves  $\text{A}_1\text{B}_1$ ,  $\text{A}_2\text{B}_2$  and  $\text{A}_3\text{B}_3$ ). A protective scale subsequently forms showing decline in the oxidation rates of the specimens (curves  $\text{B}_1\text{C}_1$ ,  $\text{B}_2\text{C}_2$  and  $\text{B}_3\text{C}_3$ ). The rest of the test runs is marked by a decreased oxidation rate of the alloy (curves  $\text{C}_1\text{D}_1$ ,  $\text{C}_2\text{D}_2$  and  $\text{C}_3\text{D}_3$ ).

The specific weight gain after 17 3-hour cycles (i.e. 51 hours) of oxidation is attained the values of about  $5.63 \text{ mg/cm}^2$ ,  $4.43 \text{ mg/cm}^2$  and  $6.0 \text{ mg/cm}^2$  for the three specimens treated.

The kinetics curves for the same alloy at  $1050^\circ\text{C}$  under thermal cycling in pure  $\text{O}_2$  at 1 atmosphere pressure are represented in Fig. 4-15. It will be observed that a protective scale is formed initially (curves  $\text{OA}_1$  and  $\text{OA}_2$ ) which suffers breakdown (curves  $\text{A}_1\text{B}_1$  and  $\text{A}_2\text{B}_2$ ). After this breakaway, a second protective scale begins to form as evident from the decrease in the rate of oxidation of the specimens (curves  $\text{B}_1\text{C}_1$  and  $\text{B}_2\text{C}_2$ ) which offers protection to the

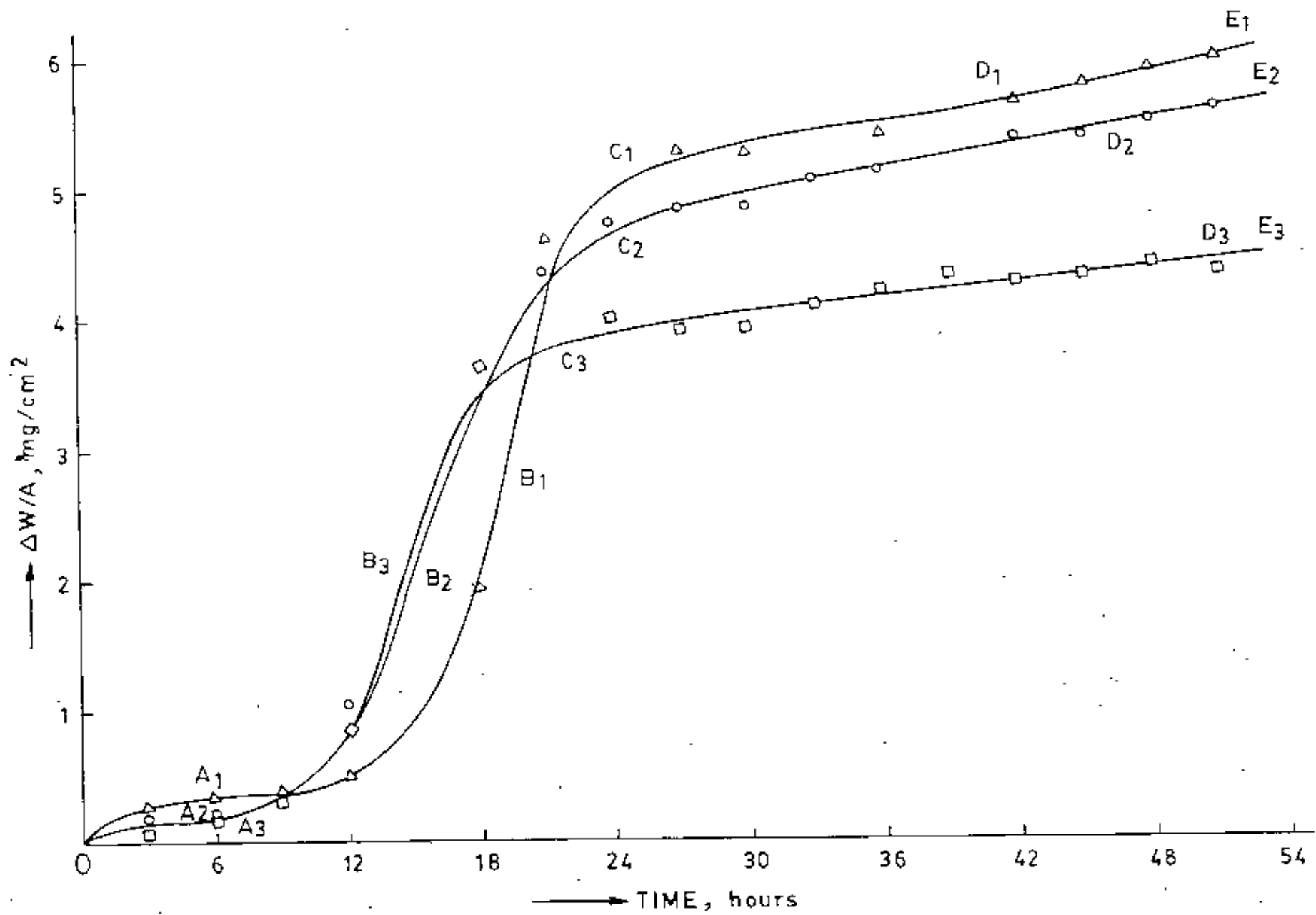


Fig. 4-14 : Cyclic oxidation kinetics of Fe-10Cr-6Al alloy at  $1000^\circ\text{C}$ .



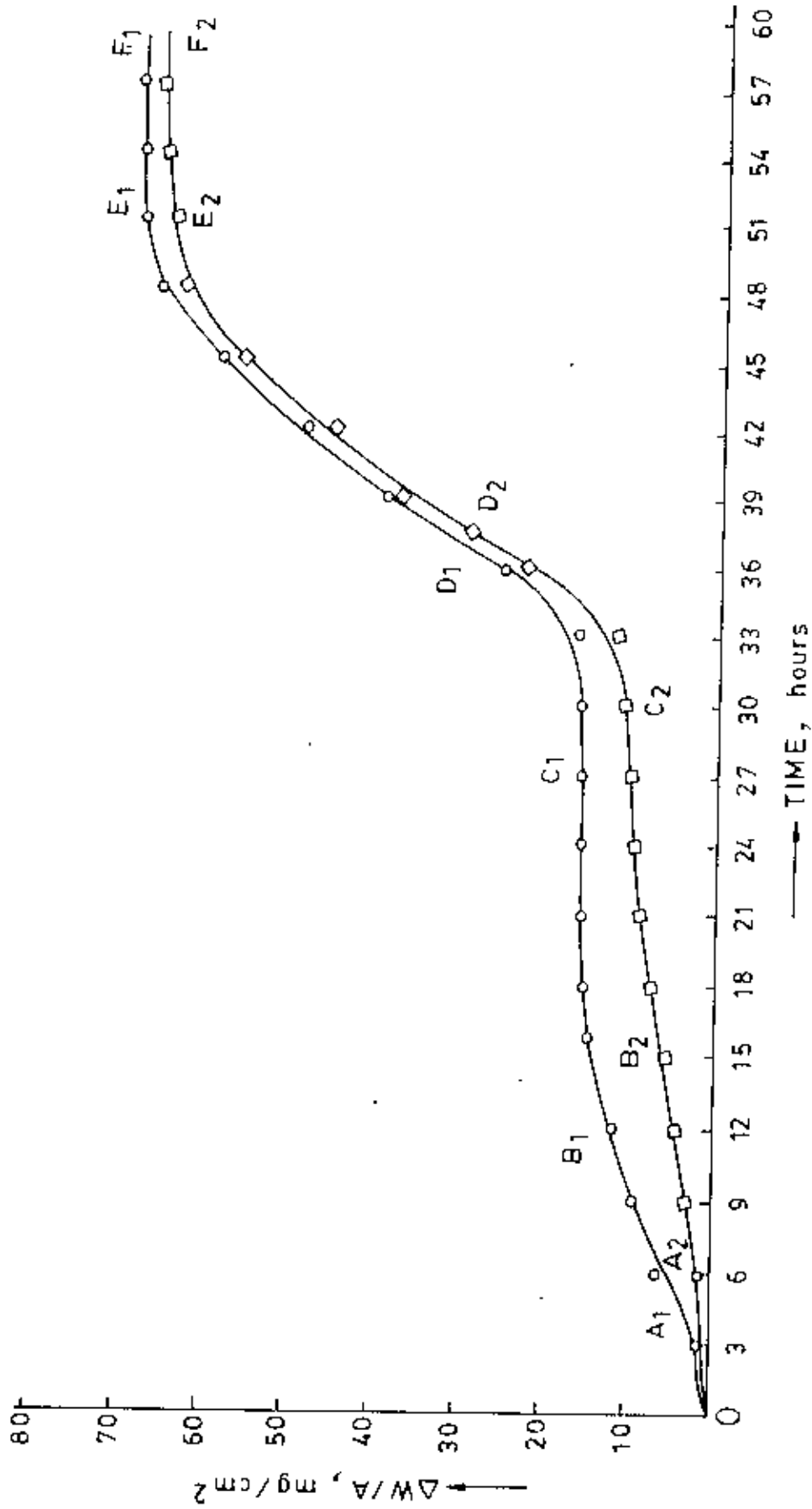


Fig. 4-15 : Cyclic oxidation kinetics of Fe-10Cr-6Al alloy at 1050°C.

alloy till about 27 hours. Unfortunately, this protective scale is also observed to breakaway resulting in a catastrophic rate of oxidation as represented by curves  $C_1D_1$  and  $C_2D_2$ . Subsequently, the catastrophic rate of oxidation subsides and ultimately settles down to a steady state rate as represented by curves  $D_1E_1F_1$  and  $D_2E_2F_2$ .

The specific weight gain values after 19 3-hour cycles (i.e. 57 hours) during oxidation shows  $67 \text{ mg/cm}^2$  on  $OF_1$  and  $65 \text{ mg/cm}^2$  on  $OF_2$  for the two specimens of this alloy.

Typical appearance of the surface upon macro-examination after oxidation of this class of alloy at the higher temperatures tested is shown in Fig.4-16. The whole of the surface is creamy brown in colour except a few nodular eruptions here and there which are grayish black in colour. For the specimen treated at  $950^\circ\text{C}$ , however, these eruptions are absent.

Spall particles are mostly in the form of a fine powder (creamy brown in color) at all temperatures being progressively in larger amounts at the higher temperatures. They are non-magnetic in nature.

The optical cross-section of this alloy after 17 3-hour cycles at  $1000^\circ\text{C}$  reveals a more or less continuous convoluted oxide scale as shown in Fig. 4-17. The substrate surface of the specimen shows the presence of voids as usual. At  $1050^\circ\text{C}$  after an exposure of 19 3-hour cycles (i.e. 57 hours), the microstructure of the same alloy represented no significant differences with regard to thickness and structure as shown in Fig. 4-18.

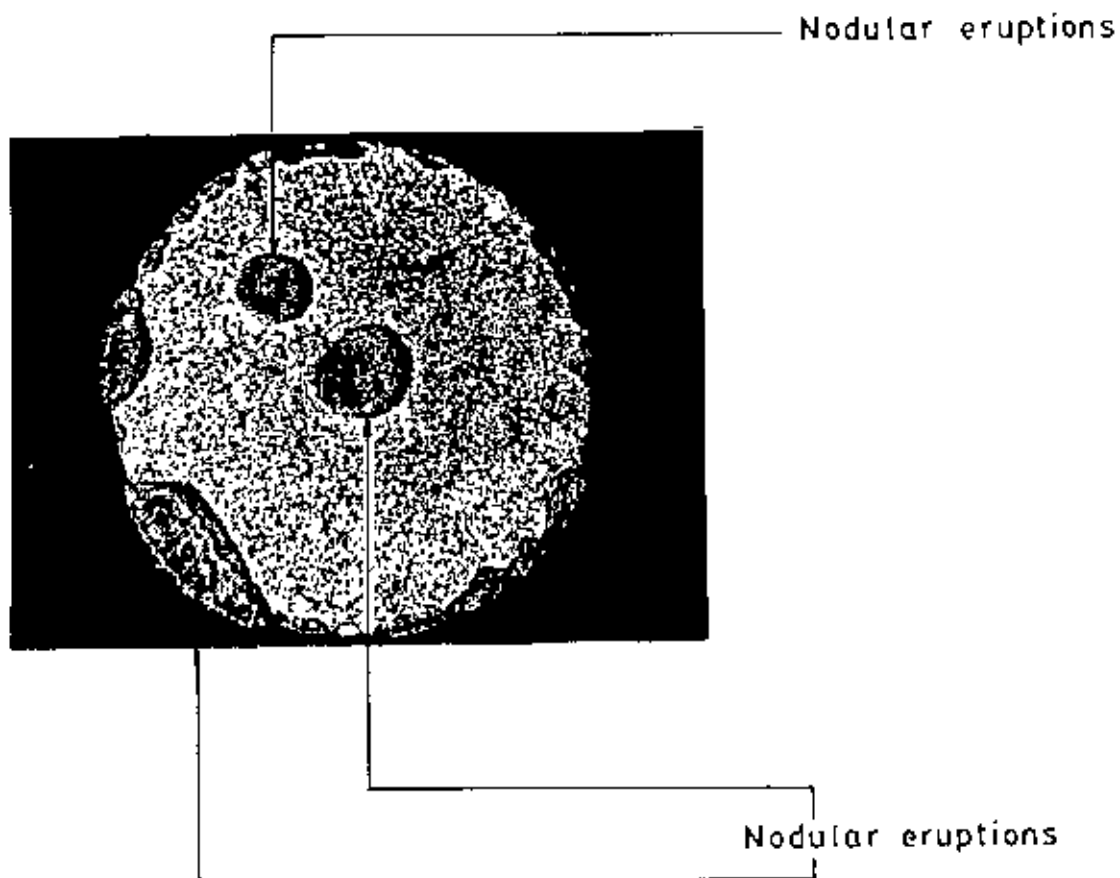


Fig. 4-16 : Macrograph of an Fe-10Cr-6Al alloy specimen (surface appearance) after 57 hours (19 3-hour cycles) of exposure at 1050°C, x 4, showing random nodular eruptions.

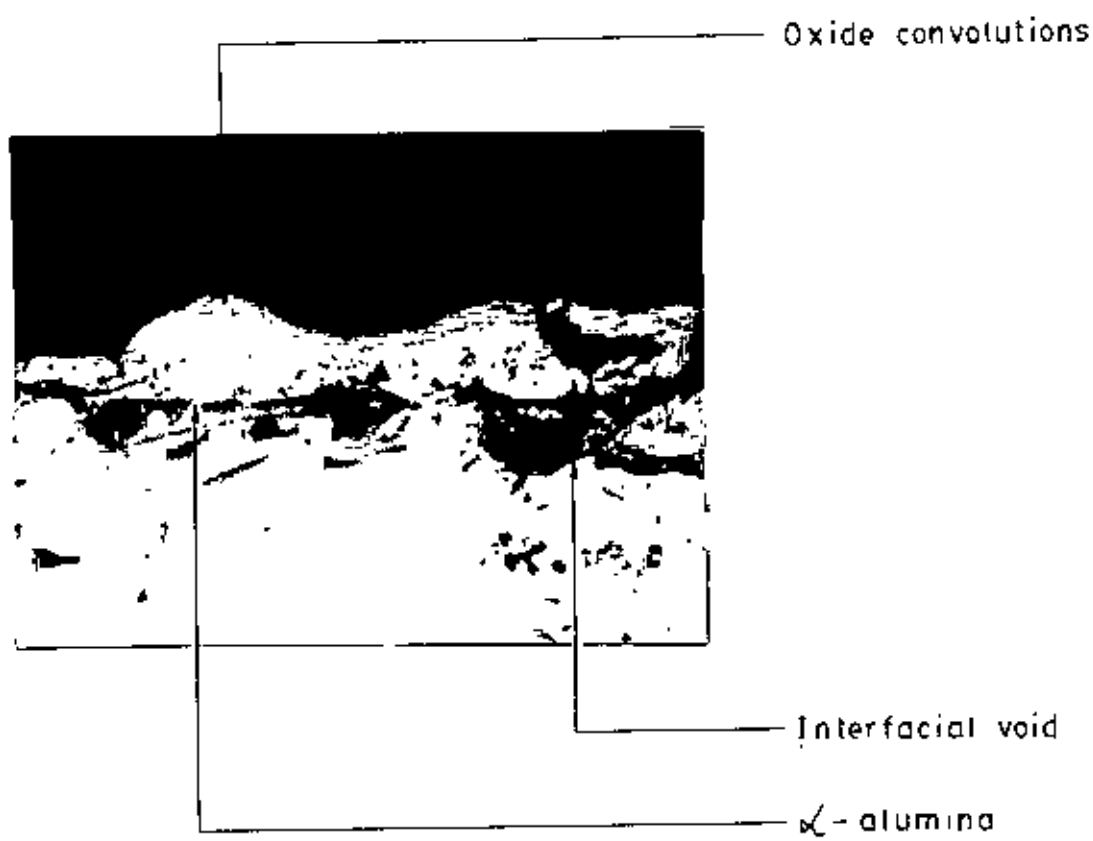


Fig. 4-17 : Optical cross-section of the oxide scale on an Fe-10Cr-6Al alloy specimen oxidized for 17 3-hour cycles at 1000°C, x 1200. The scale appears to have developed convolutions. Void formation may also be noticed at the interface region.

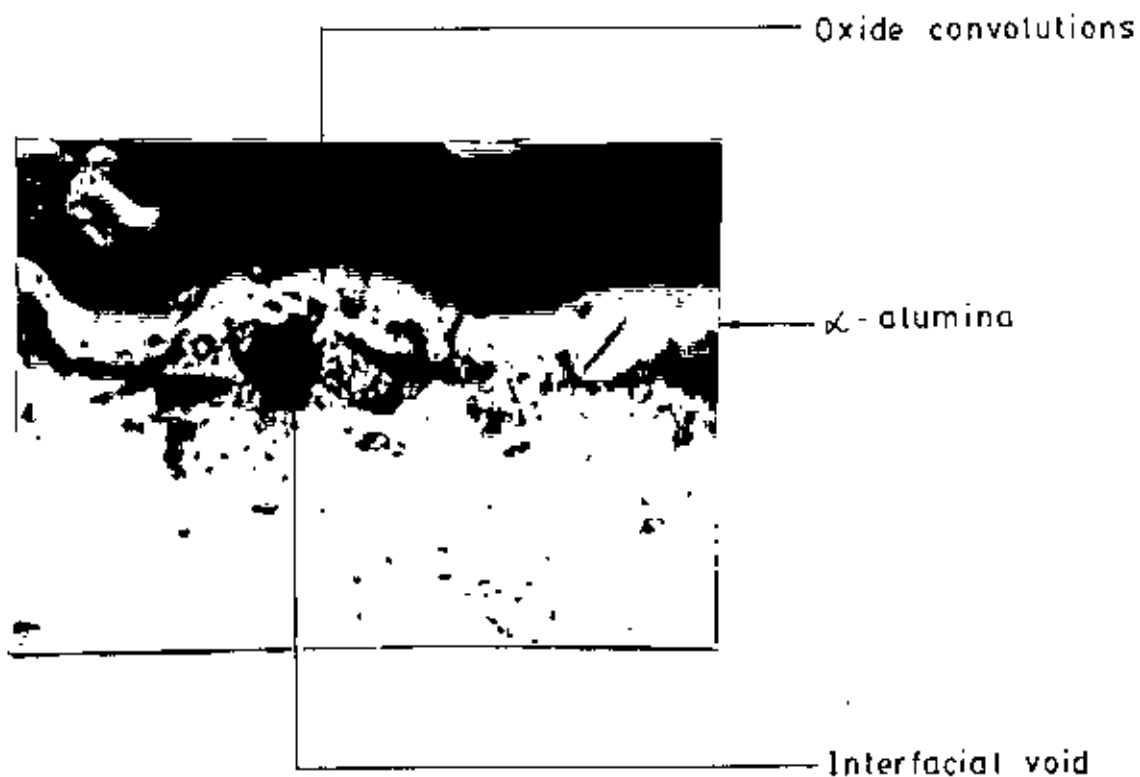


Fig. 4-18 : Microstructure of oxide scale on an Fe-10Cr-6Al alloy specimen after an exposure of 19 3-hour cycles at 1050°C, x 1200. A more or less convoluted oxide scale with void formations at the interface region may be noticed.

#### 4.24 Fe-10Cr-8Al Alloy

The oxidation kinetics of Fe-10Cr-8Al alloy at 950°C after 51 hours (17 3-hour cycles) of exposure in pure O<sub>2</sub> at 1 atmosphere pressure is presented in Fig. 4.19. The above alloy is observed to form a protective scale initially which prolongs upto 18-27 hours (curves OA<sub>1</sub> and OA<sub>2</sub>). This scale suffers breakaway resulting in an increase in the oxidation rates (curves A<sub>1</sub>B<sub>1</sub> and A<sub>2</sub>B<sub>2</sub>). After this breakaway a second protective scale begins to form which reduces the oxidation rates. This protective scale continues upto the rest of the run.

The specific weight gain values of the above alloy for 17 3-hour cycles (i.e. 51 hours) are found to be 0.82 mg/cm<sup>2</sup>, 0.57 mg/cm<sup>2</sup> and 0.55 mg/cm<sup>2</sup> for the three specimens tested.

It may be mentioned that there are virtually no eruptions on the specimen surface treated at this temperature unlike those treated at the higher temperatures. The whole surface presents a creamy brown colour free from any eruptions.

The kinetics curves for the same alloy at 1000°C under thermal cycling in pure O<sub>2</sub> at 1 atmosphere pressure are shown in Fig. 4-20. The initial oxidation behaviour at this temperature is almost identical as that for 950°C.

Initially a protective scale forms at this temperature as well which persists for only about 5-8 hours (curves OA<sub>1</sub>, OA<sub>2</sub>, OA<sub>3</sub>). This scale then starts to breakaway as marked by a gradual increase in the rate of oxidation for quite a long period (curves A<sub>1</sub>B<sub>1</sub>, A<sub>2</sub>B<sub>2</sub>,

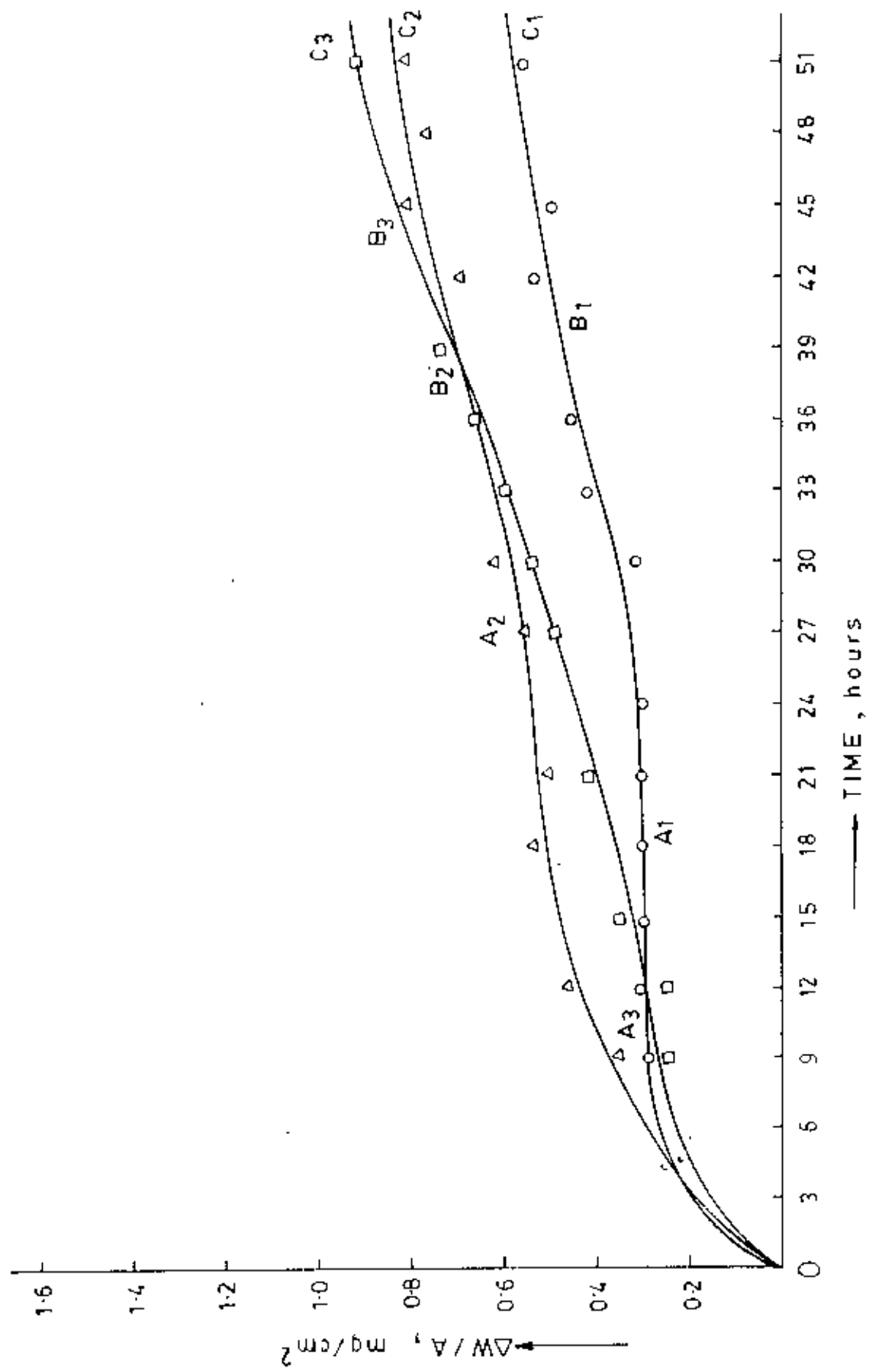


Fig. 4-19 : Cyclic oxidation kinetics of Fe-10Cr-8Al alloy at 950°C.

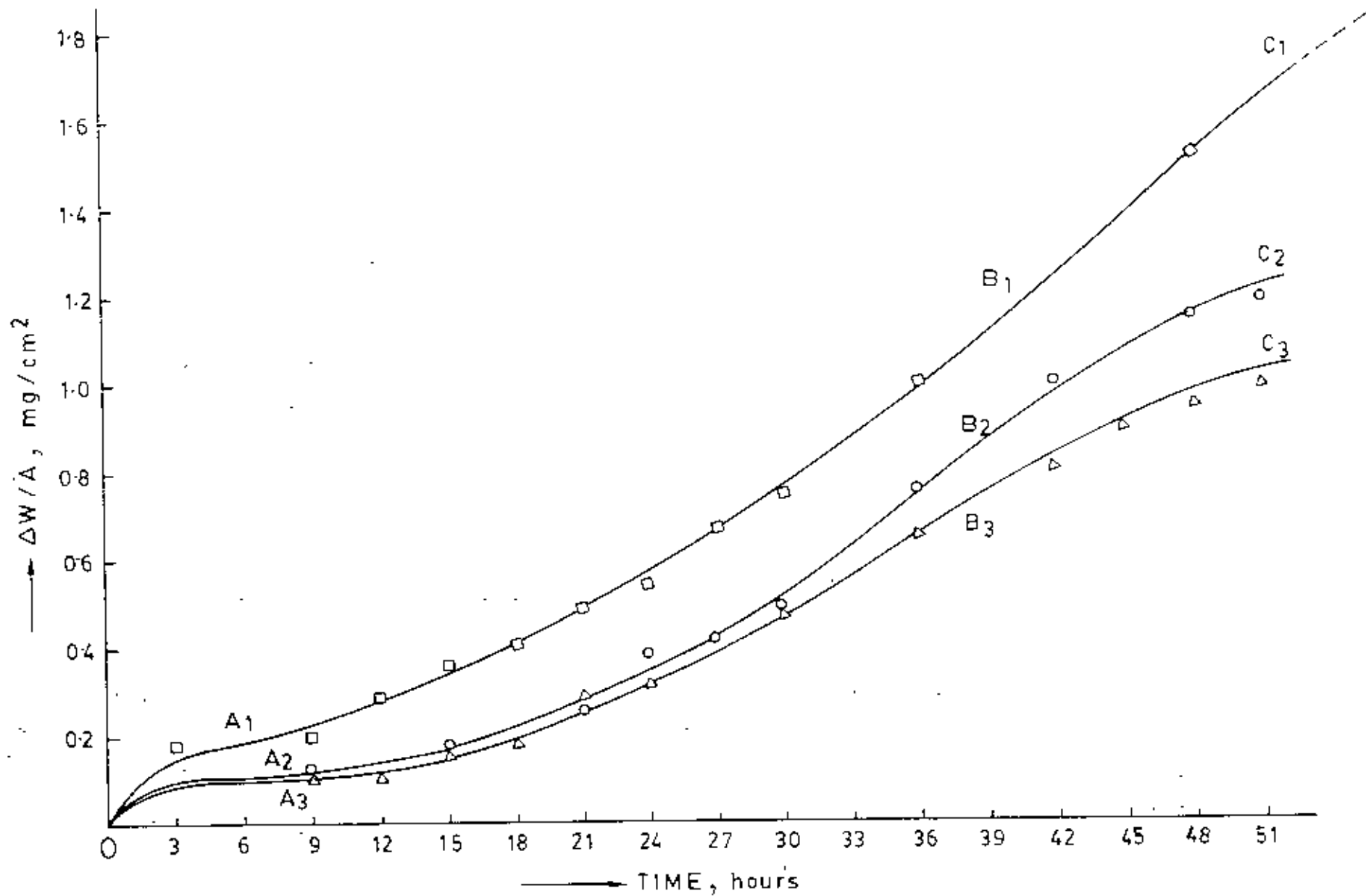


Fig. 4-20 : Cyclic oxidation kinetics of Fe-10Cr-8Al alloy at  $1000^\circ\text{C}$ .



$A_3B_3$ ). After this breakaway the rate of oxidation subsides (curves  $B_1C_1$ ,  $B_2C_2$ ,  $B_3C_3$ ) due to the formation of a second protective scale which persists till the end of the run.

From the thermogravimetric data, the specific weight gain values after a period of 17 3-hour cycles (i.e. 51 hours) during thermal treatment of the three specimens of the above alloy are recorded to be  $1.81 \text{ mg/cm}^2$ ,  $1.15 \text{ mg/cm}^2$  and  $0.99 \text{ mg/cm}^2$ . No eruptions could be observed for this 8% Al alloy at  $1000^\circ\text{C}$  as well; the whole surface, of course, is creamy brown in colour as usual.

The oxidation kinetics of the above alloy at  $1050^\circ\text{C}$  during thermal cycling in pure  $\text{O}_2$  at 1 atmosphere pressure can be observed in Fig. 4-21. The initial oxidation behaviour at this temperature is almost similar as that at  $950^\circ\text{C}$  and  $1000^\circ\text{C}$ .

It can be observed that a protective scale is also formed at this temperature as well which persists upto 3 hours as indicated in curves  $OA_1$  and  $OA_2$  and this scale suffers breakaway (curves  $A_1B_1$  and  $A_2B_2$ ). After this breakaway, a second protective scale starts to form resulting in a gradual decrease in the oxidation rates as apparent from the curves  $B_1C_1$  and  $B_2C_2$ . Unexpectedly, this second protective scale also fails to offer protection and a second stage breakdown occurs in the course of time again causing a catastrophic rate of oxidation (curves  $C_1D_1$  and  $C_2D_2$ ). Subsequently, the catastrophic rate of oxidation begins to subside as represented by curves  $D_1E_1$  and  $D_2E_2$ .

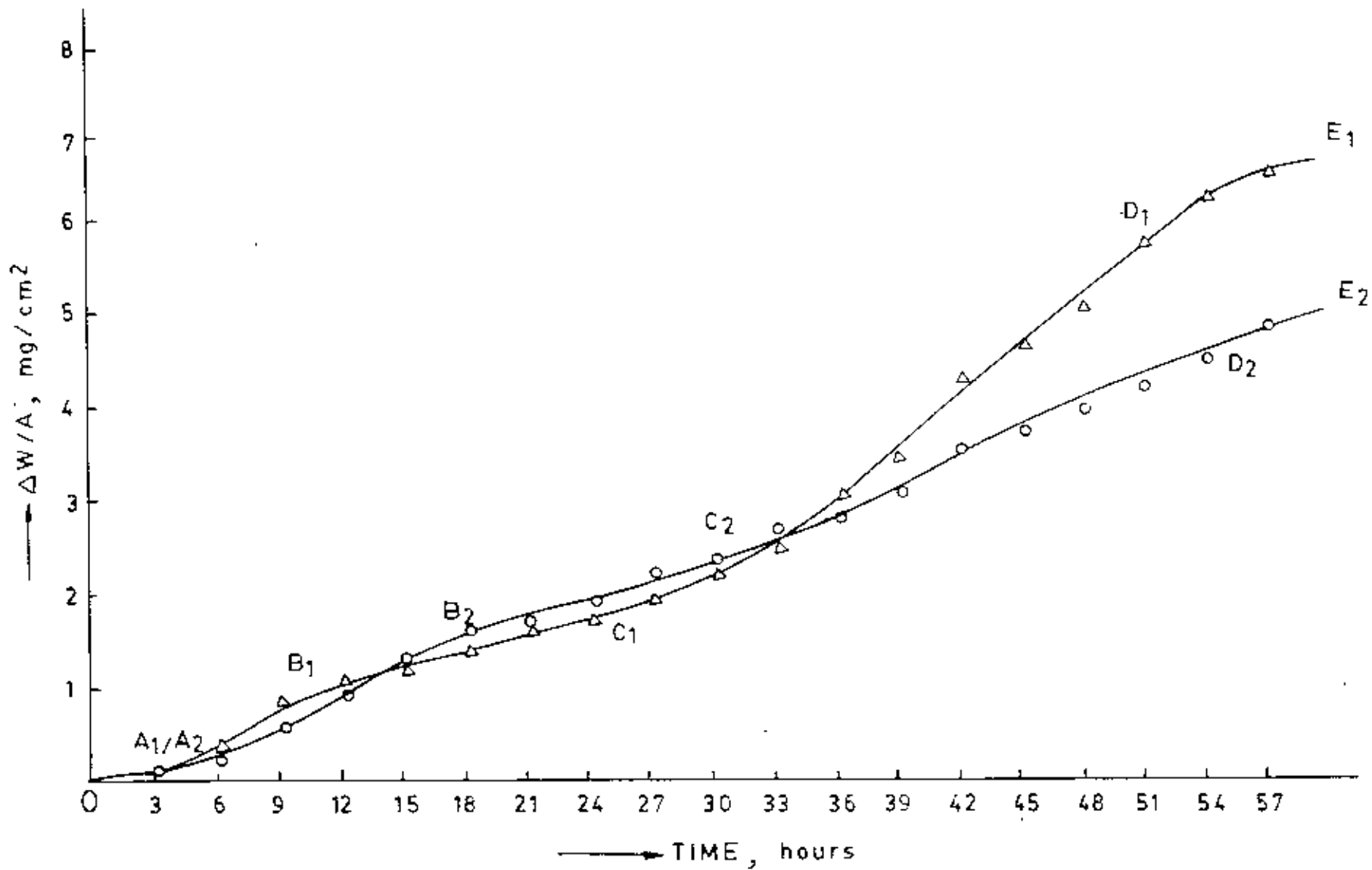


Fig. 4-21 : Cyclic oxidation kinetics of Fe-10Cr-8Al alloy at  $1050^\circ\text{C}$ .

The specific weight gain values of the above alloy after 19 3-hour cycles (i.e. 57 hours) are observed to be  $6.38 \text{ mg/cm}^2$  and  $5.54 \text{ mg/cm}^2$  at  $1050^\circ\text{C}$  for the two specimens treated.

Visual examination of the specimens at  $1050^\circ\text{C}$  reveals the existence of small grayish nodular eruptions less in quantity than that observed for Fe-10Cr-6Al alloy at the same temperature, the rest of the specimen surface being of a creamy brown colour.

Optical cross-section of this alloy after 17 3-hour cycles at  $1000^\circ\text{C}$  shows a more or less convoluted oxide scale layer as represented in Fig. 4-22. After 19 3-hour cycles (i.e. 57 hours) the same alloy represents a thin, continuous scale at  $1050^\circ\text{C}$  in the optical cross-section as observed in Fig. 4-23. The spall particles are observed in the form of a fine powder, creamy brown in colour and non-magnetic in nature at each of the temperatures, but the amount of spall particles are found to be less in quantity compared to that observed for the Fe-10Cr-6Al alloy at the same temperature.

#### 4.25 Effect of Aluminium-Content

A graph of (combined) specific weight gain vs per cent Al is shown in Fig.4-24 for all the three temperature levels ( $950^\circ\text{C}$ ,  $1000^\circ\text{C}$  and  $1050^\circ\text{C}$ ). It will be noticed that the oxidation rate, as measured by specific weight gain, declines gradually reaching a minimum value with 8% Al. This is also evident from Fig.4-25, Fig.4-26 and Fig.4-27 represented oxidation kinetics of the alloys

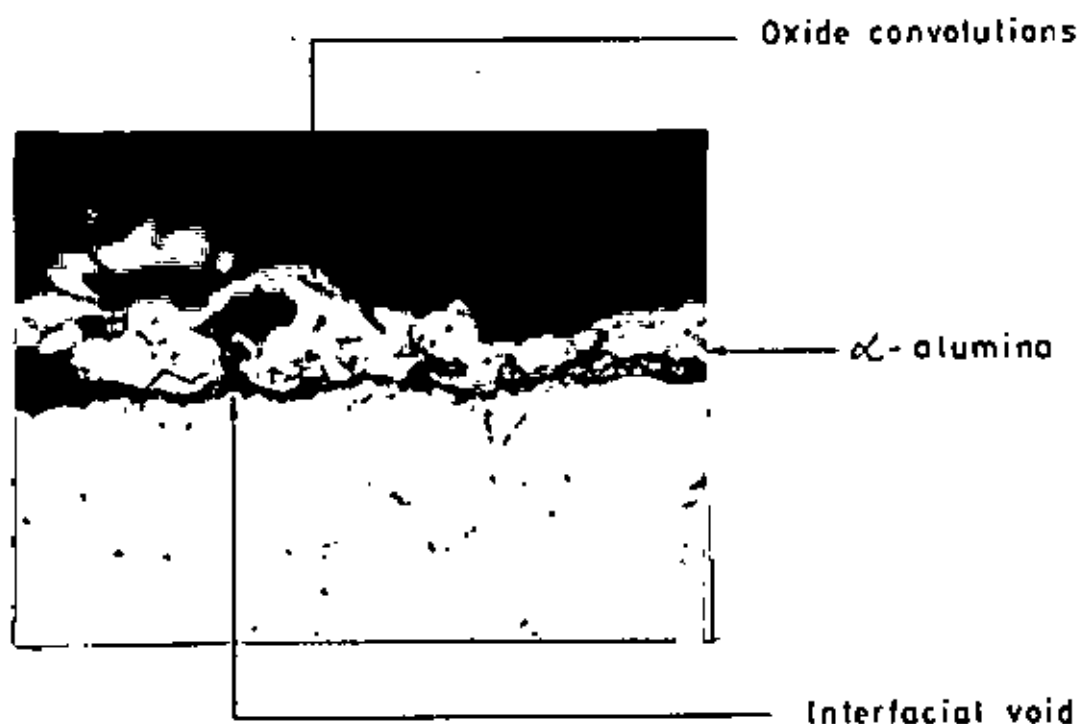


Fig. 4-22: Optical cross-section of  $\alpha$ - $\text{Al}_2\text{O}_3$  oxide scale on an Fe-10Cr-8Al alloy specimen after an exposure of 51 hours (17 3-hour cycles) at  $1000^\circ\text{C}$ , x 1200. A more or less convoluted oxide scale with void formation at the interface region may be noticed.

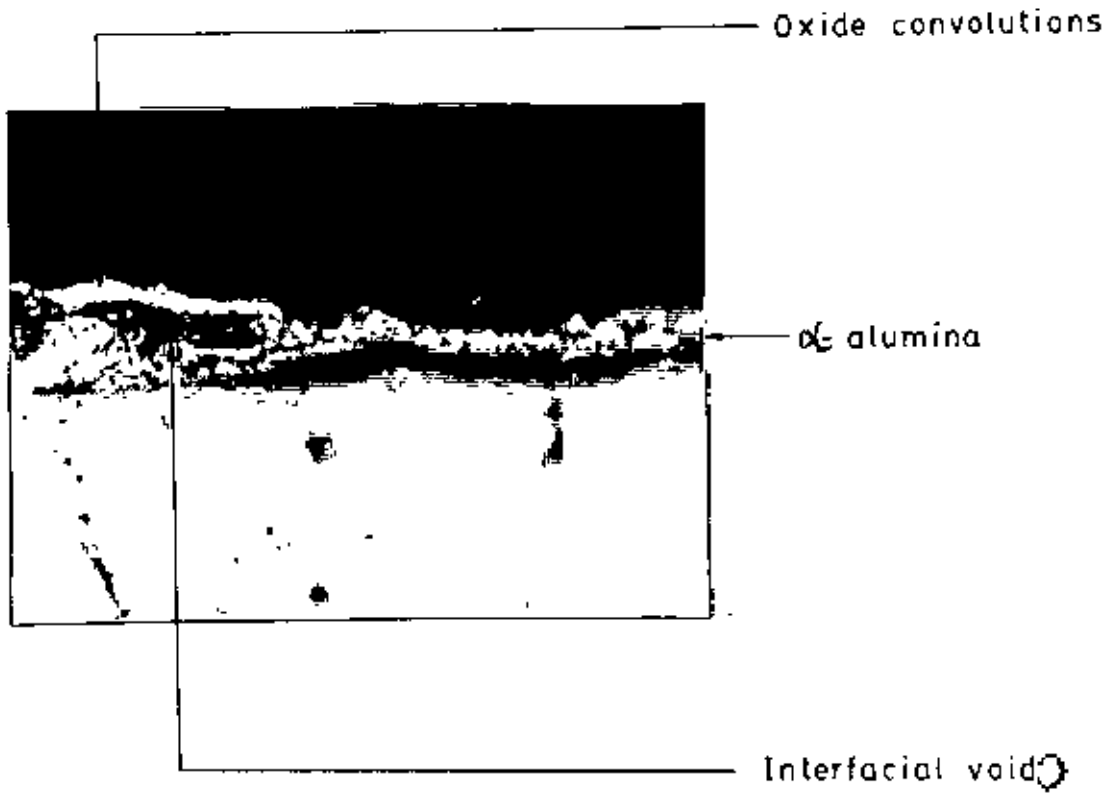


Fig. 4-23: Microstructure of oxide scale ( $\alpha$ - $\text{Al}_2\text{O}_3$ ) on an Fe-10Cr-8Al alloy specimen after an exposure for 19 3-hour cycles at  $1050^\circ\text{C}$ , x 1200. The scale appears to have developed convolutions.

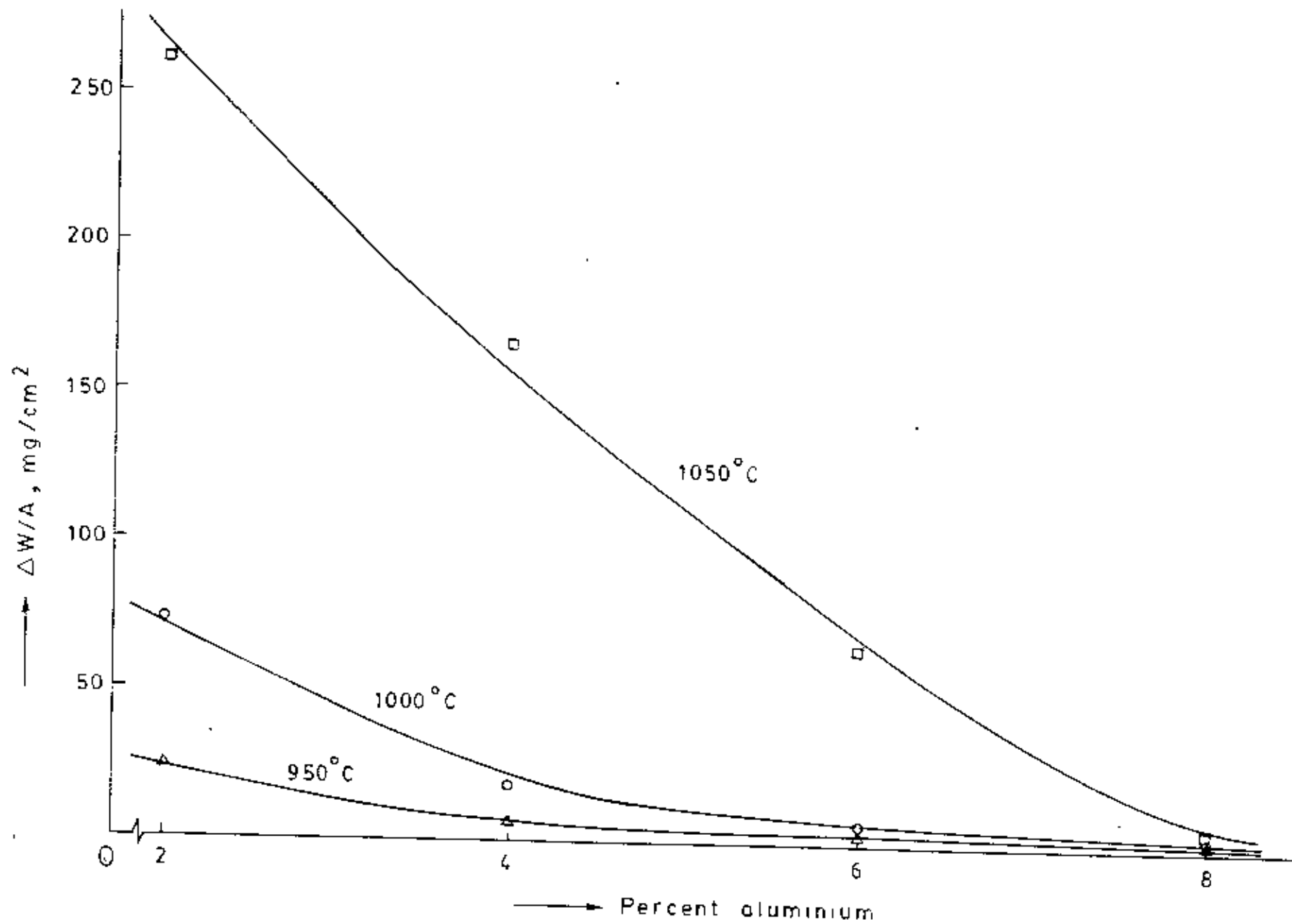


Fig. 4-24 : Effect of Al-content and temperature upon specific weight gain (48-hour basis) of the modified Fe-10Cr alloys.

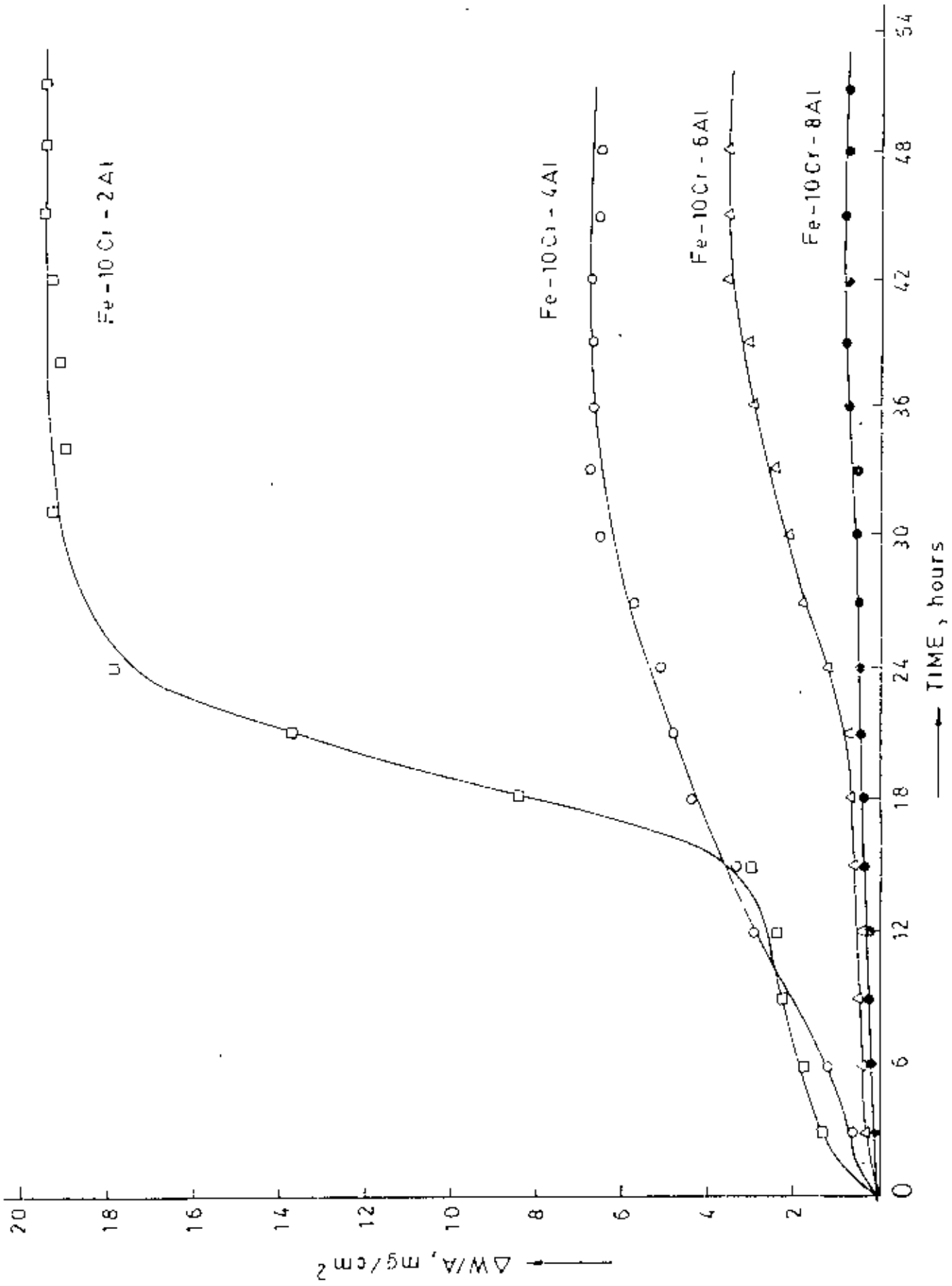


Fig. 4-25: Influence of aluminum-content on the oxidation kinetics of the modified Fe-10Cr alloys (2-8%Al) at 950°C.

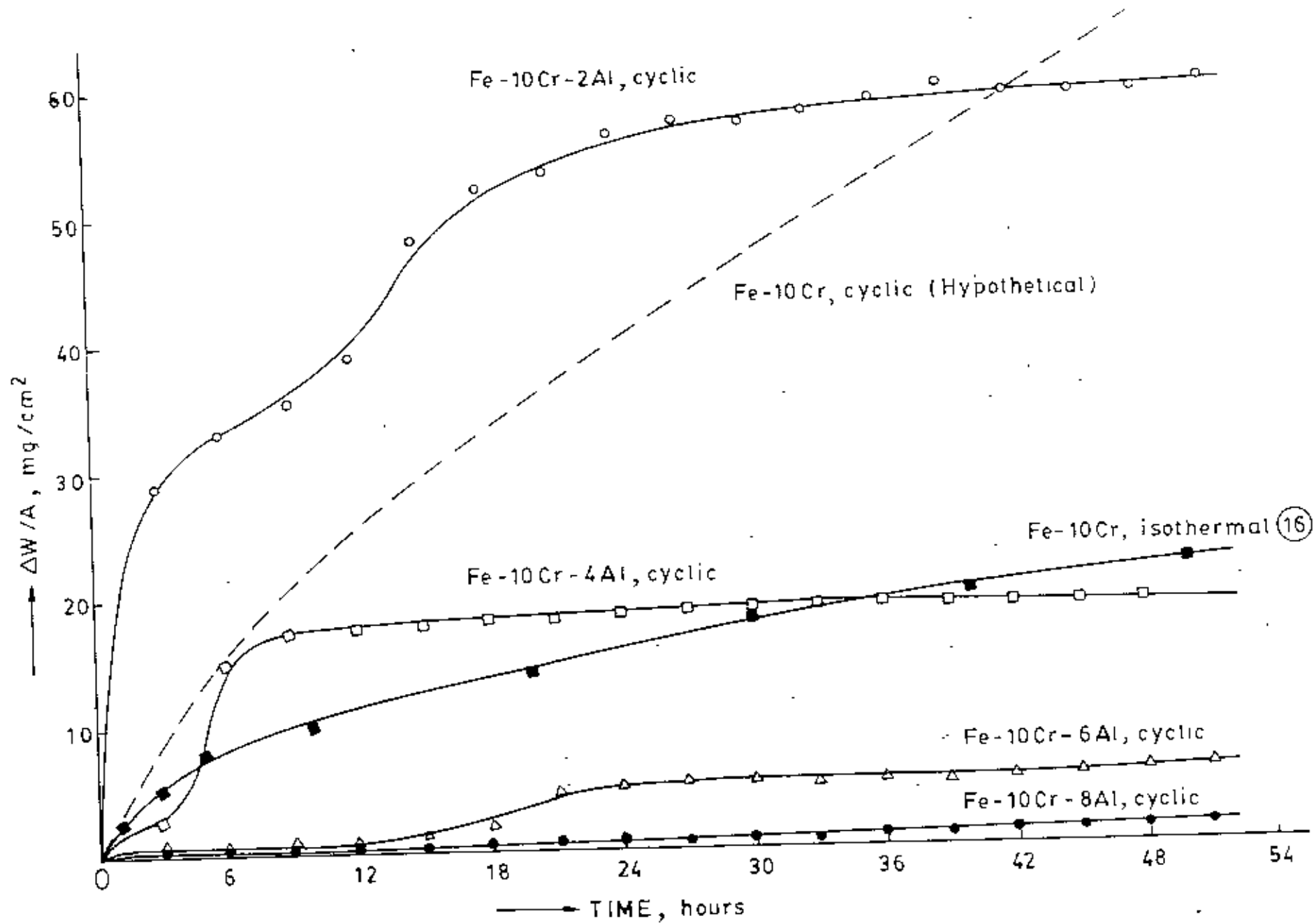


Fig. 4-26 : Comparison of cyclic oxidation kinetics of the modified Fe-10Cr alloys with 2-8% aluminium at 1000°C.



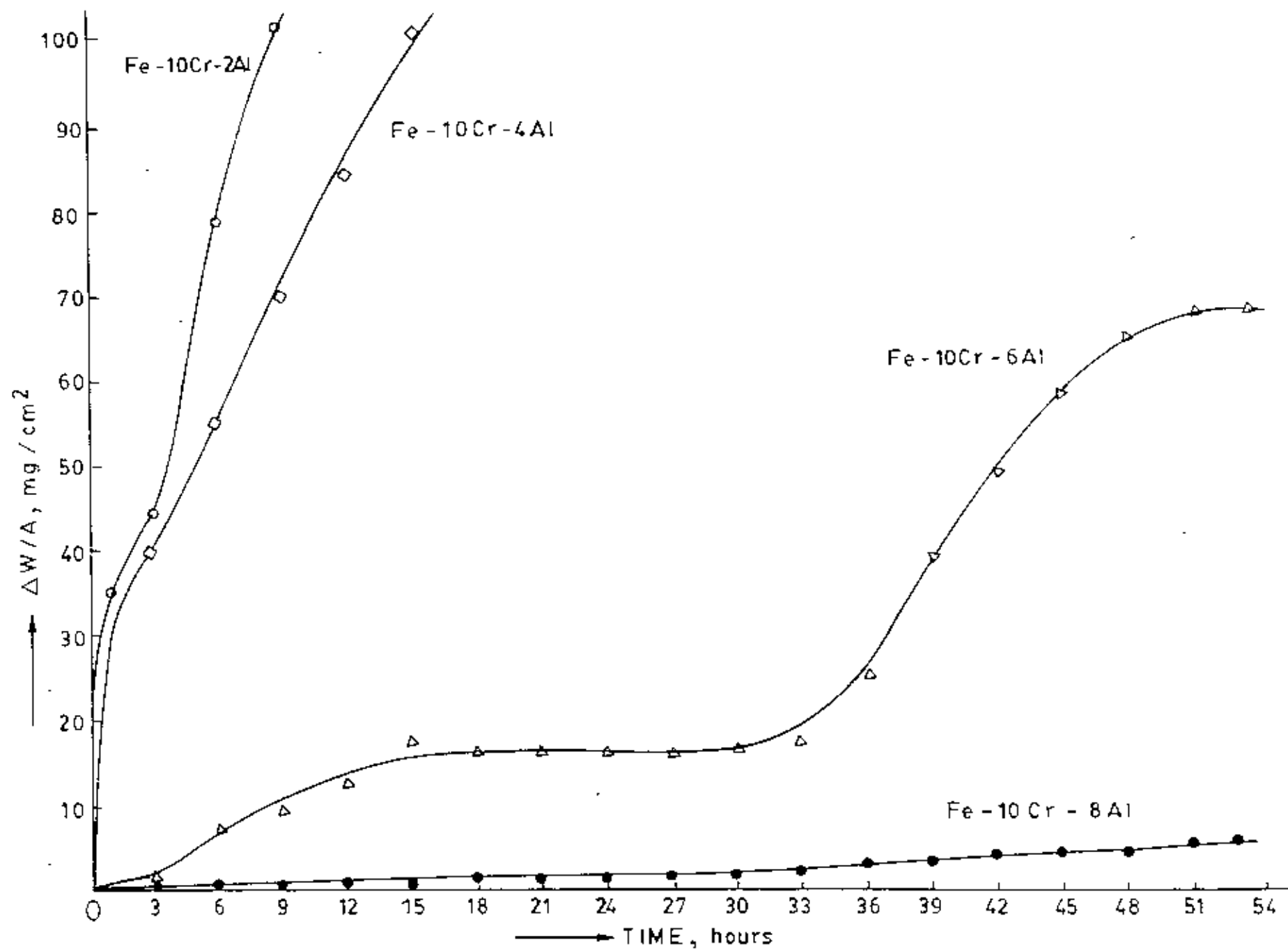


Fig.4-27: Effect of aluminium-content on the oxidation kinetics of the modified Fe-10Cr alloys (2-8%Al) at 1050°C.

at 950<sup>0</sup>C, 1000<sup>0</sup>C and 1050<sup>0</sup>C respectively, which reveals that the rate of oxidation decreases with the increase of aluminium-content.

In Fig. 4-26 the oxidation kinetics of the binary alloy-both isothermal and cyclic (hypothetical)-have been included along with the cyclic data for the modified alloys at 1000<sup>0</sup>C. The isothermal kinetics curve for the binary Fe-10Cr alloy is obviously situated much below the cyclic (hypothetical) curve. It will be also noticed that even the slope of the kinetics curve for the cyclic oxidation of the 2%Al alloy is much 'lower' than that for the binary Fe-10Cr alloy (at 1000<sup>0</sup>C) i.e. the oxidation rate of the modified alloy with the lowest Al-content is even lower than that for the binary Fe-10Cr alloy. Clearly, the alloys containing higher Al have oxidation rates much lower than the 2% Al alloy.

In general, the onset of initial spallation has been found to be delayed with increasing Al-content. The individual spall particles are noticed to be progressively finer with the increase of Al-content in the base alloy and a gradual decrease in the amount of spall particles.

To sum up the following general observation can be made:

1. Under cyclic conditions, the rate of oxidation in terms of specific weight gain attains a minimum value with 8% Al in the alloy.

2. The difference between sp. wt. gain values at various temperatures tends to increase in general as the alloy Al-content decreases, or in the other words, the effect of thermal cycling has been observed to be more severe upon the lower Al alloys.
3. The individual spall particles were grayish black in colour and are in the form of large thin flakes being magnetic in nature for 2% Al and 4% Al alloys. On the other hand, the spall particles are in the form of a very fine powder being creamy brown in colour and non-magnetic in nature for the 6% Al and 8% Al alloys.
4. On visual examination, the surface appearance shows the presence of black patches running between gray to dark gray areas with the 2% Al and 4% Al alloys, but oxidized specimens for the 6% Al and 8% Al alloys reveals creamy brown areas with a few large to gradually small nodular eruptions. The number of eruptions increases at higher temperatures.
5. Optical cross-section of the oxidized specimens at the end of the run shows the presence of  $\text{Cr}_2\text{O}_3$  and  $\text{Cr}_2\text{O}_3/\alpha\text{-Al}_2\text{O}_3$  subscale layer at the scale base in 2% Al and 4% Al alloys respectively whereas only  $\alpha\text{-Al}_2\text{O}_3$  scale can be observed in the 6% Al and 8% Al alloys under the microscope upon the oxidized specimens.

#### 4.26 Effect of Temperature

Graphs of combined specific weight gain vs time at various temperatures for 2% Al, 4% Al 6% Al and 8% Al alloys are shown in Fig. 4-28, Fig. 4-29, Fig. 4-30 and Fig. 4-31 respectively. It will be noticed that the oxidation rate in terms of specific weight gain values increases with the higher temperatures for each of the alloys.

#### 4.3 Discussion

As reported by Wood et al (29), binary Fe-Cr alloys containing Cr in the range of about 14-25% at 900-1100<sup>0</sup>C immediately forms a continuous protective scale of Cr<sub>2</sub>O<sub>3</sub> upon the surface. When a more reactive element is present (such as Ce,Al,Y,Ti etc.), this Cr<sub>2</sub>O<sub>3</sub> scale is formed even with much lower percentages of Cr i.e. 10-13% (38). Rhys-Jones et al (16) observe that such a scale is formed even with 10%Cr at 1000<sup>0</sup>C containing as little as 0.9%Ce after 10 minutes exposure in pure oxygen at 100 torr. It appears, therefore, possible that the initial scale existing on the surfaces of the Fe-10Cr alloys containing 2% Al and 4% Al at temperatures between 950<sup>0</sup>C and 1050<sup>0</sup>C is a Cr<sub>2</sub>O<sub>3</sub> scale.

The oxidation kinetics data as represented in Fig.4-2 for Fe-10Cr-2Al alloy at 950<sup>0</sup>C reveals that initially a protective scale forms on the surface of the alloy. It is apparent from the diffractometer data presented in Table 4-I that the scale is of

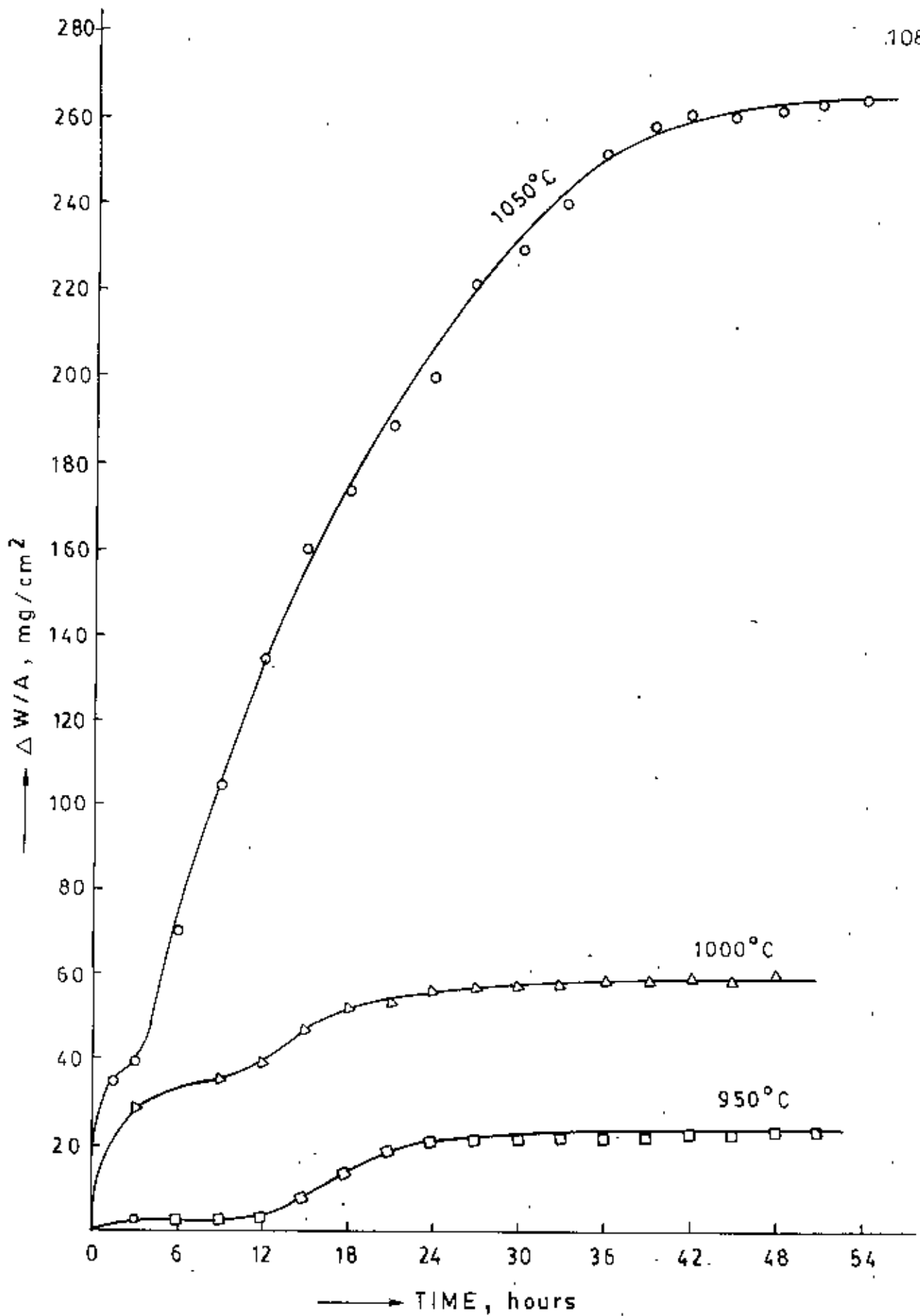


Fig. 4-28: Effect of temperature on the oxidation behaviour of Fe-10Cr-2Al alloy.

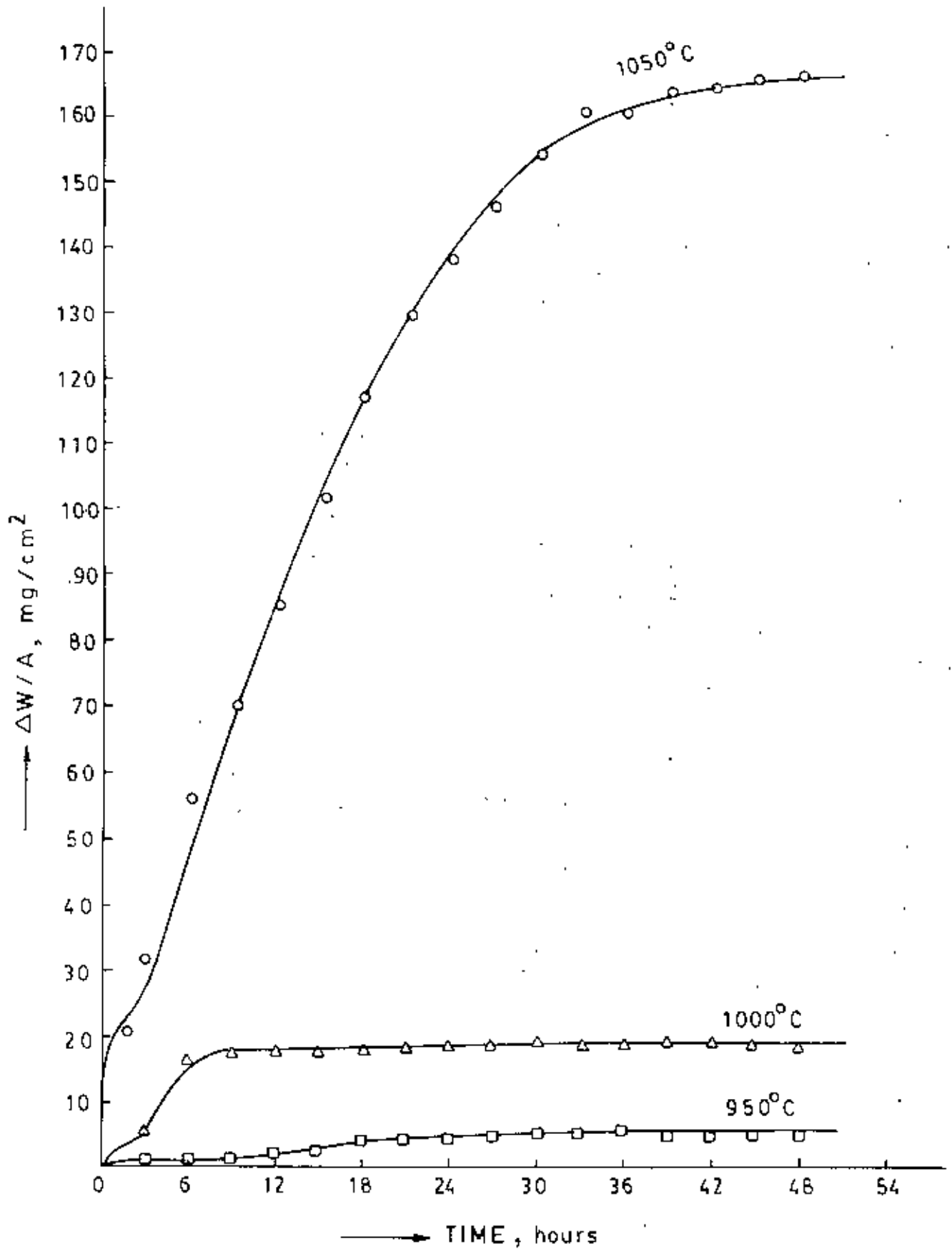


Fig. 4-29: Effect of temperature on the oxidation behaviour of Fe-10Cr-4Al alloy.

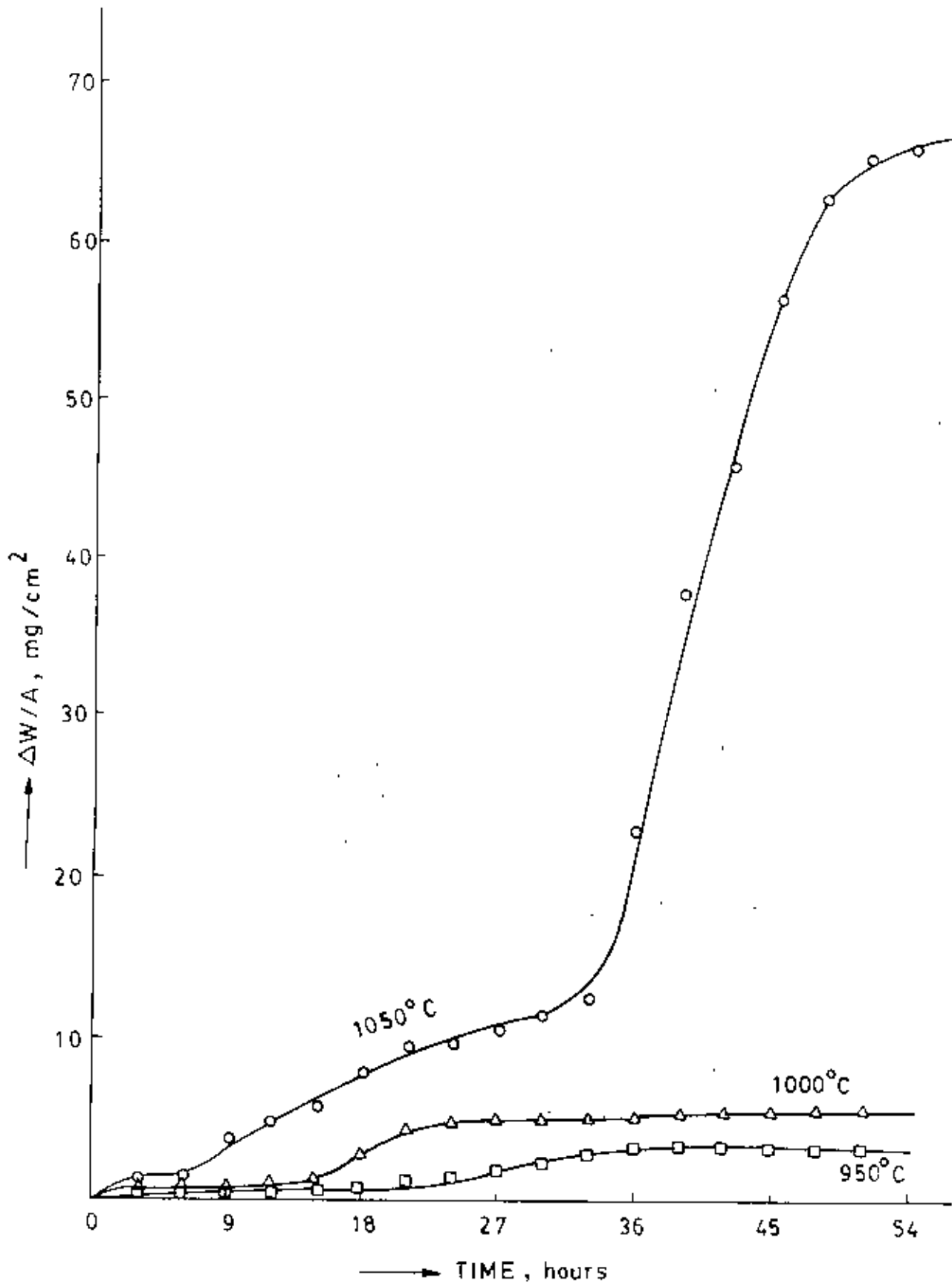


Fig. 4-30: Effect of temperature on the oxidation behaviour of Fe-10Cr-6Al alloy.

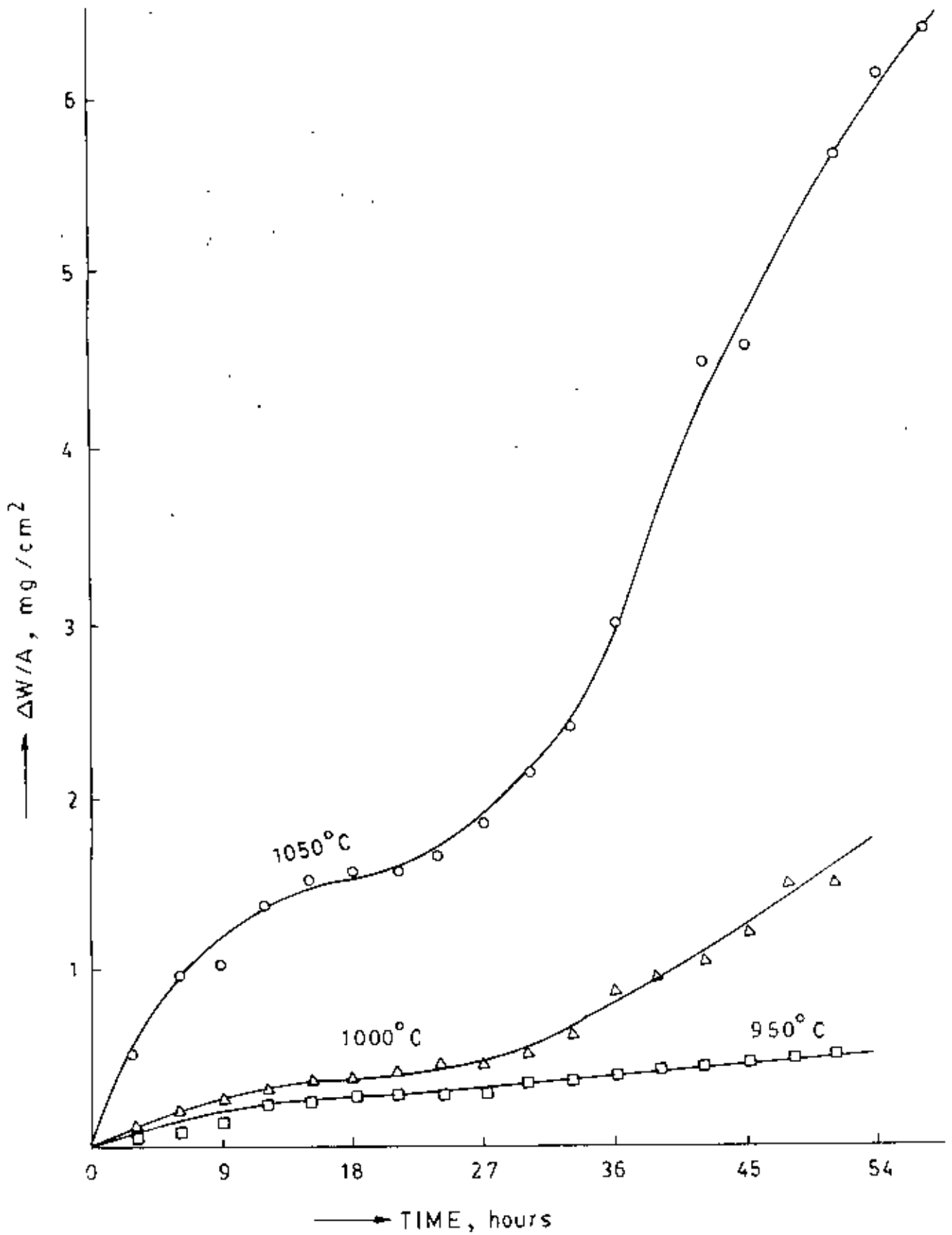


Fig. 4-31: Effect of temperature on the oxidation behaviour of Fe-10Cr-8Al alloy.



Table 4.1  
X-ray Analysis for Fe-10Cr-2Al Alloy

		Phase	$Fe_2O_3$	$Cr_2O_3$	$FeCr_2O_4$	$(Cr, Fe)_2O_3$ $Fe(Cr, Al)_2O_4$	$FeO$
950°C	51 hours	I/I <sub>0</sub>	100/75	27/37/30	32	30	29
950°C	8 hours	Phase	$(Cr, Fe)_2O_3$	$Fe_2O_3$	$Cr_2O_3$	$Fe(Cr, Al)_2O_4$	$FeO$
		I/I <sub>0</sub>	100/20	95/31	70/50	52/27	18
1000°C	48 hours	Phase	$Fe_2O_3$	$Fe(Cr, Al)_2O_4$	$Cr_2O_3$	$(Cr, Fe)_2O_3$	
		I/I <sub>0</sub>	100/30	44	16	13/10	
1000°C	6 hours	Phase	$Cr_2O_3$	$(Cr, Fe)_2O_3$	$Cr_2O_3, FeO$ $Fe(Cr, Al)_2O_4$		
		I/I <sub>0</sub>	100	19	7/6		
1050°C	54 hours	Phase	$Fe_2O_3$	$Fe_2O_3$			
		I/I <sub>0</sub>	100	18			
1050°C	9 hours	Phase	$Cr_2O_3$	$Fe_2O_3$	$Fe(Cr, Al)_2O_4$		$Fe_2O_3$
		I/I <sub>0</sub>	100/35	15	34/28		32
1050°C	4 hours	Phase	$Fe_2O_3$	$Cr_2O_3$	$(Cr, Fe)_2O_3$	$Fe(Cr, Al)_2O_4$	
		I/I <sub>0</sub>	100/43	55/35/34/30	25	21	

$\text{Cr}_2\text{O}_3$  since a strong peak for  $\text{Cr}_2\text{O}_3$  is noticeable in the diagram for 8 hours specimen. This external  $\text{Cr}_2\text{O}_3$  scale suffers breakaway after about 11 hours, ultimately reaching a more or less steady state in about 27 hours.

As breakaway proceeds Fe begins to oxidize as depletion of Cr in the bulk alloy has already taken place rapidly. This is why the oxidation rate after breakaway increases to a high value corresponding to that for the formation of  $\text{Fe}_2\text{O}_3/\text{Fe}_3\text{O}_4$ . When an iron oxide scale has thus formed upon the surface, the oxygen pressure becomes less behind this scale and hence internal oxidation of Cr takes place. In the course of time,  $\text{Cr}_2\text{O}_3$  may combine with FeO to form Fe-Cr spinel,  $\text{FeCr}_2\text{O}_4$ , and also  $\alpha\text{-Al}_2\text{O}_3$  may combine with both FeO and  $\text{Cr}_2\text{O}_3$  to form Fe-Cr-Al spinel,  $\text{Fe}(\text{Cr},\text{Al})_2\text{O}_4$ . These internal oxide particles will ultimately coalesce together to form a more or less continuous subscale layer of  $\text{Cr}_2\text{O}_3$  scale through which the diffusion of the cation is relatively slow and the oxidation rate, therefore, settles down to a more or less steady state value. The presence of the spinel layer is apparent from the X-ray data (Table 4-I) for 51 hours specimen and a more or less continuous subscale layer is visible in the photomicrograph for the scale at  $950^\circ\text{C}$  (Fig.4-5).

The photomicrograph at  $950^\circ\text{C}$  also supports the X-ray data in which a spinel layer can be observed in the inner region and an  $\text{Fe}_2\text{O}_3$  layer in the outer region. The subscale formed by the coalescence of the particles of  $\text{Cr}_2\text{O}_3$  at the alloy-oxide interface

is the principal rate-determining factor for further oxidation and the oxidation rate, therefore, settles down to a more or less steady state value.

The kinetics data for this alloy at 1000°C reveals the breakaway of the initial  $\text{Cr}_2\text{O}_3$  scale in about 7-8 hours. A final duplex scale consisting of an  $\text{Fe}_2\text{O}_3$  at the top with a spinel layer at the bottom is also believed to persist on the surface of the alloy at this temperature as well till the end of the run. This is evident from the data presented in Table 4-I (for 1000°C) after 48 hours of exposure in which a strong peak of  $\text{Fe}_2\text{O}_3$  can be identified. The optical cross-section of the scale at this temperature is observed to be similar to that shown in Fig. 4-5.

A  $\text{Cr}_2\text{O}_3$  scale also marks the initial stages of oxidation of this alloy at 1050°C. This is apparent from the diffractometer data of the specimens oxidized for 4 hours and 9 hours at this temperature. The  $\text{Cr}_2\text{O}_3$ , of course, is gradually converted to spinel, as evident from these data. The scale finally changes to oxides of iron probably due to gradual loss of the  $\text{Cr}_2\text{O}_3$  by volatilization and it is found to consist almost entirely of  $\text{Fe}_3\text{O}_4$ . It is interesting to note that although the final scale forms is  $\text{Fe}_3\text{O}_4$  for which the oxidation rate should have been considerable, yet the specific weight gain of the specimens shows no increase in their values during this stage of the run (as apparent from the kinetics curves). This paradoxical behaviour is explained by visual examination of the specimens which reveals that both the specimens

are completely oxidized probably after about 42-48 hours of exposure. On examination of the specimen, under the optical microscope, however, the specimen was observed to have been completely oxidized. This probably explains why, after about 42-48 hours the kinetics curves levels down to a constant specific weight gain value ( $\approx 220-265 \text{ mg/cm}^2$ ).

Progressive coarsening in the size of the individual spall particles with rising temperature is presumably related to a depletion of Cr from the underlying alloy with consequent changes in alloy plasticity and expansion properties at the high temperature as observed by Islam (35) during cyclic oxidation of Co-10Cr alloy between  $900-1100^\circ$ . Moreover these particles are believed to be predominantly oxides of iron as suggested by their magnetic nature and dark blackish colour.

The oxidation kinetics data of Fe-10Cr-4Al alloy represented in Fig.4-7 for this alloy at  $950^\circ\text{C}$  establishes that initially a protective  $\text{Cr}_2\text{O}_3$  scale forms on the surfaces as already observed for the 2% Al alloy. When this scale undergoes breakaway, both Al and Cr probably oxidized internally to form discrete oxide particles which render protection to the alloy in subsequent cycles. The x-ray analysis also reveals the presence of both  $\text{Cr}_2\text{O}_3$  and  $\alpha\text{-Al}_2\text{O}_3$  particles in the scale as presented in Table 4-II. The reduction in oxidation rates during the last 12 hours and subsequent flattening of the kinetics curves will bear testimony to this fact. These oxide particles coalesce to form a more or less continuous layer at

Table-4.II  
X-ray Analysis for Fe-10Cr-4Al Alloy

950°C	51 hours	Phase	$Fe_2O_3$	$Cr_2O_3$	$(Cr, Fe)_2O_3$	$Fe(Cr, Al)_2O_4$ $\alpha-Al_2O_3$ (2)		
		I/I <sub>0</sub>	100/25 /14	20	18	13		
1000°C	48 hours	Phase	$Fe_2O_3$	$Fe(Cr, Al)_2O_4$	$\alpha-Al_2O_3$	$Cr_2O_3$		
		I/I <sub>0</sub>	100/38	88	61	41		
1000°C	6 hours	Phase	$Fe_2O_3$	$Fe(Cr, Al)_2O_4$	$\alpha-Al_2O_3$	$(Cr, Fe)_2O_3$	FeO	$Cr_2O_3$
		I/I <sub>0</sub>	100	55	50	34	30	25
1050°C	48 hours	Phase	$Fe_2O_3$	$\alpha-Al_2O_3$	$Cr_2O_3$	$Fe(Cr, Al)_2O_4$	$(Cr, Fe)_2O_3$	
		I/I <sub>0</sub>	100/34	71/29	68/28	51/29		28/27

the scale base which eventually levels down the oxidation rate to a negligible value. As usual, the presence of  $\text{Fe}_2\text{O}_3$  and spinel,  $\text{Fe}(\text{Cr},\text{Al})_2\text{O}_4$  are also observed in the scale on the alloy surface from the X-ray data.

Optical cross-section of the alloy at this temperature can be observed in Fig.4-11 in which a duplex scale consisting of  $\text{Fe}_2\text{O}_3$  at the top and spinel at the bottom with a  $\text{Cr}_2\text{O}_3$  and/or  $\alpha\text{-Al}_2\text{O}_3$  subscale at the base is produced by the internal oxidation of Cr and Al upon breakaway of the initial external scale.

This alloy when treated at  $1000^\circ\text{C}$  is observed to be protective in the initial period of about 1-3 hours as revealed by oxidation kinetics data due to the formation of a  $\text{Cr}_2\text{O}_3$  scale. Then breakaway of the  $\text{Cr}_2\text{O}_3$  scale occurs within a short time. A final duplex scale consisting of  $\text{Fe}_2\text{O}_3$  and spinel is believed to exist on the surface of the alloy at this temperature with an  $\alpha\text{-Al}_2\text{O}_3$  and/or  $\text{Cr}_2\text{O}_3$  subscale at the base which prevails till the end of the run. This is evident from the X-ray data presented in Table 4-II (for  $1000^\circ\text{C}$ ) in which strong peaks of  $\text{Fe}_2\text{O}_3$  and  $\text{Fe}(\text{Cr},\text{Al})_2\text{O}_4$ , spinel can be identified for the 48 hour specimen. This is also supported by optical cross-section which represents an iron oxide ( $\text{Fe}_2\text{O}_3$ ) layer in the outer region and  $\text{Fe}(\text{Cr},\text{Al})_2\text{O}_4$ , spinel layer in the inner region in Fig. 4-10 with a more or less continuous subscale layer of  $\text{Cr}_2\text{O}_3$  and/or  $\alpha\text{-Al}_2\text{O}_3$  internal oxide particles. Subscale formation at the alloy oxide interface due to the internal oxidation of Cr and/or Al has been observed by Islam (35) and also others in their

works on high chromium Co-Cr alloys containing reactive element additions. The flattening of the curves in the final stages at this temperature of the above alloy is believed to be due to the existence of the subscale layer (bottom) together with the presence of the duplex scale layer upon the surface.

It is believed that a  $\text{Cr}_2\text{O}_3$  scale also marks the initial stages of oxidation for this alloy at  $1050^\circ\text{C}$  as that at  $1000^\circ\text{C}$ . The scale upon continued thermal cycling, subsequently changes to spinel  $\text{FeCr}_2\text{O}_4/\text{Fe}(\text{Cr},\text{Al})_2\text{O}_4$ . The breakaway, of course, results in the rapid formation of  $\text{Fe}_3\text{O}_4$  as well. This is apparent from the X-ray diffractometer data of the specimens oxidized for 48 hours (16 3-hour cycles) in Table 4-II. Formation of internal oxide particles of  $\text{Cr}_2\text{O}_3$  and/or  $\alpha\text{-Al}_2\text{O}_3$  also are believed to have taken place as before. As a result, the oxidation rate of the treated alloy is primarily controlled by the rate of diffusion of ions ( $\text{Fe}^{3+}$ ) through this subscale layer and eventually settles down to a very much reduced rate of oxidation.

The optical cross-section of the oxidized specimens at this temperature is shown in Fig. 4-12. Bright patches, probably of  $\alpha\text{-Al}_2\text{O}_3$ , can be observed in the figure.

Progressive coarsening in the size of the individual spall particles at higher temperature is also observed in this alloy as already explained in case of Fe-10Cr-2Al alloy. More over these particles are presumably oxides of iron as confirmed by their magnetic nature and a dark blackish colour.

Moseley et al (28), Golightly et al (51) and Rapp et al (38) indicate that binary Fe-Cr alloys containing Cr of about 14-28% along with a more reactive element like Al in the range of 4-5% initially forms an  $\alpha$ - $\text{Al}_2\text{O}_3$  scale. Moseley et al (28) establishes that an  $\alpha$ - $\text{Al}_2\text{O}_3$  is present as a significant phase on specimens of Fe-16Cr-5Al alloy oxidized for 2 hours at 1000°C in air and also on specimens oxidized for 24 hours at 1200°C in air.

The oxidation kinetics of Fe-10Cr-6Al alloy between 950°C and 1050°C represents that an external protective scale forms initially which suffers breakaway within a short period. Subsequently, a second or even a third protective scale has been observed till the end of the run and the rates of oxidation, therefore, level down to a more or less steady state value. It is apparent from the X-ray diffractometer data for the alloy at 950°C presented in Table 4-III, that a number of strong peaks for  $\alpha$ - $\text{Al}_2\text{O}_3$  has been observed. Also the spall particles released from the specimens are in the form of a fine powder, non-magnetic in nature, creamy brown in colour and very small in quantity. On the other hand, the spall particles obtained from the Fe-10Cr-2Al and from the Fe-10Cr-4Al alloys are magnetic in nature, grayish black in colour, larger in quantity and in the form of broken platelets distinctly different from those released by the high-aluminium alloys.

The surface of the oxidized specimen for the above alloy (6%Al) at 950°C is creamy brown in colour, quite free from any black eruption, whereas in case of the previous alloys (2%Al and



Table-4 III  
X-ray Analysis for Fe-10Cr-6Al Alloy

950°C	48 hours	Phase	$\alpha\text{-Al}_2\text{O}_3$	$\text{Fe}_2\text{O}_3$ $(\text{Cr}, \text{Fe})_2\text{O}_3$		
		I/I <sub>0</sub>	100/78/65/60	35		
1000°C	51 hours	Phase	$\alpha\text{-Al}_2\text{O}_3$	$\text{Fe}(\text{Cr}, \text{Al})_2\text{O}_4$	$\text{Fe}_3\text{O}_4$	
		I/I <sub>0</sub>	100/57/53	56	25/21	
1000°C	6 hours	Phase	$\alpha\text{-Al}_2\text{O}_3$	$\text{Fe}(\text{Cr}, \text{Al})_2\text{O}_4$		
		I/I <sub>0</sub>	100/35	65		
1050°C	57 hours	Phase	$\alpha\text{-Al}_2\text{O}_3$	$\text{FeCr}_2\text{O}_4$	$\text{Fe}_3\text{O}_4$	$\text{Fe}(\text{Cr}, \text{Al})_2\text{O}_4$
		I/I <sub>0</sub>	100/24/28	71/29	10	18

4%Al) dark black patches running between gray to dark gray areas have been observed.

It may, in the light of the above features, be considered that the protective scale existing on the surface of the Fe-10Cr-6Al alloy at 950°C from the very beginning till the end of the run is of  $\alpha$ -Al<sub>2</sub>O<sub>3</sub>. As it is believed that the layer of the  $\alpha$ -Al<sub>2</sub>O<sub>3</sub> forms at this relatively low temperature is extremely thin and it is not possible to be observed under ordinary optical microscope.

This alloy, when treated at 1000°C and 1050°C, can be observed to behave in an almost identical manner as that at 950°C. The kinetics curves are featured by the formation of a second protective scale at 1000°C and even by a third at 1050°C. The surfaces of the specimens at both these temperatures, when visually examined presented grayish black eruptions here and there, the rest of the surface being of a creamy brown colour all over without eruption. The spall particles are powdery, non-magnetic in nature and of a creamy brown colour as before, X-ray diffractometer data at the end of the runs for both temperatures after 51 hours and 57 hours of exposure respectively, as shown in Table 4-III, confirms the formation and presence of strong  $\alpha$ -Al<sub>2</sub>O<sub>3</sub> peaks with subsidiary peaks for spinel.

Microstructure of the scales at 1000°C and at 1050°C can be observed in Fig. 4-17 and Fig. 4-18 respectively. It will be apparent that the scale surfaces bear marks of convoluted growth with void formation at the interface region. The scale also appears

to have cracked here and there. The convolutions are believed to be the result of the development of compressive stresses due to lateral growth of the oxide scale (51) and also due to the differential contraction of the oxide scale and metal during thermal cycling (33). These two factors are supposed primarily to be responsible for the formation of cracks in the scale through which contacts between the hot alloy surface and the oxidizing environment occurs. This factor together with void formation at the scale-alloy interface is believed to be responsible for spallation of the oxide scale in the present instance as well. The X-ray data, the nature of the spall particles, the surface appearance of the specimens at the end of the runs, the microstructure of the oxide scale which is conspicuous by the formation of convolutions upon the surface with void formation at the scale metal interface-all support the formation and persistence of an  $\alpha$ - $\text{Al}_2\text{O}_3$  scale on the alloy surface and the interaction of the various factors responsible for bringing about the consequent failure or breakdown of the protective scales.

The phenomena of multiple breakaway and repeated protective scale formation, as observed, in the oxidation of this alloy at  $1050^\circ\text{C}$ , has been known in earlier literatures (37). Failure of the initial external protective scale definitely produces depletion of the alloy-content in the interface region which may even reach the minimum level of the alloying element necessary for the re-formation of the protective scale, but this depletion may be

eventually replenished to a higher level of alloy content to enable the formation of a second protective scale. This phenomenon may repeat as long as the factors responsible for such formation are favourable. Although such observation is not possible metallographically in the present instance, but the kinetics curves sufficiently indicate such a possibility and the relevant X-ray data definitely confirm the existence of an  $\alpha$ - $\text{Al}_2\text{O}_3$  scale till the end of the run. That the repeatedly-formed scales upon the alloy surface are  $\alpha$ - $\text{Al}_2\text{O}_3$  and not  $\text{Cr}_2\text{O}_3$  needs no further emphasis.

It has been postulated that the generation of a complete protective scale of alumina on the alloy surface requires the aluminium-content in the alloy to be above a certain critical value which is a function of temperature. For example, an Fe-4.9%Al alloy forms iron oxide and  $\text{FeAl}_2\text{O}_4$  - spinel below  $570^\circ\text{C}$  and aluminium oxide scales above  $570^\circ\text{C}$  (59). An alloy with as little as 4.4%Al is also reported to form aluminium oxide scales at  $900^\circ\text{C}$  and above (60). In the present study, it is observed that a  $\text{Cr}_2\text{O}_3$  subscale forms with the 2%Al alloy which has been subsequently replaced by an external  $\alpha$ - $\text{Al}_2\text{O}_3$  scale with the 6%Al alloy. The 4%Al alloy, however, forms a mixed subscale layer. It, therefore, appears possible that a minimum limit for aluminium also exists with the present series of alloys marking the establishment of an external protective  $\alpha$ - $\text{Al}_2\text{O}_3$  scale. In fact, the 6%Al alloy did form such a scale, whereas this was not possible with the 4%Al alloy. This finding confirms the same fact that the minimum level of aluminium

necessary for the formation and maintenance of an  $\alpha$ - $\text{Al}_2\text{O}_3$  scale on the alloy surface is about 5% in the present instance as well.

The oxidation kinetics data as represented in Fig. 4-19 for the Fe-10Cr-8Al alloy at  $950^\circ\text{C}$  may suggest the formation of an external  $\alpha$ - $\text{Al}_2\text{O}_3$  scale initially as explained in the case of Fe-10Cr-6Al alloy. It is believed that this  $\alpha$ - $\text{Al}_2\text{O}_3$  scale suffers breakaway due to lateral growth of the scale. On continued cycling, another protective  $\alpha$ - $\text{Al}_2\text{O}_3$  scale starts to form which subsequently decreases the rate of oxidation. Examination of spall particles indicates that these particles consist of  $\alpha$ - $\text{Al}_2\text{O}_3$  as characterized by their non-magnetic property, characteristic colour and fine state of subdivision. The above statement is also confirmed from the X-ray diffractometer data for 51 hours specimen as shown in Table 4-IV, in which a strong peak of  $\alpha$ - $\text{Al}_2\text{O}_3$  can be observed.

Similar explanation may be put forward to justify the oxidation kinetics at  $1000^\circ\text{C}$  for this alloy as that at  $950^\circ\text{C}$ . The kinetics data of the above alloy at  $1000^\circ\text{C}$  reveals the formation of an initial  $\alpha$ - $\text{Al}_2\text{O}_3$  scale. This is evident from the X-ray analysis data presented in Table 4-IV, in which a strong peak of alumina scale has been observed at  $1000^\circ\text{C}$  for the specimen after 6 hours of exposure. As breakaway proceeds, a second protective  $\alpha$ - $\text{Al}_2\text{O}_3$  scale is believed to form which offers protection to the alloy till the end of the run. A number of strong peaks of  $\alpha$ - $\text{Al}_2\text{O}_3$  scale can be observed in the X-ray diffractometer data for the specimen exposed for 51 hours as shown in Table 4-IV. Examination of spall particles

Table-4.IV  
X-ray Analysis for Fe-10Cr-8Al Alloy

950°C	51 hours	Phase	$\alpha\text{-Al}_2\text{O}_3$	$\text{Fe}(\text{Cr,Al})_2\text{O}_4$	
		I/I <sub>0</sub>	100/10/8	20	
1000°C	51 hours	Phase	$\alpha\text{-Al}_2\text{O}_3$	$\text{Fe}(\text{Cr,Al})_2\text{O}_4$	
		I/I <sub>2</sub>	100/44/24/26	26	
1000°C	6 hours	Phase	$\alpha\text{-Al}_2\text{O}_3$	$\text{Fe}(\text{Cr,Al})_2\text{O}_4$	
		I/I <sub>0</sub>	100/13	35	
1050°C	57 hours	Phase	$\alpha\text{-Al}_2\text{O}_3$	$\text{Fe}_3\text{O}_4$ $\text{Fe}(\text{Cr,Al})_2\text{O}_4$	$\text{Fe}_2\text{O}_3$
		I/I <sub>0</sub>	100/82/66/58/21	32	21

indicates that these are  $\alpha$ - $\text{Al}_2\text{O}_3$  particles as before, as they are non-magnetic and creamy brown in colour and in the form of a fine powder.

Unlike the others (at  $950^\circ\text{C}$  and  $1000^\circ\text{C}$ ), the kinetics curves of this alloy at the highest temperature are marked by two breakaways with multiple protective  $\alpha$ - $\text{Al}_2\text{O}_3$  scale formation. An initial  $\alpha$ - $\text{Al}_2\text{O}_3$  scale forms as at the lower temperatures but failure occurs within a short time as marked by a rapid increase in the oxidation rate of the alloy (curves  $A_1B_1$  and  $A_2B_2$ ) in Fig. 4-21. When a second protective scale forms at this high temperature, however, a rapid failure again occurs within a short time as evident from curves  $B_1C_1$  and  $B_2C_2$ . The oxidation rate finally decreases indicating the subsequent re-formation of a third protective scale (curves  $D_1E_1$  and  $D_2E_2$ ). That the scale formed at each of the stages are all  $\alpha$ - $\text{Al}_2\text{O}_3$ , is borne out by the non-magnetic nature and the characteristic colour of the spall particles in every stages. This is also confirmed by the X-ray data presented in Table 4-IV, in which a number of strong peaks of  $\alpha$ - $\text{Al}_2\text{O}_3$  are identified for the 51 hours specimen. Such a multiple breakaway and repeated protective  $\alpha$ - $\text{Al}_2\text{O}_3$  scale formation have been reported by Golightly (37) in his work with Fe-14Cr-4Al alloy at  $1200^\circ\text{C}$  as shown in Fig. 2-5.

The microstructure of the scale at the higher temperatures are illustrated in Fig. 4-22 and Fig. 4-23. From the convoluted morphology of the scale, presence of crack and void formation at

the metal-scale interface, it may similarly be argued that the scale forms at 1000°C is an  $\alpha$ -Al<sub>2</sub>O<sub>3</sub> scale.

The above statement for the existence of an  $\alpha$ -Al<sub>2</sub>O<sub>3</sub> scale is also apparent from the optical cross-section of this alloy at 1050°C as shown in Fig. 4-23 in the present work. It represents presumably the presence of  $\alpha$ -Al<sub>2</sub>O<sub>3</sub> layer at the alloy oxide interface in this case. The scale morphology, nature of spall particles, the specimen surface all confirmed that an  $\alpha$ -Al<sub>2</sub>O<sub>3</sub> persists on the alloy surface at this temperature. Although an  $\alpha$ -Al<sub>2</sub>O<sub>3</sub> scale is believed to have formed upon the alloy surface at 950°C as supported by the X-ray analysis and the character of the spall particles, yet such a scale layer could not be identified under the optical microscope for obvious reasons.

The rate of oxidation decreases with the increase of Al-content due to rapid oxidation of base metal in the lower Al alloys. It is evident from the observation of Moseley et al (28) that oxides of base metal (iron) initially grow more rapidly - outwards from the metal surface - but ultimately the surface becomes covered by a layer of the more stable oxides (alumina) and oxidation of base metal ceases in higher Al alloys.

The effect of temperature i.e. thermal cycling has been observed to be more severe upon the lower Al alloys. This is supported by Islam (35) that the effect of increasing the maximum temperature is found to result in an increased rate of attack with an earlier initiation of spallation. Earlier failure of the



protective scale occurs with the increase of temperature resulting in an increase in the oxidation rate.

The size of the individual spall particles is observed to be progressively finer and smaller with the increase of Al-content. As the rate of oxidation increases, oxide layers being thick and stratified and coarsen the spall particles in lower Al alloys. Such a situation is observed by Moseley et al (28), when the reactive element is present, the outward movement of cations is thought to be suppressed so that there is no growth of stresses and hence no spalling ensues.

Distinctive colour of the spall particles and of the oxidized specimens is likely due to the compositional changes in the oxide layers. As per cent Al increases in the alloy, oxidation of Fe and Cr almost ceases and Al begins to oxidize preferentially. This is why, the spall particles released from the 6% Al and 8% Al alloys has been observed to be creamy brown in colour (most identical to the appearance of  $\alpha$ - $\text{Al}_2\text{O}_3$  particles)

## CHAPTER 5 : CONCLUDING REMARKS

### 5.1 Conclusions

The following conclusions can be drawn regarding the present studies with the modified Fe-10Cr alloys containing 2-8 per cent aluminium:

1. A general reduction in the rate of oxidation in terms of specific weight gain values was noticed with increasing aluminium-content.
2. The amount of spallation decreased with increasing aluminium-content. The individual spall particles become smaller in size and progressively finer accompanied by a change in colour from blackish to creamy brown.
3. Tendency towards the formation of  $\alpha$ -Al<sub>2</sub>O<sub>3</sub> scale was definite and conspicuous with the increase of aluminium-content in the alloy.
4. Scale thickness reduced progressively with increasing aluminium-content marked by an almost complete cessation of spallation with the 8% Al alloy.

5. Following the rapid attainment of alloy coverage by oxide, subsequent oxide growth was slow with increasing aluminium-content, with maximum beneficial effect of aluminium in the range of 6-8%.
6. Failure of a scale was inhibited either through the immediate re-formation of an external protective scale or through the internal oxidation and subsequent formation of a subscale layer.
7. A minimum level of aluminium, depending upon temperatures, exists for the formation of a complete protective scale on the alloy surface.

## 5.2 Suggestions for Future Work

The following are some of the suggestions for further work:

1. To study the effects of addition of a more reactive element in order to change the growth mechanism of  $\alpha$ - $\text{Al}_2\text{O}_3$  scale which will stabilize the  $\alpha$ - $\text{Al}_2\text{O}_3$  on the alloy surface and result in an adherent scale.
2. To study the effects of Al above 8% both under cyclic and isothermal conditions in Fe-10Cr alloy.
3. To determine the minimum Al-content for the formation of an external protective oxide scale on Fe-10Cr alloy under cyclic and isothermal conditions.
4. To study the effects of temperatures at  $1100^\circ\text{C}$  or above on Fe-10Cr alloy with increasing Al-content both under cyclic and isothermal conditions.
5. To study the influence of varying Cr-content with gradually increasing of Al-content both under cyclic and isothermal conditions.

## REFERENCES

1. T. Tsuji, S. Kobayashi, M. Oda and K. Naito: High Temperature Corrosion of Advanced Materials and Protective Coating, Proc. Conf., Tokyo, December 1990, p. 115.
2. D. Clemens, K. Bongartz, W. Speier, W.J. Quadackers and R.J. Hussey : Fresenius J. Anal. Chem., 1993, Vol. 346, Nos. 1-3, p. 318.
3. D.S. Clark and W.R. Varney: Physical Metallurgy for Engineers, CBS publishers and Distributors, Delhi, First Indian Edition 1987, p. 318, 348.
4. R.J. Welsh and G. Waller: The Gas Turbine Manual, Publ. Temple Press Ltd., London, p. 25.
5. High Temperature Steels and Alloys for Gas Turbines (Special Report no.43), Iron and Steel Institute , 1952.
6. H. Shimizu, K. Ishii, F. Togashi, K. Yoshioka and T. Kawasaki: Applications of stainless steel, Proc. Conf., Stockholm, 1992, Vol. 2, p. 1101.
7. A. K. Biswas: Principles of Blast Furnace Iron making, (Theory and practice), SBA publications, Delhi, First Indian edition, 1984, (Reprinted: 1991), p. 66.
8. E. Gregory and W.W. Stevenson: Chemical Analysis of Metals and Alloys, Blackie and Son Ltd, London and Glasgow, 2nd Edition, 1942, p. 68.

9. O. Kubascewski and B.E. Hopkins: Oxid. Metals and Alloys Butterworths, London, 2nd Edition, 1957, p. 11.
10. C.S. Tedmon: J. Electrochem. Soc., 1966, Vol. 113, p. 766.
11. E. A. Gulbransen and K. F. Andrew: J. Electrochem. Soc., 1957, Vol. 104, p. 334.
12. C.A. Phalnikar, E.B. Evans and W.M. Baldwin: Jr. J. Electrochem. Soc., 1956, Vol. 103, p. 429.
13. D. Mortimer and M.L. Post: Corr. Sci., 1968, Vol. 8, p. 499.
14. B.G. Seong, J.H. Song, S.Y. Hwang and K.Y. Kim: High temperature corrosion of Advanced Materials and protective coatings, Proc. Conf., Tokyo, December 1992, p. 123.
15. Y. Matsuanaga: Japan Nickel Review, 1933, Vol.1, p. 347.
16. T.N. Rhys-Jones, H.J. Grabke and H. Kudielka: Corr. Sci., 1987, Vol. 27, No. 1, p. 49.
17. D.J. Gardiner. C.J. Littleton, K.M. Thomas and K.N. Strafford: Oxidation of Metals, 1987, Vol. 27, p. 57.
18. S.C. Tjong, J. Endridge and R.W. Hoffman: Appl. Surface Sci., 1982-83, Vol. 14, p. 297.
19. S.C. Tjong, Mat. Res. Bull., 1983, Vol. 18, p. 157.
20. F.I. Wei and F.H. Stott: Corr. Sci., 1989, Vol.29, No.7, p.839.
21. R.G. Richards and J. White: Trans. Brit. Ceramic Soc., 1954, Vol. 53, p. 422.
22. R.L. Rickett and W.P. Wood: Trans. A.S.M., 1934, Vol. 22, p. 347.

23. H.M. McCullough, M.A. Fontana and F.H. Beck: *ibid*, 1950, Vol. 43, p. 404.
24. H.J. Yearian, E.C. Randell and T.A. Longo: *Corrosion*, 1956, Vol. 12, p. 515t.
25. P.E. Wretblad: *Z. Anorg. Chem.*, 1930, Vol. 189, p. 329.
26. D. Caplan and M. Cohen: *Journal of the Electrochem. Soc.*, 1965; Vol.112, No.5, p. 471.
27. A.U. Seybolt: *Journal of the Electrochem. Soc.*, 1960, Vol.107, No.3, p. 147.
28. P.T. Moseley, K.R. Hyde, B.A. Bellamy, G. Tappin: *Corr. Sci.*, 1984, Vol. 24, No.6, p. 547.
29. G.C. Wood, T. Hodgkiess and D.P. Whittle: *Corr. Sci.*, 1966, Vol.6, p. 129.
30. G.C. Wood, and T. Hodgkiess: *J. Electrochem. Soc.*, 1966, Vol. 113, p. 319.
31. J.S. Wolf and G.D. Sandrock: *NASA-TN/D-4715*, 1968.
32. G.C. Wood and D.P. Whittle: *Corr. Sci.*, 1964, Vol. 4, p. 263.
33. C.E. Lowell and W.L. Deadmore: *Oxid. Metals*, 1973, Vol.7, p. 55.
34. J.O. Edstrom: *J. Iron steel Inst.*, 1957, Vol. 185, p. 450.
35. M.S. Islam: *Ph.D. Thesis, University of Liverpool*, 1978.
36. T. Hodgkiess: *Ph.D. Thesis, Univ. Manchester*, 1966.
37. P.A. Golightly : *Ph.D. Thesis, Univ. Manchester*, 1970.
38. R. A. Rapp and B. Pieraggi: *The Electrochem Soc.*, 1992, Vol. 92-22, p. 51.

39. A.M. Huntz and M. Schutze: *Materials at High Temperatures*, 1994, Vol. 12, No. 2-3, p.151.
40. D.P. Whittle: *Corr. Sci.*, 1972, Vol. 12, p. 869.
41. G.C. Wood, I.G. Wright, T. Hodgkiess and D.P. Whittle: *Werkstoffe und Korrosion*, 1970, Vol.21, p. 900.
42. D.P. Whittle, D.J. Evans, D. B. Scully and G.C. Wood: *Acta Met.*, 1967, Vol. 15, p. 1421.
43. Lucas Aerospace Ltd., Report No. B-49-105, 1973.
44. P.Y. Hou and J. stringer: *Oxidation of metals*, 1992, Vol. 38, Nos 5/6, p. 323.
45. V.R. Howes: *Corr. Sci.*, 1968, Vol. 8, p. 221.
46. J.K. Tien and F.S. Pettit: *Met. Trans.*, 1972, Vol.3, p. 1587.
47. J. Stringer: *Corr. Sci.*, 1970, Vol. 10, p. 513.
48. N.B. pilling and R.E. Bedworth: *J.Inst. Metals*, 1923, Vol. 29, p. 529.
49. R.F. Tylecote: *J. Iron Steel Inst.*, 1960, Vol. 195, p. 380.
50. F.N. Rhines and J.S. Wolf: *Met. Trans.*, 1970, Vol. 1, p. 1701.
51. F.A. Golightly; F. H. Stott: *Oxid. metals*, 1976, Vol. 10, p. 163.
52. G.C. Wood: *Werkstoffe und Korrosion*, 1971, Vol.22, p. 491.
53. C.A. Barrett and C.E. Lowell: NASA-TN-D-7615, 1974.
54. F. Wang, H. Lou and W.U. Waitao: *High Temperature Corrosion of Advanced Materials and Protective Coatings*, Proc. Conf., Tokyo, 1990, p. 103.



55. M.W. Brumm and H.J. Grabke: *Corr. Sci.*, 1992, Vol. 33, No. 11, p. 1677.
56. J. Jedlinski, G. Borchardt: *The Electrochem. Soc.*, 1992, Vol. 92-22, p. 67.
57. L.V. Ramanathan: *Corr. Sci.*, 1993, Vol.35, No.5-8, p. 871.
58. F. Clemendot, J.M. Gras, J.C. Van Duysen and G. Zacharie: *Corr. Sci.*, 1993, Vol.35, Nos.5-8, p. 901.
59. W.E. Baggs: *J. Electrochem. Soc.*, 1971, Vol. 118, p. 906.
60. W.C. Hagel: *Corrosion*, 1965, Vol. 21, p. 316.

